Worcester Polytechnic Institute
Digital WPI

2012-04-26

Cell Printing: A novel method to seed cells onto biological scaffolds

Chirantan Kanani
Worcester Polytechnic Institute

Follow this and additional works at: https://digitalcommons.wpi.edu/etd-theses

Department of Biomedical Engineering

Cell printing: A novel method to seed cells onto biological scaffolds

A Thesis

Submitted to the faculty of

WORCESTER POLYTECHNIC INSTITUTE

In partial fulfillment of the requirements for the

Degree of Master of Science

Submitted by: _____

Chirantan Kanani

Approved by:

_____   _____

Glenn Gaudette, PhD   Raymond Page, PhD

_____

Qi Wen, PhD

1

Acknowledgements

Abstract

Bioprinting, defined as depositing cells, extracellular matrices and other biologically relevant materials in user-defined patterns to build tissue constructs de novo or to build upon pre-fabricated scaffolds, is among one of the most promising techniques in tissue engineering. Among the various technologies used for Bioprinting, pressure driven systems are most conducive to preserving cell viability. Herein, we explore the abilities of a novel bioprinter - Digilab, Inc.'s prototype cell printer. The prototype cell printer (Digilab Inc., Holliston, MA) is an automated liquid handling device capable of delivering cell suspension in user-defined patterns onto standard cell culture substrates or custom-designed scaffolds. In this work, the feasibility of using the cell printer to deliver cell suspensions to biological sutures was explored.

Cell therapy using stem cells of various types shows promise to aid healing and regeneration in various ailments, including heart failure. Recent evidence suggests that delivering bone-marrow derived mesenchymal stem cells to the infarcted heart reduces infarct size and improves ventricular performance. Current cell delivery systems, however, have critical limitations such as inefficient cell retention, poor survival, and lack of targeted localization. Our laboratories have developed a method to produce discrete fibrin microthreads that can be bundled to form a suture and attached to a needle. These sutures can then be seeded with bone-marrow derived mesenchymal stem cells to deliver these cells to a precise location within the heart wall, both in terms of depth and surface localization. The efficiency of the process of seeding cells onto fibrin thread bundles (sutures) has previously been shown to be 11.8 ± 3.9 %, suggesting that 88% of the cells in suspension are not used. Considering that the proposed cell-therapy model for treatment of myocardial infarction contemplates use of autologous bone-marrow derived stem cells, an improvement in the efficiency of seeding cells onto the fibrin sutures is highly desirable.

The feasibility of using Digilab's prototype cell printer to deliver concentrated cell suspension containing human mesenchymal stem cells (hMSCs) directly onto a fibrin thread bundle was explored in this work, in order to determine if this technology could be adapted to seed cells onto such biological sutures. First the effect of the printing process on the viability of hMSCs was assessed by comparing to cells dispensed manually using a hand-held pipette. The viability of hMSCs 24 hours post-dispensing using the cell printer was found to be 90.9 ± 4.0 % and by manual pipetting was 90.6 ± 8.2 % (p = ns). Thereafter a special bioreactor assembly composed of sterilizable Delrin plastic and stainless steel pins was designed to mount fibrin thread bundles onto the deck of the cell printer, to deliver a suspension containing hMSCs on the bundles. Highly targeted delivery of cell suspension directly onto fibrin thread bundles (average diameter 310 µm) was achieved with the bundle suspended in mid-air horizontally parallel to the printer's deck mounted on the bioreactor assembly. To compare seeding efficiency, fibrin thread bundles were simultaneously seeded with hMSCs using either the cell printer or the current method (tube-rotator method) and incubated for 24 hours. Seeded thread bundles were visualized using confocal microscopy and the number of cells per unit length of the bundle was determined for

each group. The average seeding efficiency with the tube rotator method was 7.0 ± 0.03 % while the cell printer was $3.46 \pm 2.24\%$ (p = ns).

In conclusion, the cell printer was found to handle cells as gently as manual pipetting, preserve their viability, with the added abilities to dispense cells in user-defined patterns in an automated manner. With further development, such as localized temperature, gas and humidity control on the cell printer's deck to aid cell survival, the seeding efficiency is likely to improve. The feasibility of using this automated liquid handling technology to deliver cells to biological scaffolds in specified patterns to develop vehicles for cell therapy was shown in this study. Seeding other cell types on other scaffolds along with selectively loading them with growth factors or multiple cell types can also be considered. In sum, the cell printer shows considerable potential to develop novel vehicles for cell therapy. It empowers researchers with a supervision-free, gentle, patterned cell dispensing technique while preserving cell viability and a sterile environment. Looking forward, de novo biofabrication of tissue replicates on a small scale using the cell printer to dispense cells, extracellular matrices, and growth factors in different combinations is a very realistic possibility.

Contents

Table of Figures

Table of Tables

Chapter 1: Introduction

Bioprinting can be defined broadly as depositing or dispensing live cells and biologically relevant substances in user-defined patterns in two or three dimensions (1). Several technologies have been adapted for bioprinting: ink-jet printing (or drop-on-demand printing) (2) (3) (4), laser-induced forward transfer (LIFT) (5) or its modifications such as BioLP (6), and syringe-based gel deposition (7), (8), (9). However, success of these techniques in terms of tissue engineering applications of these technologies remains limited and largely confined to individual laboratories or groups which have developed these technologies.

One of the most crucial factors for wider acceptance of such bioprinting technologies in tissue engineering applications is the commercial availability of the device with standardized configuration at reasonable cost, which has been tested successfully for particular applications. Even when such a device is standardized, available for purchase and use, reproducibility of success in the hands of different users can be reasonably assured only when parameters for its successful use for a particular application (protocol) are clearly defined by rigorous testing. Digilab, Inc.'s bioprinter – the Cell Jet, is relatively inexpensive motorized-syringe pump based bioprinter, with a time-tested automated liquid handling technology at its core. A prototype version of the cell printer, which was used in this project for the purpose of more flexibility of operation and easy hardware changes, is precursor for its commercial product. It has the same technology of cell dispensing as the commercial version.

Working towards a larger goal of exploring the use of a bioprinting technology towards a specific tissue engineering application, Digilab, Inc.'s prototype cell printer was evaluated as a tool for seeding cells onto biological sutures as vehicles for cell therapy for cardiac dysfunction.

Cardiac failure is a major health burden in the United States and worldwide (10). The main reason for disease being a major health cost is that the heart lacks the ability to regenerate clinically (11). Cell therapy shows promise to regenerate the heart. Among other cell types, human mesenchymal stem cells (hMSCs) have been observed to contribute to cardiac function by increasing vascularity as well as limiting scarring in the infarction zone (12), (13). However, current methods of cell delivery are inefficient with cell engraftment rates ranging from $1 - 25\%$ depending upon the method (14), (15). Fibrin microthread bundles, developed by Cornwell *et al.,* have shown to be more effective vehicles to deliver human mesenchymal stem cells to the rat heart myocardium compared to direct myocardial injection (16), (17), (18). The process of seeding hMSCs onto fibrin microthread bundles currently has an efficiency of about 12%, with the remaining 88% of the cells remaining un-utilized (18). If an autologous source of cells is to be contemplated for cell therapy using this mode of delivery, an improvement in seeding efficiency, to deliver a much higher proportion of therapeutically relevant cells to the target tissue, is highly desirable.

The current method uses a slowly rotating assembly consisting principally of a sterile silastic tubing of 1.98 mm inner diameter filled with cell suspension into which the fibrin thread bundle is placed in an incubator for 24 hours. Among the various possible reasons for low cell seeding efficiency, a major contributing factor is likely to be the dead space around the fibrin thread bundle inside the silastic tubing, in which the cells keep floating in suspension while the assembly rotates, without getting an opportunity to settle and attach onto the bundle. If the dead space around the bundle is eliminated, with the cell suspension remaining in contact with the fibrin thread bundle throughout the duration of the incubation period, an increase in seeding efficiency is likely.

Digilab's prototype cell printer is an automated liquid handling device modified to handle live cells, capable of delivering cell suspensions to substrates in user-defined patterns, including a linear pattern onto a target such as a fibrin thread bundle. If cell suspension could be delivered to the fibrin thread bundles directly, and conditions favorable to cell seeding be maintained on the bundle for a period long enough to allow cell attachment, the dead space in the current assembly could be done away with.

With this rationale in mind, the cell printer was first evaluated for the effects of cell dispensing process on the viability of hMSCs. It was hypothesized that the viability of the hMSCs would be unaffected by the printing process. A big advantage of this motorized-syringe pump based cell printer is that the physical forces acting upon the cell suspension when it is aspirated and dispensed by the cell printer are very similar to those encountered while aspirating and dispensing using a hand-held pipette. This is unlike other methods of cell printing such as thermal inkjet or laser assisted bioprinting, wherein the cell suspension is momentarily exposed to temperatures up to $600^{o}C$ (2), or is subjected to high acceleration and deceleration during dispensing process (5), respectively. To test the hypothesis, viability of hMSCs dispensed using the cell printer was compared to the viability of cells dispensed manually using a handheld pipette.

Second, a bioreactor assembly was developed to mount the fibrin thread bundle onto the cell printer's deck. The printer was programmed to aspirate a concentrated volume of cell suspension and dispense it directly onto the thread bundle, distributing it uniformly through the length of bundle. It was hypothesized that the cell printer would be able to deliver cell suspension to the thread bundle so as to result in attachment of the cells on the bundle. Additionally, factors critical to better seeding of cells onto fibrin thread bundles, and scaffold in general, using this novel method were identified in this study.

Chapter 2: Background

The broad aim of this project was to explore the capabilities of Digilab's prototype cell printer to dispense and deliver delicate cells (such as human mesenchymal stem cells) in minute volumes in user-defined patterns at targeted locations, in order to develop useful applications in tissue engineering. This lab being a cardiac tissue engineering lab, tissue engineering approaches to quantify and improve cardiac pump function in cardiac disease are studied here. One of the main focuses of the lab is development of scaffold based delivery of various types of stem cells for *in vivo* cardiac tissue regeneration. Previous work done in the lab illustrated that biological threads made of fibrin and/or collagen, are capable of serving as a scaffold for human mesenchymal stem cells (hMSCs) (17). It has also been shown that sutures made of such biological threads show a higher rate of *in vivo* hMSC-engraftment as compared to direct myocardial injection in a rat heart model (18). However, the rate of seeding of hMSCs onto fibrin thread bundles (seeding efficiency) using the current seeding method which uses a slowly rotating bioreactor made of silastic tubing is only about 12%, with abundant scope for improvement.

With this serving as motivation, this work was aimed at exploring the feasibility use of this cell printing technology to seed cells onto relatively thin linear print targets such as a biological thread bundle, and identify factors necessary to adapt this novel tool to efficiently seed cells onto such scaffolds.

An overview of Cell Printing and various technologies used for the same is presented in this chapter. Thereafter, a brief background of role of fibrin microthread bundles as scaffolds for cell therapy in cardiac disease is presented.

2.1: Cell printing: an overview

2.1.1: Definition
Cell printing can be defined as automated deposition or dispensing of live cells in user-defined patterns in 2 or 3 dimensions on cell culture substrates or pre-formed scaffolds using various liquid handling/deposition technologies. Although a categorical definition of the term was not found after an exhaustive literature survey, it has been used in the said sense in scientific works by several independent groups – Vladimir Mironov *et al.* (19), Thomas Boland *et al.* (2), Anthony Atala *et al.* (3), Wei Sun *et al.* (20), and Makoto Nakamura *et al.* (4) among others. A more technical term is used by certain authors to describe the same process - 'Direct Cell Writing' (20), (21).

The term 'cell printing' must be distinguished from a similar-sounding term 'Cell Transfer Printing', also known as 'Cell Stamping' (22), which refers to transferring cells attached to a source surface of user-defined geometry or pattern (called the 'stamp'), to a target or destination

surface by bringing the two surfaces in contact with each other ('stamping' the cell stamp on the destination surface), so as to deposit cells on the destination surface in the pattern of the 'stamp'. This is an entirely different concept that relies on the interactions between cells and the surface properties of source and destination materials in order to dislodge cells from the former and make them adhere to the latter.

Cell printing can be considered a subset of **Bioprinting**, a more generic term that includes deposition or dispensing of any biologically relevant substance, not just live cells, in an automated manner in user-defined patterns in two or three dimensions (19). In addition to live cells, biologically relevant substances may include scaffold materials as Collagen, Fibrin, Gelatin, Alginate, Agarose and others usually in a hydrogel form, growth factors, nutrient media or other substances as may be relevant.

A closely related term, **Biofabrication,** has been broadly defined as "the production of complex living and non-living biological products from raw materials such as living cells, molecules, extracellular matrices, and biomaterials" (1). Biofabrication usually requires assembling, arranging or 'putting together' of the biologically relevant entities at certain stage(s) in the process, which forms the bulk of the process, and finally results into the 'product'.

Conceptually speaking, Biofabrication is an approach for tissue engineering, while Bioprinting may be regarded as a method.

2.1.2: Technologies employed for cell printing

All technologies employed to dispense cells in patterns are modification of pre-existing printing or automated liquid dispensing technologies. Being a relatively young concept, born a little over a decade ago, technologies and devices used for cell printing are in their nascent stage and are constantly evolving with time. Development of cell printing technologies is ongoing and will continue as new applications emerge. At the core, all technologies are being modified so as to handle live cells gently, causing minimal unwanted perturbation to them.

A current literature survey revealed the following basic technologies employed for cell printing:

A. Ink-jet bioprinters (2), (3), (4) utilize either a heating element (thermal inkjet) or a piezo-electric element (piezo-electric inkjet) to dispense small droplets of cell suspension or other biologically relevant liquid load in a cartridge. The paper loading tray of the printer is replaced with a Z-stage containing a cell culture dish or other substrate.

B. Laser Induced Forward Transfer and related laser-based bioprinters (5), (6), (23) utilize a highly targeted pulse of laser to impart energy to a film of cells in suspension placed on a dispense 'cartridge', which causes cells in that part of the cartridge to detach and transfer to a print substrate placed opposite the cartridge. Patterns are formed on the basis of parts of the cartridge that are pulsed by the laser, as defined by the user.

C. Syrige-based bioprinters (7), (9) utilize a syringe pump to aspirate and dispense cell suspensions through a small diameter nozzle (similar to a hypodermic needle) mounted on a 'print-head'. Pressure is generated inside the syringe (to either aspirate (negative pressure) or dispense (positive pressure)) using either compressed air (Pneumatic pressure-driven syringe-based bioprinters) or a motorized-piston or plunger (displacement-driven syringe-based bioprinters). In either case, when negative pressure is applied by the syringe onto the nozzle on the-print head, cell suspension is drawn up through the nozzle into the syringe (or a system of tubing connecting the syringe to the nozzle). The print-head is moved with respect to the print deck in X, Y and Z directions of space using motion control robots. This determines the position, movement velocity and acceleration of the print head and of the nozzle. When positive pressure is applied by the syringe onto the nozzle, the cell suspension is dispensed onto the print substrate positioned on the printer's deck (or stage). The syringe usually works in tandem with a valve positioned in between the syringe and the nozzle, the firing of which at different rates allows different volumes of the cell suspension to be dispensed. The combination of X, Y, Z position and movement pattern of the print-head as controlled by the motion control robot and the pressure applied by the syringe on the cell suspension determines the pattern in which cell suspension is dispensed onto the print substrate.

Digilab's Bioprinter belongs to the third category – syringe-based bioprinters, specifically plunger-displacement based bioprinters, versus pneumatic (compressed air) bioprinters.

Detailed discussion of mechanisms of printing of various bioprinters is beyond the scope of this work. However, representative images of the principle types of bioprinters are given below.

A sample inkjet bioprinter developed by modifying a standard HP Deskjet 550 by Boland *et al* (2) (Clemson University, Clemson, SC) is shown in Figure 1.

A pneumatic pressure based bioprinter built from scratch by Lee *et al.* (Brigham and Women's Hospital, Boston, MA) is shown in Figure 2.

The mechanism of droplet formation for a modified version of laser induced forward transfer, known as Absorbing-Film Assisted LIFT (AFA-LIFT) is shown in Figure 46, in the Discussion chapter. The mechanics of printing of LIFT based bioprinters are similar to the one described.
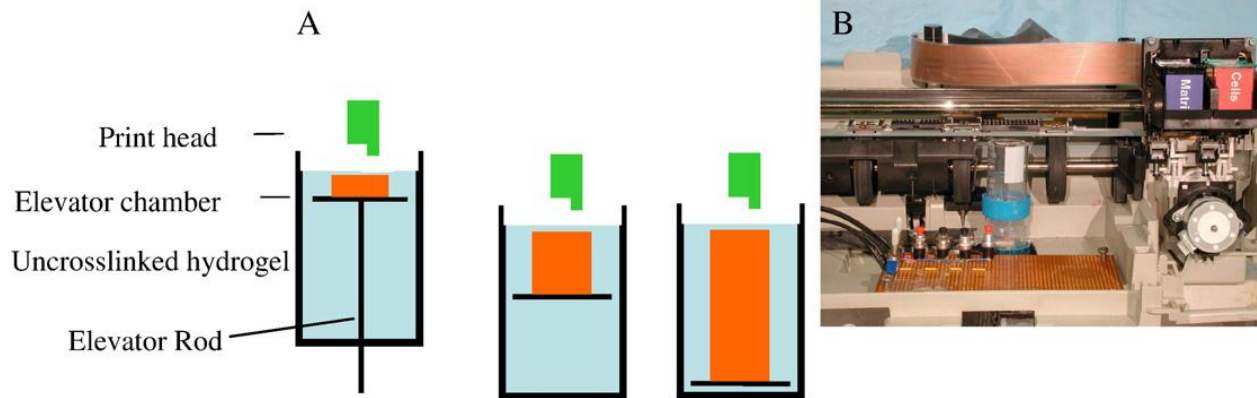
Figure 1: Example of Ink-jet Bioprinter. Hewlett-Packard DeskJet 550 printers were modified to adapt them to print cells by Boland *et al.* (figure adapted from their journal publication titled "Drop-on-demand printing of cells and materials for designer tissue constructs" - **(2)**). A schematic view of the Z-stage mechanism is shown in the schematic on the left (A), and the actual printer with the cover taken off, and Z-stage chamber placed in place of the paper-feed system is shown in the image on the right (B). Z-stage mechanism (A): After each printed layer, the elevator rod is lowered. Since the total volume inside the chamber was constant during the lowering of the stage, uncrosslinked hydrogel would flood onto the printed areas. After the rod reached the bottom of the chamber, a printed hydrogel structure was formed on the stage.
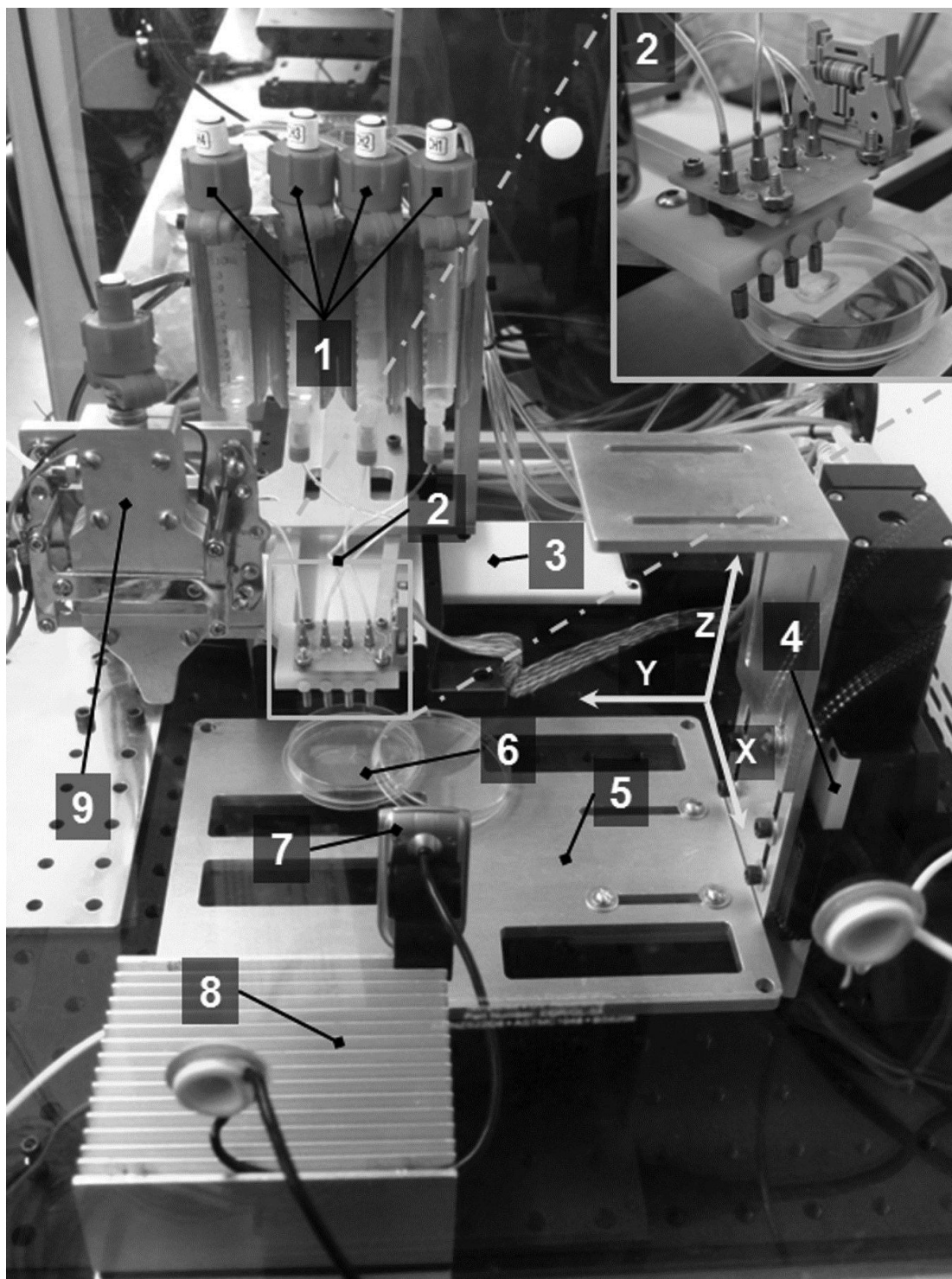
Figure 2: Syringe-based bioprinter: Pneumatic pressure-driver. Lee *et al.* (**24**). Side view of a pneumatic pressure driven 3D bioprinter platform shown with: 1. a four-channel syringe array as cartridges for cells and hydrogel precursors; 2. a four-channel dispenser array; 3. X-Y axes control; 4. Z-axis control; 5. the vertical stage; 6. the target substrate; 7. a video camera for the monitoring of 3D printing process; 8. a vertical stage heater/cooler; and 9. independent heating/cooling unit for a dispenser. Inset: a close-up view of the four-channel dispenser array.

Several bioprinters are now manufactured commercially by companies worldwide. The prominent ones among them that surfaced during literature review are listed below:

- Envision TEC, Gladbeck, Germany - 3D Bioplotter
- Sciperio / nScript, Orlando, FL – 'BioAssembly Tool'
- Neatco, Toronto, Canada - Laboratory Bioprinter 'LBP', in collaboration with MUSC Bioprinting Research Center, Charleston, SC
- Digilab, Inc., Holliston, MA - Cell Jet cell printer
- Organovo, San Diego, CA – Novogen MMX bioprinter

2.1.3: Top-down versus Bottom-up approach:

Two approaches towards forming tissue constructs are described in the literature (25):

A. A "top-down" approach, wherein cells are seeded on pre-fabricated biodegradable scaffolds made of materials such as poly (glycolic acid) (PGA) or others. (26) (27) (28) (29). In this approach, which is a more conventional approach, cells are expected to populate a scaffold and create appropriate extra-cellular matrix, often with the aid of perfusion, growth factors, and/or physical stimuli such as mechanical or electrical conditioning. Despite advances in core engineering competencies, top-down approaches have limitations of not being able to create the intricate micro-architecture of tissues, such as small vasculature.

B. A "bottom-up" approach, also known as "modular tissue engineering", aims at creating smaller building blocks or "modules" made of cells and/or scaffolding material having the microarchitecture of native tissue, which can then be assembled to create larger functional tissues. Individual modules can be created and/or arranged using various techniques such as self-assembled aggregation (30), micro-fabrication of cell-laden hydrogels (31), creation of cell sheets (32), or direct printing of tissues (19).

Bioprinting and Biofabrication are bottom-up approaches in principle. However, the current project involves use of a cell printing technology to deliver cells to a pre-formed scaffold (biological suture made of fibrin microthreads). The technique thus represents a fusion of the two approaches for tissue engineering: a technology used traditionally for bottom-up construction of tissues has been employed to deliver cells to a pre-fabricated scaffold with the intent of populating the scaffold efficiently.

Novel solutions to difficult tissue engineering problems may emerge by applying such a combined approach, keeping in mind native development of tissues.

2.2: Human mesenchymal stem cells and fibrin microthread sutures for cardiac regeneration

2.2.1: Cardiovascular disease

Cardiovascular disease is currently the leading cause of death in the United States (33). Nine hundred twenty thousand people in the United States annually suffer from myocardial infarction. After a myocardial infarction occurs, 22% of men and 46% of women are diagnosed with heart failure within six years. At this point, the heart is unable to pump a sufficient amount of blood to the body's organs, significantly altering a patient's ability to perform even basic physical tasks. Myocardial infarction and coronary heart disease cost patients in the United States over $156 billion a year (34). The importance of dealing with this disease burden cannot be understated.

After a myocardial infarction, the heart cannot clinically repair itself. Post-infarction scar tissue forms over the dead tissue where the cardiac myocytes perished. If the infarction is not treated, the scar tissue will begin to thin and the dimensions of the left ventricle start to change (35). Myocardial infarction also has profound effects on the general function of the heart. Ejection fraction, the amount of blood in the ventricle that is ejected with each stroke of the heart, decreases depending on the size of the infarction. Compensatory responses to restore the ejection fraction increase the stress in the ventricular wall because of the extra pressure and volume applied. The increase in stress on the non-contractile, thinned-out infarcted scar tissue that replaced infarcted myocardium can cause complications including aneurysms and rupture (35).

2.2.2: Current treatment for myocardial infarction

The current treatments for myocardial infarction aim at restoring blood flow to infarcted region or restoring the normal shape of the heart from a spherical shape to the natural, more efficient elliptical shape.

Procedures to restore blood flow to the ischemic myocardium

Procedures commonly performed that restore blood flow to the ischemic region of the heart include coronary artery bypass grafting (CABG) and percutaneous coronary interventions (PCI).

Coronary Artery Bypass Grafting (CABG) involves harvesting a segment of a blood vessel having a diameter comparable to the coronary artery such as the internal mammary artery (36) or saphenous vein (autograft), and anastomosing the harvested blood vessel to the coronary artery proximal and distal to the blocked segment of the artery so as to bypass the blockage and thus restore the blood flow to the damaged myocardium.

Percutaneous Coronary Interventions (PCI) refers to a group of interventions wherein a flexible catheter is introduced into one of the major peripheral arteries, most commonly the femoral artery, and guided inside the lumen of the vessel using a variety of live imaging techniques to reach the root of the aorta where the coronary arteries originate. The tip of the catheter is then guided into the blocked coronary vessel to reach the blocked segment. A variety

of interventions may then be performed to relieve the block (such as blowing up a cylindrical balloon to dislodge the thrombus and widen the narrowed segment), with or without additional interventions to maintain patency of the vessel (such as plain or drug-eluting stent placement).

Even though these procedures may serve to restore blood flow to damaged myocardium, they do not regenerate the myocardium if it is infarcted (37). Cardiac pump failure that results from the infarction is not treated by these methods.

Procedures to restore shape of the heart
A myocardial infarction that is replaced by non-contractile scar tissue undergoes remodeling over time, where the shape of the ventricle and the heart overall becomes more spherical than the normal elliptical one. The abnormal shape contributes significantly to the lowered pump function of the heart. Thus, surgical procedures to restore to the natural, more efficient elliptical shape of the heart have been developed. Most common procedures include **direct linear closure** and **endocardial patch plasty (Dor procedure)** (38). Both these procedures serve to restore ventricular dimensions. However they do not address the problem of pump failure actively. The overall function of the heart remains compromised because the infarcted tissue does not contribute to the pump function.

Thus, none of the treatment options currently available for myocardial infarction are aimed at regenerating contractile myocardial tissue to restore the pump function of the ventricle.

2.2.3: Cell therapy and biomaterials for myocardial regeneration:
Cellular therapy aims to restore damaged or non-functional tissue back to its functional state by implanting specific types of cells in the tissue that can provide necessary cues for regeneration and healing. In case of heart failure, instead of excising the infarcted or scarred tissue, it aims to regenerate healthy contractile myocardial tissue at the site of the scar tissue.

A variety of cell types have been used for myocardial cellular therapy: bone marrow stem cells, skeletal myoblasts, embryonic stem cells, and cardiac stem cells (39) (40) (41) (42). Ethical issues are involved in the use of embryonic stem cells, along with the increased risk of tumor formation. Skeletal myoblasts are unable to electrically integrate with cardiac myocytes. There is lack of consensus about the existence of cardiac stem cells (43), (44), (45). Considering these factors, human mesenchymal stem cells derived from the bone marrow are being explored for cell therapy for myocardial regeneration in our laboratory and were used in this project.

Human mesenchymal stem cells (hMSCs) represent 0.001% to 0.01% of the total nucleated cells in the bone marrow, from where they are acquired (43). They are multipotent adult stem cells, and have been shown to induce angiogenesis, differentiate into cardiac myocyte-like phenotype after being delivered to the heart, and are capable of being utilized without causing an immune

response (43) (44) (45). In terms of tissue regeneration, these cells are ideal due to their relatively high proliferation rate, genetic stability, and ease of isolation (6) (43) (46).

hMSCs have been shown to improve metrics of cardiac function post-delivery including increase in ventricular performance and reduction in infarct size in many studies (39), (46), (47), (48), (49), (50). The exact mechanisms that are responsible for these improvements are not completely understood. The theories regarding possible mechanisms include: differentiation of delivered hMSCs, cell fusion, a presence of passive cells in the myocardial wall, and paracrine signaling (51). Even though controversy surrounds the mechanisms by which hMSCs bring about improvement in cardiac function, researchers agree hMSCs help restore a portion of cardiac function. For all of the above reasons, hMSCs are used in our laboratory to study cardiac regeneration in a rat heart model.

Despite the great potential shown by hMSCs for cardiac regeneration, their therapeutic effect is limited due to lack of an efficient delivery method. Direct intramyocardial injection involves the injection of a certain volume of cell suspension directly into a myocardial infarction in a beating heart. The main limitation of this method is that once the injection needle is removed, the cells are pushed out due to the contraction of the heart muscle (11). Systemic delivery of therapeutic cells lacks localization. When cells are delivered systemically, a majority of the cells engraft in other organs including lungs, liver, and spleen (49), (52). Due to lack of localization, low cell attachment and high rate of cell death, myocardial engraftment rate ranges from 1 to 10% with various routes of injection (11), (53).

The limitations of myocardial cellular therapy due to inefficient delivery methods can be overcome by attaching therapeutically relevant cells to suitable biomaterials that can be implanted specifically to the site of delivery. Numerous scaffolds have been created for use in cardiac applications using gelatin, fibrin, collagen, and alginates in the form of gels or 3D scaffolds (14), (15), (54), (55), (56), (57), (58), (59), (60). Despite improved cell survival, injectable gel mediated cell delivery has problems of cell and gel retention (41), (54), (59). 3D scaffolds used for myocardial regeneration have shortcomings of having insufficient nutrient diffusion and vascularization (46), (54). There is a need to develop a scaffold that would improve cell viability and aid targeted cell delivery in therapeutically significant numbers to the myocardium.

Discrete fibrin microthreads, developed by Cornwell *et al*. (61), can be bundled to form thread bundles that have higher tensile strengths than fibrin gels and sufficient mechanical properties to be pulled through the myocardium using a surgical suture needle. Proulx *et al.* showed that fibrin thread bundles support viability and proliferation of hMSCs without affecting their multipotency (62). They were also able to seed thread bundles with physiologically relevant number of hMSCs for cardiac regeneration. Additionally, fibrin microthread bundles can be coated with growth factors or other biologically relevant molecules to aid cellular attachment and function towards

cardiac regeneration. Due to these reasons, fibrin microthreads have been used as vehicles to deliver hMSCs to the rat heart in our lab to study myocardial regeneration.

Fakharzadeh *et al*. showed that delivering hMSCs seeded on biological microthreads is a more efficient method of delivering the cells to a beating rat heart as compared to a direct myocardial injection (18). Higher localization of delivery of hMSCs was also achieved (more hMSCs could be delivered to the sub-endocardial portion of the myocardium) as compared to myocardial injection of the same number of cells, effectively targeting therapeutically relevant portions of the myocardium.

With better efficiency of seeding hMSCs onto biological sutures made of fibrin thread bundles, this method has a potential to be developed into an improved treatment modality for heart failure resulting from myocardial infarction for millions of patients worldwide.

Chapter 3: Hypothesis and Specific Aims

It was hypothesized that the Digilab's prototype cell printer can dispense human mesenchymal stem cells (hMSCs) that have viability comparable to manual pipetting and further that it can dispense cells suspension containing hMSCs onto fibrin microthread bundles in a manner that delivers the entire cell suspension onto the thread bundle to allow attachment of the cells (seeding) onto the thread bundles.

The hMSCs were dispensed using the cell printer or manually into wells of 96-well plates and incubated for 24 hours, stained for viability and examined microscopically. Viability in both groups was compared. The cell printer was used to deliver a small volume of concentrated cell suspension containing hMSCs onto fibrin microthread bundles. Cells were seeded onto fibrin thread bundles using the current method (tube rotator method) in parallel for comparison. The seeded bundles were incubated for 24 hours, stained with fluorescent dyes and examined microscopically. The number of cells seeded per unit length of thread bundle in both groups was determined and efficiency of cell seeding compared.

Specific Aim 1: Determine the viability of human Mesenchymal Stem Cells (hMSCs) after dispense ("post-printing") using the cell printer

For this specific aim, we hypothesized that the viability of hMSCs dispensed (or "printed") using the cell printer will be comparable to those dispensed manually using a pipette. In order to test this specific aim, we dispensed equal volume of hMSC suspension having a known cell concentration into wells of 96-well plates pre-filled with warmed cell culture medium, using either the prototype cell printer or a micropipette. Cells were incubated for 24 hours at 37°C, under atmospheric oxygen, 5% carbon dioxide and 85% relative humidity. Cell culture media was removed and cells were then stained with Live-Dead Viability/Cytotoxicity kit for mammalian cells (Invitrogen) and Hoechst 33342 dye (Invitrogen). The Hoechst dye stained nuclei of all cells, and was used to identify cells during image analysis using software (CellProfiler). The Live-Dead dyes stained the cytoplasm of viable cells and nuclei of damaged/dead cells. Every well of the 96-well plate into which hMSCs were dispensed and stained with the above dyes was visualized using an inverted fluorescent microscope with 3 filters: one for Hoechst dye (for nuclei of all cells), another for Calcein (stain for the cytoplasm of viable cells) and a third one for Ethidium Homodimer-1 (stain for the nuclei of dead or damaged cells). Images from the three filters for each region in the well were merged using Adobe Photoshop to generate a single image showing both live and dead cells. Multiple such images representing different regions of a well were stitched using Adobe Photoshop to generate a single image of the entire well showing all cells in that particular well. Images for all wells were obtained and processed similarly, and analyzed using software – CellProfiler, open source software from Broad Institute, Cambridge, MA, to obtain percentage of viable cells in each well. Mean viability of cells in all wells belonging to either group was used for comparison.

Specific Aim 2: Determine the ability of the cell printer to deliver cell suspension containing hMSCs onto linear scaffolds such as fibrin microthread bundles to seed the scaffold with the delivered cells

For this specific aim, we hypothesized that the cell printer will be able to dispense cell suspension containing a known concentration of hMSCs onto fibrin microthread bundles (one bundle at a time) in a manner that allows attachment of the cells to the bundle. The efficiency of cell seeding (the number of cells that attach onto the bundle divided by the total number of cells used for seeding that bundle) was compared to the efficiency of seeding obtained on a bundle seeded in parallel using the current method of seeding (tube rotator method) to gauge the preliminary effectiveness of the method. To test this, a bioreactor assembly was designed to anchor fibrin thread bundles into position inside a sterile 6-well plate (one thread bundle per assembly per well), which was then mounted onto the cell printer. A print program was written on the software controlling the cell printer, to dispense ("print") cell suspension onto a pre-wet thread bundle held in place in the 6-well plate so as to distribute the suspension evenly on the bundle. The thread bundle on the assembly was incubated for 20 minutes (without adding culture media) at 37°C under atmospheric oxygen, 5% carbon dioxide and 85% relative humidity, to allow initial cellular attachment while minimizing cell dehydration due to drying. The bundle was then transferred into a pre-sterilized polyethylene tubing bioreactor assembly (similar to the one used in the tube rotator method), and 100 μL of culture medium was added. The bioreactor polyethylene tubing bioreactor assembly was then mounted onto the tube rotator and incubated for 24 hours under atmospheric oxygen, 5% carbon dioxide and 85% relative humidity.

For comparison, fibrin thread bundles of the same length and diameter were seeded in parallel using the current tube-rotator method (using cell suspension obtained from the same cell culture flask as for the cell printer group) and incubated for 24 hours under the same conditions. To quantify cell seeding, seeded thread bundles from both groups were fixed and stained with Phalloidin (dye for Actin cytoskeletal fibers present in the cytoplasm) and Ethidium Homodimer-1 (dye for nucleic acids which is taken up strongly by nuclei of cells) after 24 hours. Each thread bundle was examined using confocal microscopy to visualize cells seeded on one side (half of the circumference) of the bundle from end to end. For this, the seeded bundles were visualized on the confocal microscope in partly overlapping segments from one end of each bundle to the other and a maximum projection of each segment was generated. Maximum projections for all segments were then stitched together using Adobe Photoshop to generate the image of one side (half the circumference) of the entire length of that thread bundle. Number of cells visible on one half of each thread bundle were counted manually and normalized to the length of that bundle. To calculate the total number of cells seeded, the number of cells counted on one side of the thread was multiplied by two, under the assumption that cells seed evenly on all sides of the circumference. Seeding efficiency for each thread bundle was calculated by dividing the total number of cells attached to the bundle by the total number of cells used to seed the bundle, normalized to the length of the bundle. Mean seeding efficiency in both groups was compared.

Chapter 4: Materials and Methods

In this chapter, materials used and protocols followed to accomplish the specific aims are presented. Components and functioning of Digilab's prototype cell printer are described along with its basic functioning. Evaluation of effect of dispensing ('printing') process on the viability of cells is also described. Fibrin microthread production and bundling is detailed along with the current method used to seed the thread bundles with hMSCs (tube-rotator method).Next, the bioreactor assembly developed for this project in order to position the fibrin thread bundles onto the cell printer to allow the printer to dispense cell suspension onto the bundles, and the protocol followed during the cell seeding process, is explained. Thereafter, the cell counting method, calculations of seeding efficiency and comparison made are presented.

4.1: Digilab's Prototype Cell Printer

The prototype cell printer (Digilab, Inc., Holliston, MA) (Figure 3) (referred to as 'cell printer' hereinafter) is an automated liquid handling device. It has two main functional components: Digilab's proprietary automated liquid handling technology - synQUAD, and a high-precision motion control robot. The synQUAD technology allows the user to control the volume of liquid aspirated or dispensed, while the motion control robot (X, Y, Z stage) allows the user to specify patterns in 3D in which the liquid is to be dispensed. Different combination of parameters such as dispense speed, inter-droplet pitch, droplet volume, XYZ stage speed, etc. yield different patterns. The cell printer can print on any substrate that can be accommodated on the printer's deck. To use the printer to dispense cells, a sterile environment is essential. For this reason, the cell printer is housed inside a biosafety cabinet.

Head with Y, Z-motion, dispense tips and reservoir for aspirated cells

synQUAD Pumps

Deck with X-motion, plate holders, wash & vacuum station
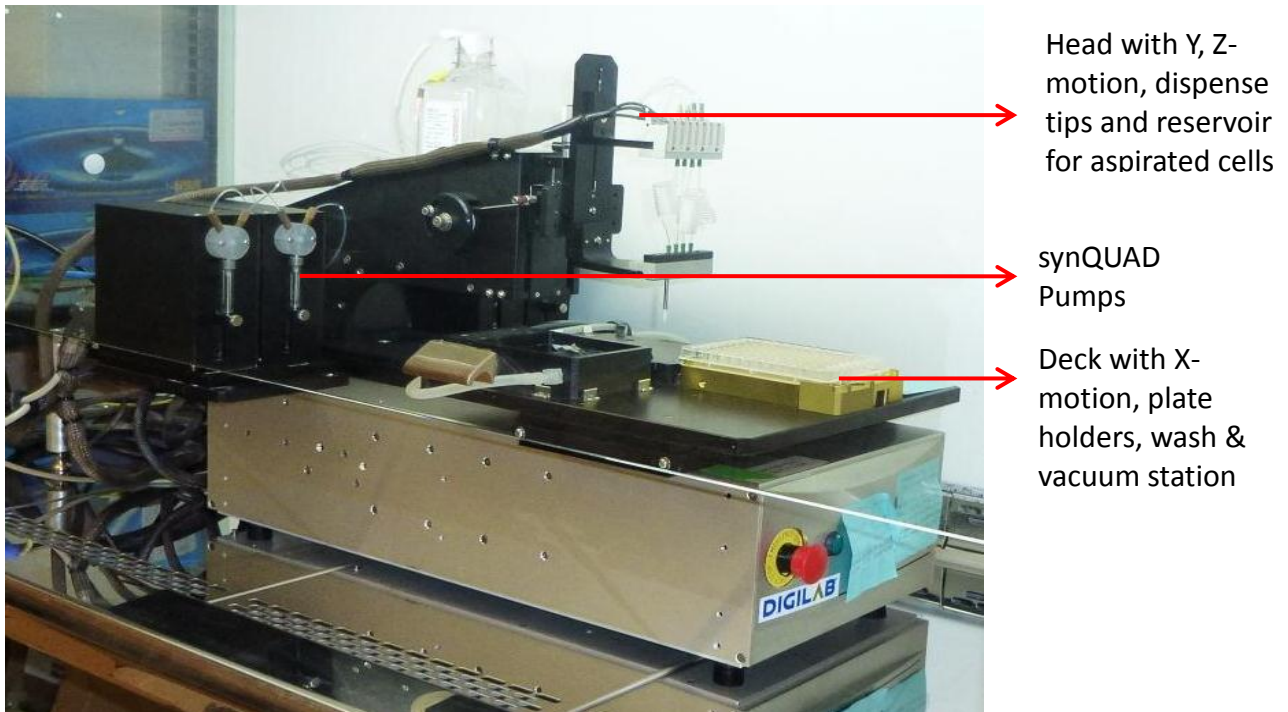
Figure 3: Digilab's prototype cell printer housed inside a biosafety cabinet
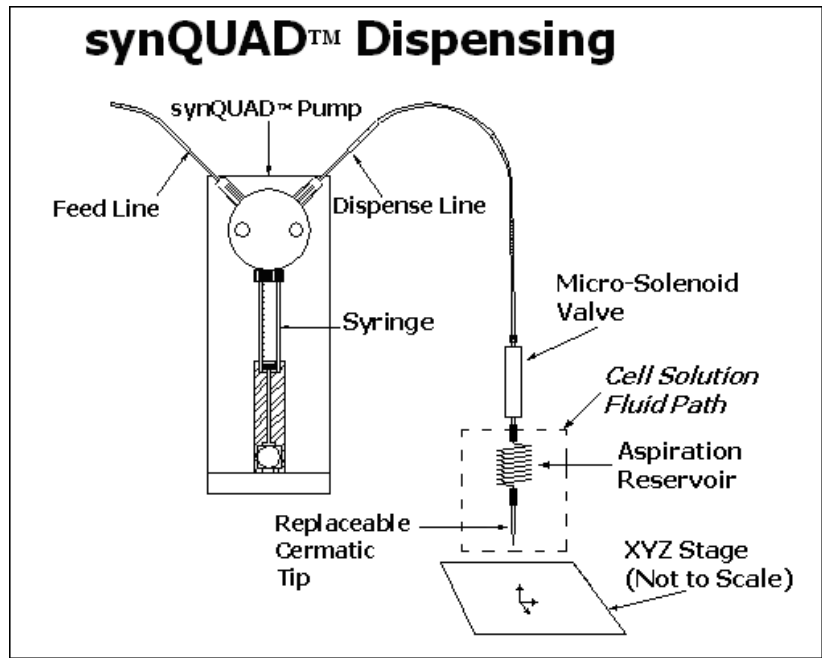
Figure 5: Schematic describing basics of synQUAD dispensing (courtesy Digilab, Inc.)
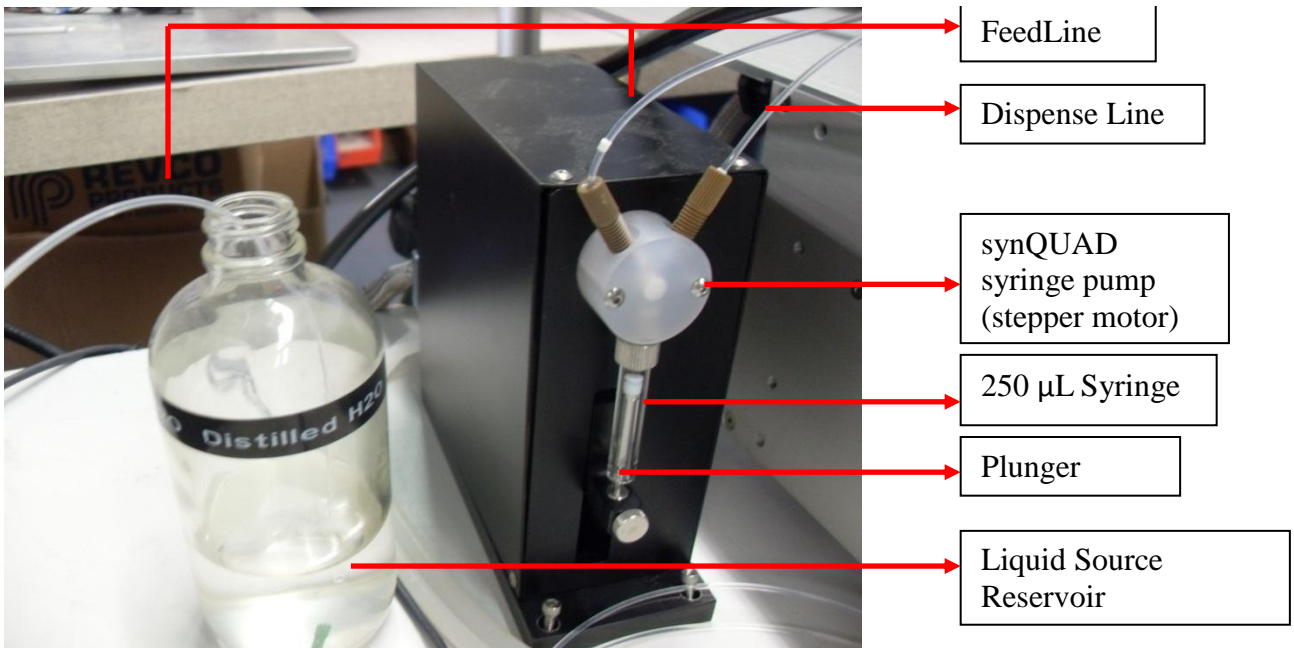
Figure 4: SynQUAD pump (courtesy Digilab, Inc.)

4.1.1: SynQUAD Technology:

SynQUAD technology was developed to dispense droplets of minute volumes ranging from a few nanoliters to a few microliters per droplet (typically 50 nL to 4 µL). The technology is a combination of a stepper-motor powered motorized syringe pump and a high-frequency microsolenoid valve that are controlled synchronously by a computer.

When the cell printer is first installed, each synQUAD pump on the printer is connected to a reservoir of buffer liquid such as sterile phosphate-buffered saline (PBS) at one end and the solenoid valve (and liquid path distal therefrom) mounted on the dispense head at the other end, via a system of sterile transparent plastic tubing which is filled with the buffer solution. This forms an air-tight column of the buffer solution in the tubing with the motorized syringe pump of the synQUAD situated in the path of the liquid column. (Figure 5, Figure 4). When the stepper motor on the pump moves the plunger of the glass syringe, it creates a pressure inside this closed system of tubing which drives the liquid inside this system of tubing. The direction in which the column of liquid moves is determined by a 3-way valve situated in between the feed line, the dispense line and the syringe (Figure 5).

A high-frequency microsolenoid valve is placed in the path of the liquid at the dispensing end of the system of tubing on the dispense head. The valve is closed by default. When the syringe pump drives the liquid towards the dispense head, the liquid encounters the closed microsolenoid valve. The liquid is ejected from the dispense head only if the valve opens. The frequency of opening and total open time of this valve determines how much volume of liquid gets dispensed. A dispensing tip made of ceramic is fitted distal to the microsolenoid valve on the dispense head and forms the very end of the path of the column of liquid, before it is ejected. This tip has a narrow orifice which helps dispense liquid with high positional precision on to the printer's deck. The position at which the liquid is dispensed is determined by X, Y, and Z co-ordinates specified by the user (Figure 5).

The syringe pump pushes the plunger into the syringe displacing the column of liquid inside the system of tubing. However, because the microsolenoid valve is closed by default and opens only when voltage is applied to it, the pressure builds up in this column of liquid inside the closed system of tubing. At this point, the microsolenoid valve opens momentarily for a very short duration typically lasting a few hundred microseconds, which allows a very small volume of this pressurized liquid to escape at high velocity through the dispense tip in the form of a droplet. The volume of the droplet depends on the displacement of the plunger affected by the motorized syringe pump and the duration of opening of the microsolenoid valve, both of which are controlled by a Windows PC-based proprietary software – AxSys. The X, Y and Z position of the dispense head relative to the printer's deck and the speed and acceleration of movement of the dispense head are also controlled by AxSys software.

4.1.2: AxSys Software and Programming the Cell Printer

Digilab's cell printer is controlled by a Windows XP PC based software named **AxSys**. The computer connects to the cell printer via serial two serial cables that relay commands to the synQUAD pumps and the X, Y, Z motion-controlling motors on the printer. It is the only means through which the cell printer can be accessed and used; there are no on-board motion controls or dispense/aspirate buttons on the cell printer itself.

The AxSys software is structured like a high-level computer programming language. It consists of a set of basic commands that the cell printer can execute. Each command is depicted graphically and has parameters that the users need to specify. A 'print-program' consists of a group of such commands specified by the user in sequential logical order as per the function the user wants the cell printer to carry out. When this print program is executed or 'Run', the AxSys relays each of these commands to the cell printer in sequential order, starting from the first one (at the top of the list)going through subsequent commands until it reaches the end of the commands (at the bottom of the list) or encounters an error. Constructing a print program on AxSys, or 'Programming', involves adjusting the parameters within individual commands within a pre-specified allowable range, with the parameter adjusted and the range differing from command to command. Due to the inherent complexity with the number of possible combinations, a considerably steep learning curve is associated with the AxSys software. Once mastered, however, it allows for tremendous flexibility in the patterns that can be printed using cell suspension in media or hydrogel, or only hydrogel, on a flat surface as well as in 3D. (Figure 6)

Figure 6: Programmed patterns printed by the cell printer inside wells of a 6-well plate using 1% Sodium Alginate. Top row: left to right: 2 wells with vertical parallel lines, 3rd well with horizontal parallel lines. Bottom row: left to right: square with diagonals, the letters WPI, 3 concentric circles.

4.1.2.1: Detailed description of the AxSys software

The Graphic User Interface (GUI) of the AxSys software upon launch is shown below. (Figure 7)
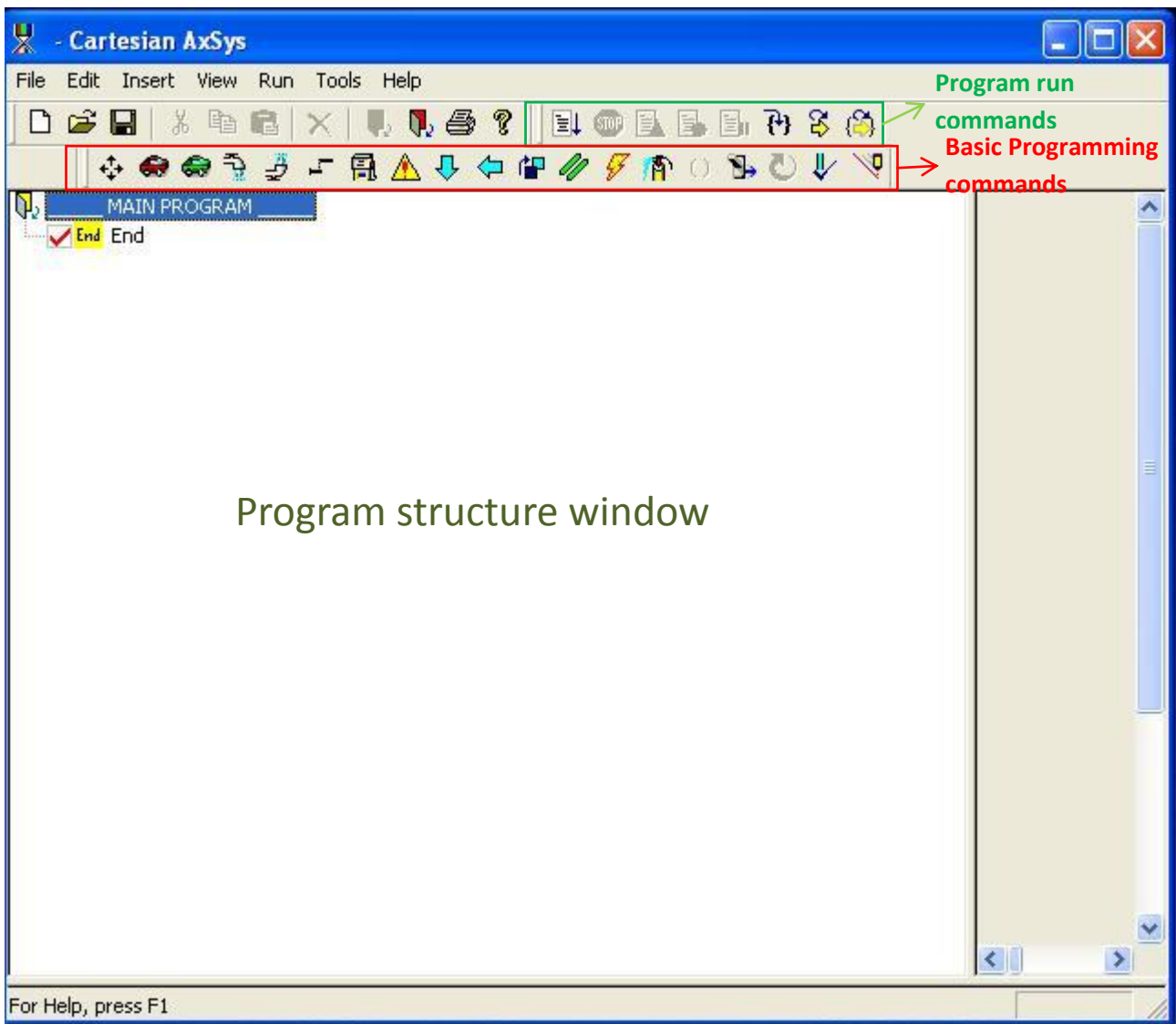
Figure 7: The AxSys Graphic User Interface (GUI) when the program is launched. The AxSys GUI consists of some features that are typical to most windows interfaces – menus such as 'File, Edit, View, Help' while the rest are specific – 'Insert, Run, Tools'. The toolbar across the top contains the commands that the user can give to the cell printer in the form of a 'print program'. A typical print program consists of a sequence of basic commands (boxed in red) that are executed from the top to the bottom when the program is run. The commands comprising the current program are listed in the 'program window' (boxed in olive green) which is empty in this image.

A brief descriptions of most commonly used commands follow in Figure 8, Figure 9, Figure 10, Figure 11, Figure 12, Figure 13, Figure 14, and Figure 15.
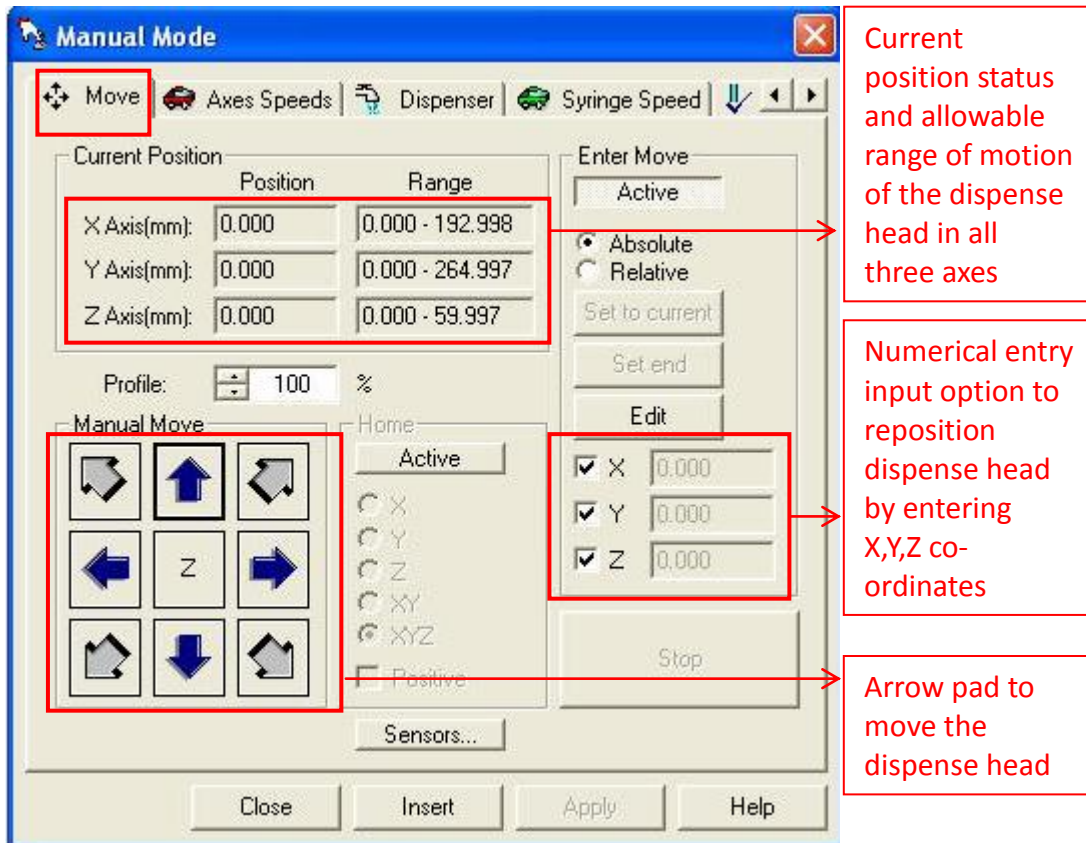
Figure 8: The 'Move' Command in AxSys. The move command repositions the dispense head of the cell printer to any position on the deck of the printer. Changing the X position (either by numerical entry or by pressing either left or right arrows) causes the dispense head to move left to right (or right to left) with respect to the deck. Similarly, changing the Y position causes the head to move forward or backwards with respect to the deck, and changing the Z position causes the head to move up or down (away-from or closer-to respectively, to the deck).

The default position when the printer is initialized is the called 'Home' which is assigned the co-ordinates 0, 0, and 0 in the X, Y and Z axes, and which corresponds to the dispense head being stationed at the left-lower corner of the deck in the X, Y axes and all the way to the top (furthest away from the deck) in the Z axis. Any movement of the dispense head is with respect to this home position. Movements occur in increments of 1 μm (0.001 mm) in all three axes.

Plate-holders and a wash-waste-vacuum station are positioned at definite sites on the printer's deck. In order to move the dispense head between these stations, nearly all print programs require the use of the 'Move' command multiple times in a program.

29
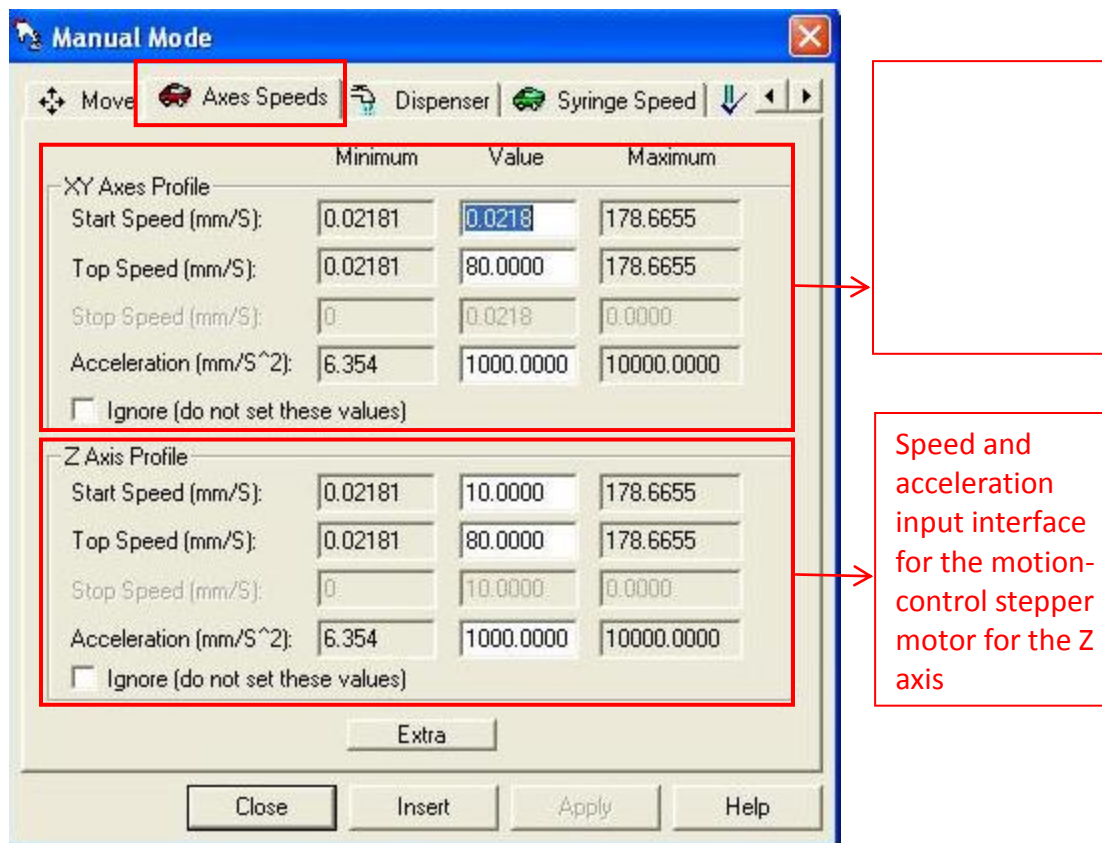
Figure 9: The 'Axes Speeds' command in AxSys. The speed and acceleration with which the head gets repositioned with the 'Move' command each time can be changed by using the 'Axes Speeds' command.

High-resolution stepper-motors control the motion of the dispense head with respect to the deck in all three axes; each axis has a dedicated stepper-motor. When the cell printer is initialized, these stepper-motors are engaged and hold the dispense head in position actively.

The default maximum speed and acceleration of the motors controlling all three axes is set to 80 mm/sec and 1000 mm/sec^2 respectively. It has been observed empirically that these settings work well for moving the dispense head from station to station. However, for dispensing cell suspension or other liquids in certain fine patterns, a lower speed and acceleration of movement of the dispense head is often required. This can be done by inserting the 'Axes speeds' command in the program window prior to a 'Move' command in which the delicate motion is required, and adjusting the speed and acceleration of all three axes as need be. When such fine motion is no longer required, another 'Axes speeds' command may be inserted at that stage in the program, to set the speed and acceleration to a higher number to suit head mobility in between stations or whatever else is required.

For example, the XY axes speed setting used for the 'Line dispense' command to gently dispense cell suspension containing hMSCs onto fibrin thread bundles was a maximum speed of 5 mm/sec and an acceleration of 10 mm/sec^2.
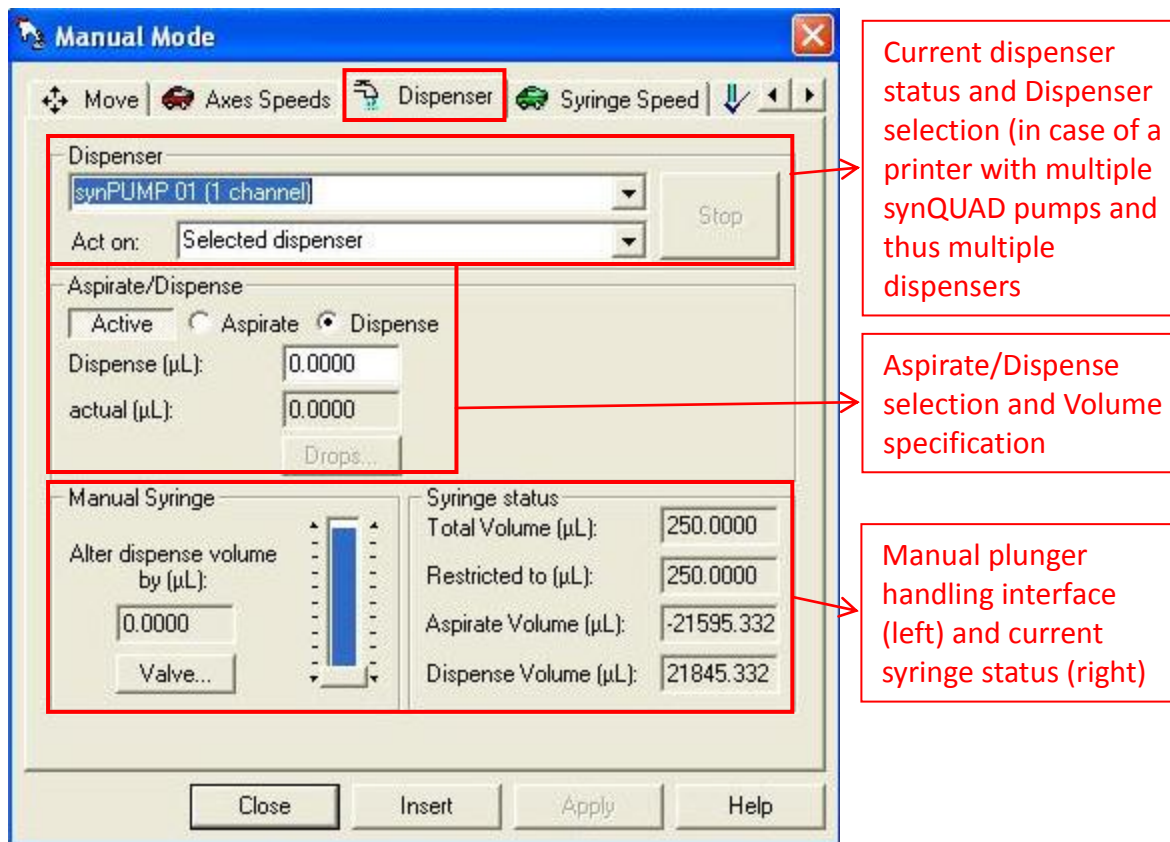
Figure 10: The 'Dispenser' command in AxSys. This command is used for instructing the synQUAD pump(s) on the cell printer to aspirate or dispense liquid (cell suspension or media) via the dispensing tip (shown in Figure 5andFigure 4).

The cell printer may have anywhere from 1 up to 8 synQUAD pumps mounted on a single unit, and thus 1 to 8 distinct aspirating and dispensing channels. All channels have one solenoid valves and one dispensing ceramic tip per channel, in addition to one synQUAD pump per channel. All the channels are mounted on to the head one which they separated by a distance of 9 mm. Because the tips are mounted along the X-direction on the head, the X co-ordinate that would position the dispensing tip at the target location would differ for each channel. Because of this, planning ahead which channel is to be used to aspirate or dispense would be vital to in programming the 'Move' commands. This is done through the 'Dispenser' command. The prototype used in this project has 4 channels; only 1 of them was used for most experiments.

Additionally, using this command, the user can specify whether to aspirate or dispense and how much volume to aspirate or dispense (within the allowable range – zero to 250 µL) using a particular channel. The manner in which the volume is to be aspirated or dispensed (in terms of number of droplets and volume of each droplet) also can be specified. E.g. if 100 µL of volume of a liquid needs to be dispensed, it can be done in 100 droplets of 1 µL or 1000 droplets of 0.1 µL (or 100 nL) or similar such combinations. Depending upon the task at hand, the right combination of channel number, aspirate/dispense and droplet size is selected. For mechanism of dispensing, see Figure 5, and Figure 4.
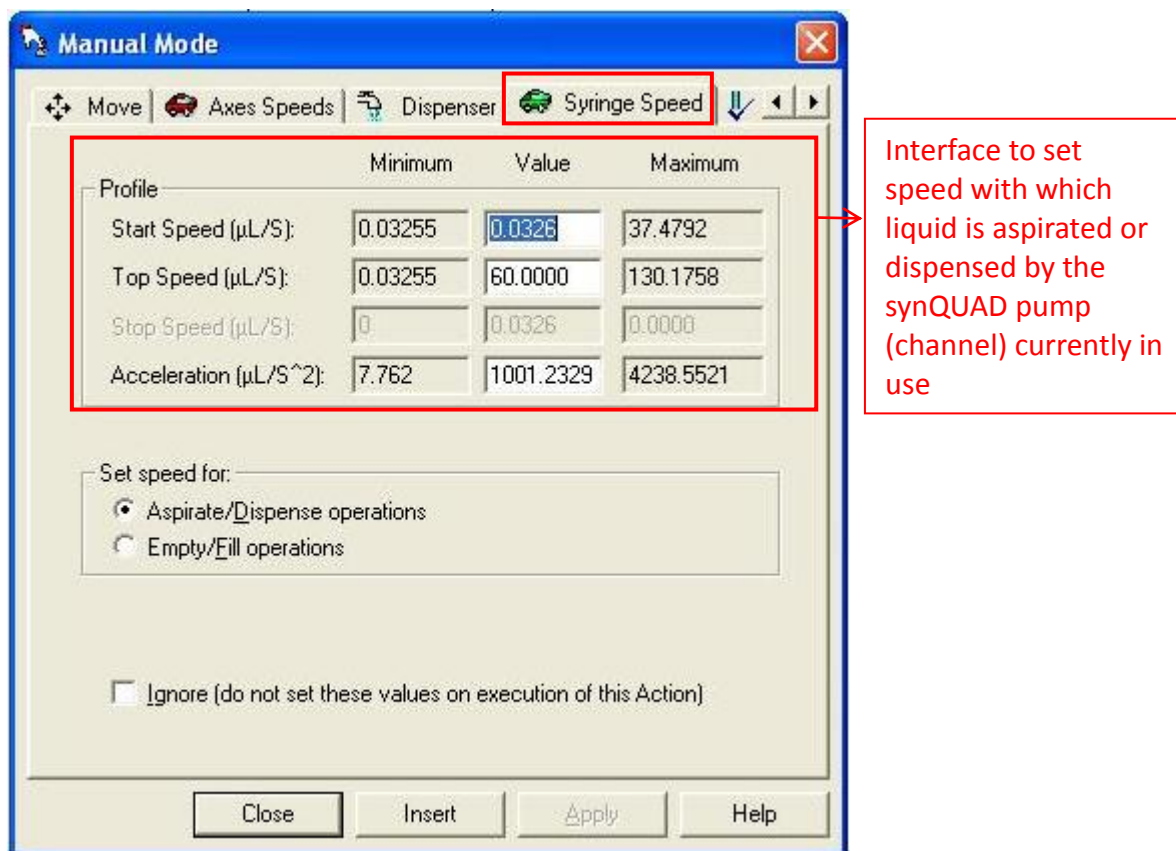
Figure 11: The 'Syringe Speed' command in AxSys. This command is used to adjust the velocity of flow of liquid dispensed or aspirated through a channel. It is necessary to alter the flow velocity according to the type of liquid being dispensed and the type of aspirate/dispense function being performed.

For gentle handling of cells in suspension, dispensing or aspirating flow velocities must be kept relatively low. This is to prevent damage to the cells that would occur due to shear stresses caused at high flow velocities through the narrow orifice of the dispensing tip. (Dispensing tip diameters can be 100, 150, 250, 350, or 500 μm. The diameter of the tip is selected based on the application for which use of the cell printer is contemplated). For aspirating and dispensing cell suspensions, a top speed in the range of 5 to 20 μL/sec is recommended (Product manual – Digilab, Inc.).

At the other end of the spectrum, high flow velocities are required when the channels are being cleaned such as during synQUAD pump priming steps (see Figure 12). To eject any debris that may be lingering in the channel-in-use from previous programs or current use, the flow velocity is set to a high speed (between 60 to 100 μL/sec) and the 'Prime' command is called which flushes the channel at the set high velocity. High flow velocities are also used for bulk dispensing of liquids not containing cells such as reagents or cell culture media.

Whenever a change in the flow velocity is required in a particular channel, this command is inserted in the print program just prior to the 'Dispenser' command (dispense/aspirate step) or 'Prime' command for which that flow velocity is needed.
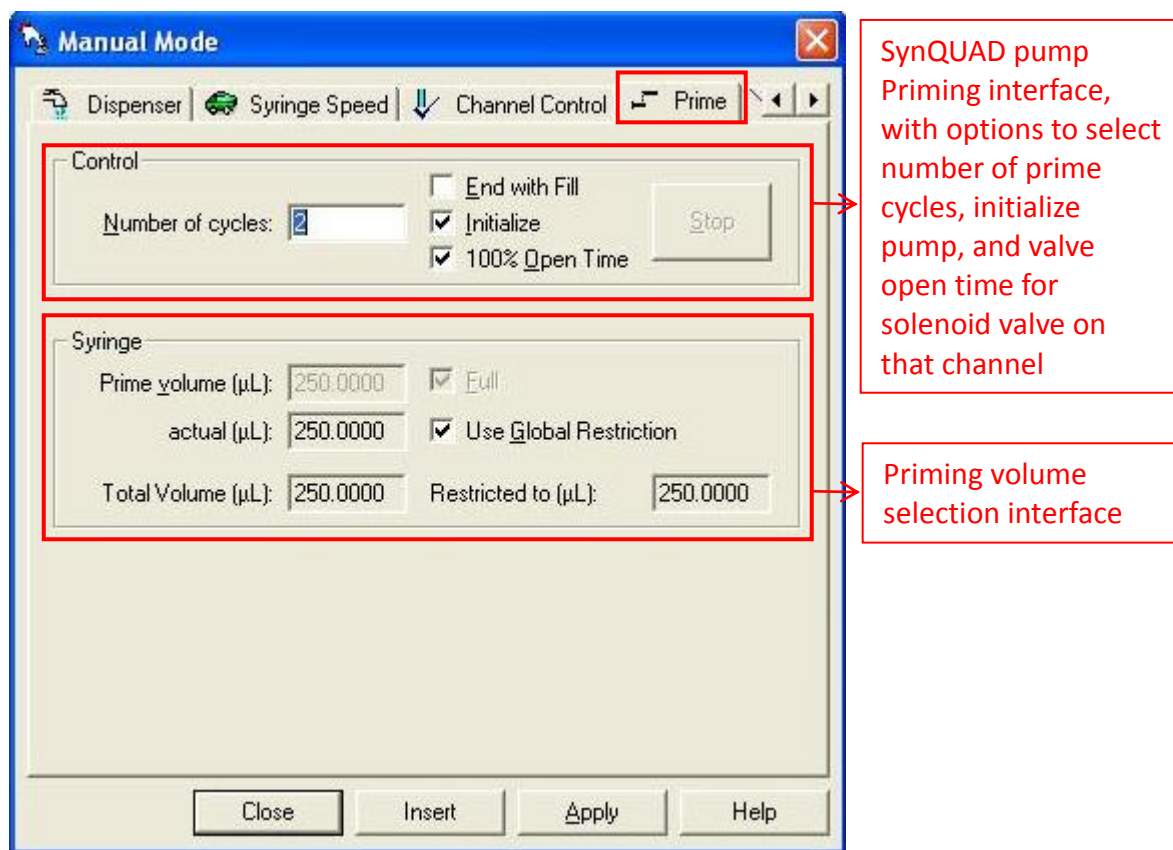
Figure 12: The 'Prime' command in AxSys. This command is used to 'prime' a synQUAD pump selected using the 'Dispenser' command. The process of priming a synQUAD pump begins with 'initializing' the pump (unless otherwise specified by the user) which realigns and engages the stepper-motor driving the plunger. The motor then repositions the plunger to its default position, pushing it all the way into the glass syringe emptying out any sterile buffer solution contained in the syringe back into the reservoir. This is followed by rapid drawing (aspirating) of 250 μL of buffer solution from the reservoir, filling up the glass syringe to capacity, followed by rapid emptying of the same volume through the dispense tip. This process is generally done at a high flow velocity. As a result, the entire channel gets flushed removing any debris or air bubbles within it.

A priming step is usually done at the beginning and end of each program, repeated twice or more at each instance generally. All synQUAD pumps used in a particular program are primed. The priming step at the start is essential to initialize the synQUAD pumps before they can be used for aspirate or dispense functions. It also gets rid of any waste within the channels that may be left over from previous use. A priming step at the end cleans the channels of any waste or residual liquid not dispensed during the program run.

During the dispensing phase of a prime cycle wherein liquid is ejected out through the dispense tip, because of the high flow velocity of the liquid dispensed and the narrow tip orifice, the liquid jets out in a straight stream pointing vertically downwards. This 'straightness' of this stream is a useful gauge of how clean the dispense tip is. If there is dust or other type of blockage inside tip, the liquid jets out at an angle, or sprays out in multiple streams, or doesn't come out at all, depending upon the degree and type of blockage. The tip is cleaned or replaced in such a situation.

33
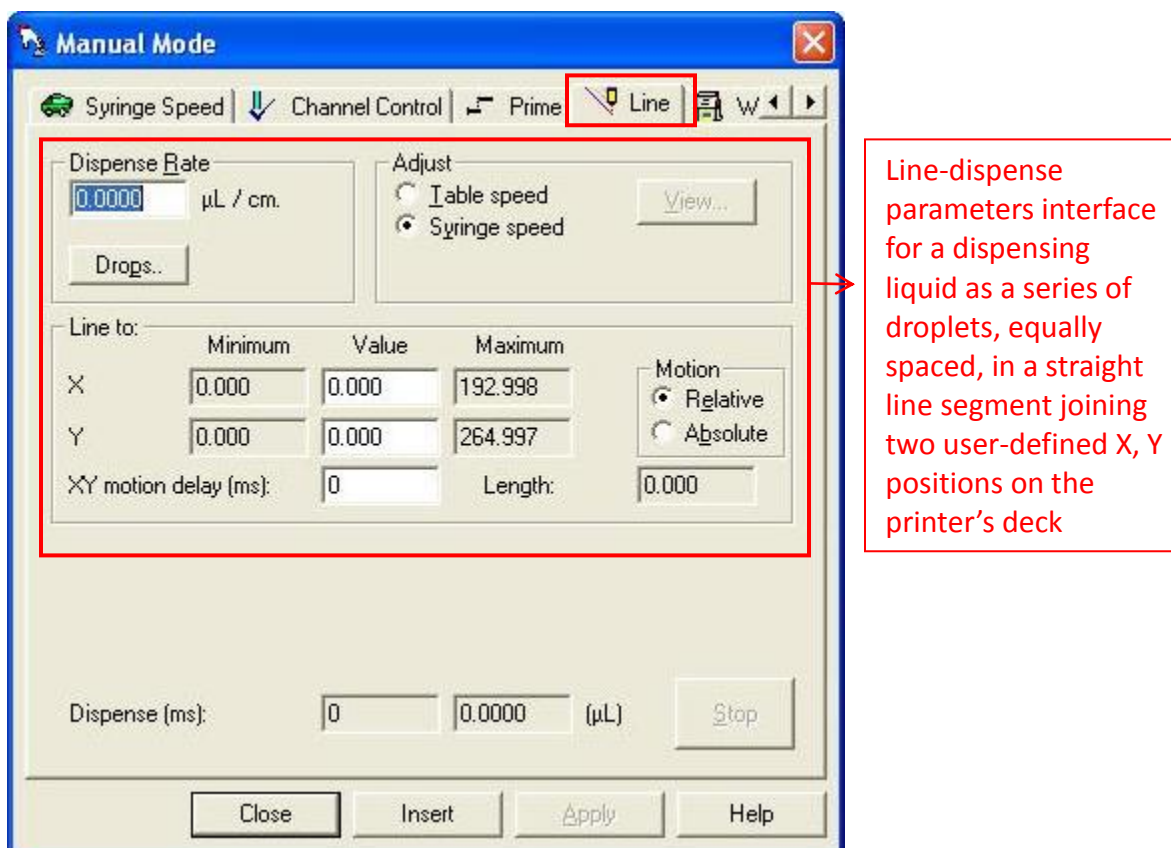
Figure 13: The 'Line' command in AxSys. The 'Line' command, also known as the 'Line Dispense' command, is used for dispensing a series of droplets of equal volume, equally spaced, along a straight line. This is a separate command, distinct from the 'Dispense' command, in that the dispensing action and the movement of the dispense head with respect to the deck occur simultaneously when this command is executed by the cell printer. In the 'Dispense' command, only dispensing (or aspirating) function is performed; the dispense head cannot be moved simultaneously.

The 'Line' command takes inputs of the volume is to be dispensed per unit length (per centimeter), the inter-droplet pitch (the distance between two consecutive droplets), the volume of each droplet, and the X, Y co-ordinates of the start and end point of the line-segment. These parameters are set according to the pattern desired. For example, for a straight continuous line, the inter-droplet is kept less than the expected drop diameter on the print surface so that adjacent droplets fuse to form a single line. For an array of droplets equally spaced, inter-droplet distance is kept much larger than the drop diameter so that individual droplets remain comfortably spaced and do not touch each other.

This command is very useful for rapidly dispensing small volumes at regularly spaced intervals such as into wells of microtitre plate – a 96, 384 or 1536-well plate or other similar targets. This command was used in this project for dispensing hMSC suspension onto fibrin microthread bundles, along the length of each bundle evenly distributing the suspension for uniform cell seeding.
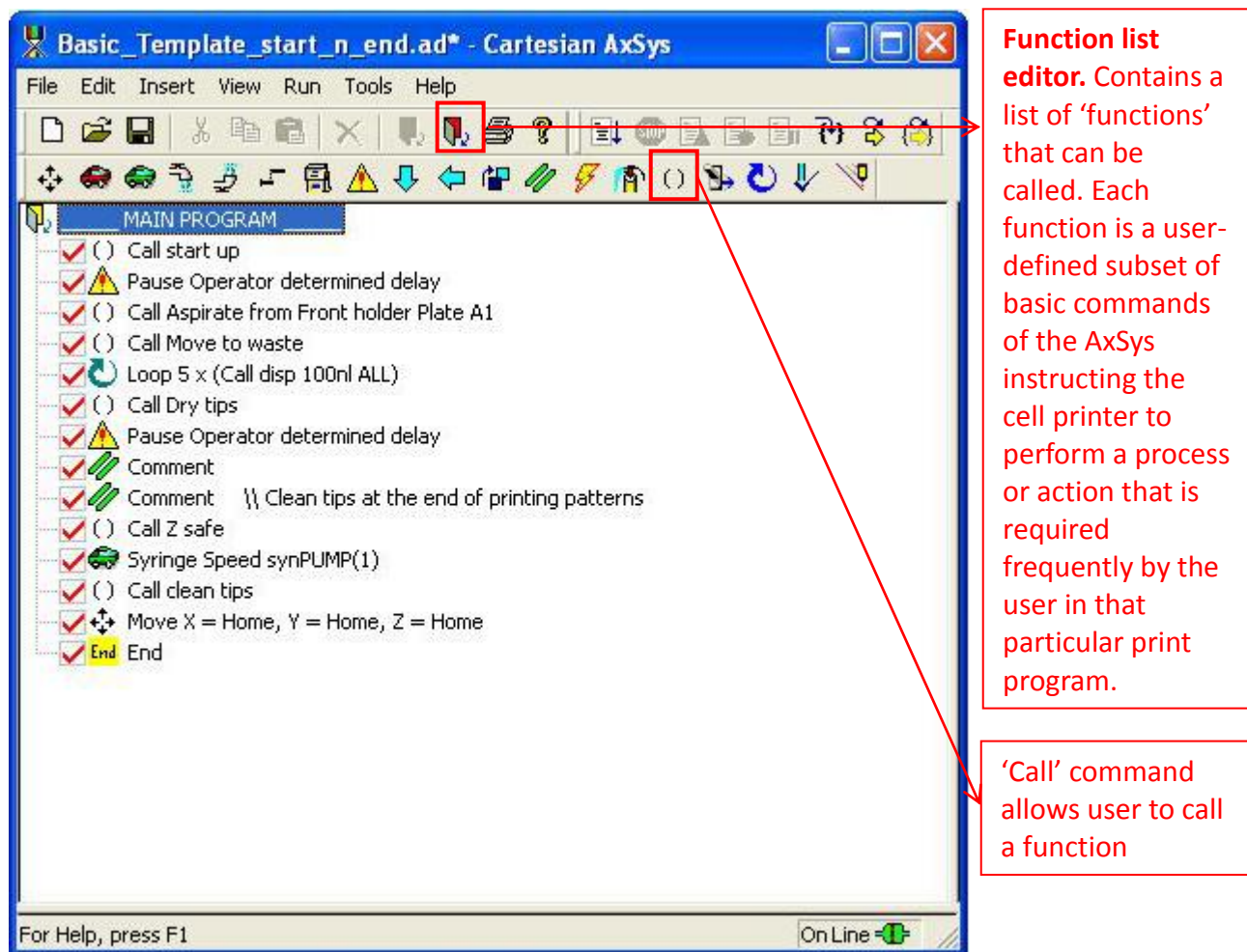
Figure 14: The concept of a 'Function' and the 'Function list editor' in the AxSys. The image above shows a sample program written in the AxSys. The icon towards the top boxed in red represents the 'Function list editor'. AxSys allows the user to store a set of commands representing an action that is used repeatedly or has special importance in the print program, to be stored as a sub-program called a 'Function'. Each function must be assigned a unique name by the user. All such 'functions' created by the user are listed in the 'Function list editor' and may be 'called' at any point in the print program using the 'Call' command (icon with ( ) boxed in red on the top-right). Using the 'Function list editor', new functions can be created, and exiting ones modified or deleted.

All functions created by the user are stored in a library assigned to that particular print program. Each time the program is loaded from computer memory, the library of functions associated with it is loaded automatically. This list is accessed using the 'Function list editor'. Each print program has a unique function library.

In the print program depicted in the image above, the functions called using the 'Call' command include 'start up', 'Aspirate from front holder plate A1', 'Move to waste', 'Dry tips', and 'Z-safe'. Functions are usually named meaningfully, with the name specifying what action it represents and distinguishing it from other similar actions. One or more functions can be called within a function, which in turn can call several functions within them. Such nesting of functions allows the user to create complex print programs in an organized manner and navigate through them with ease.

35
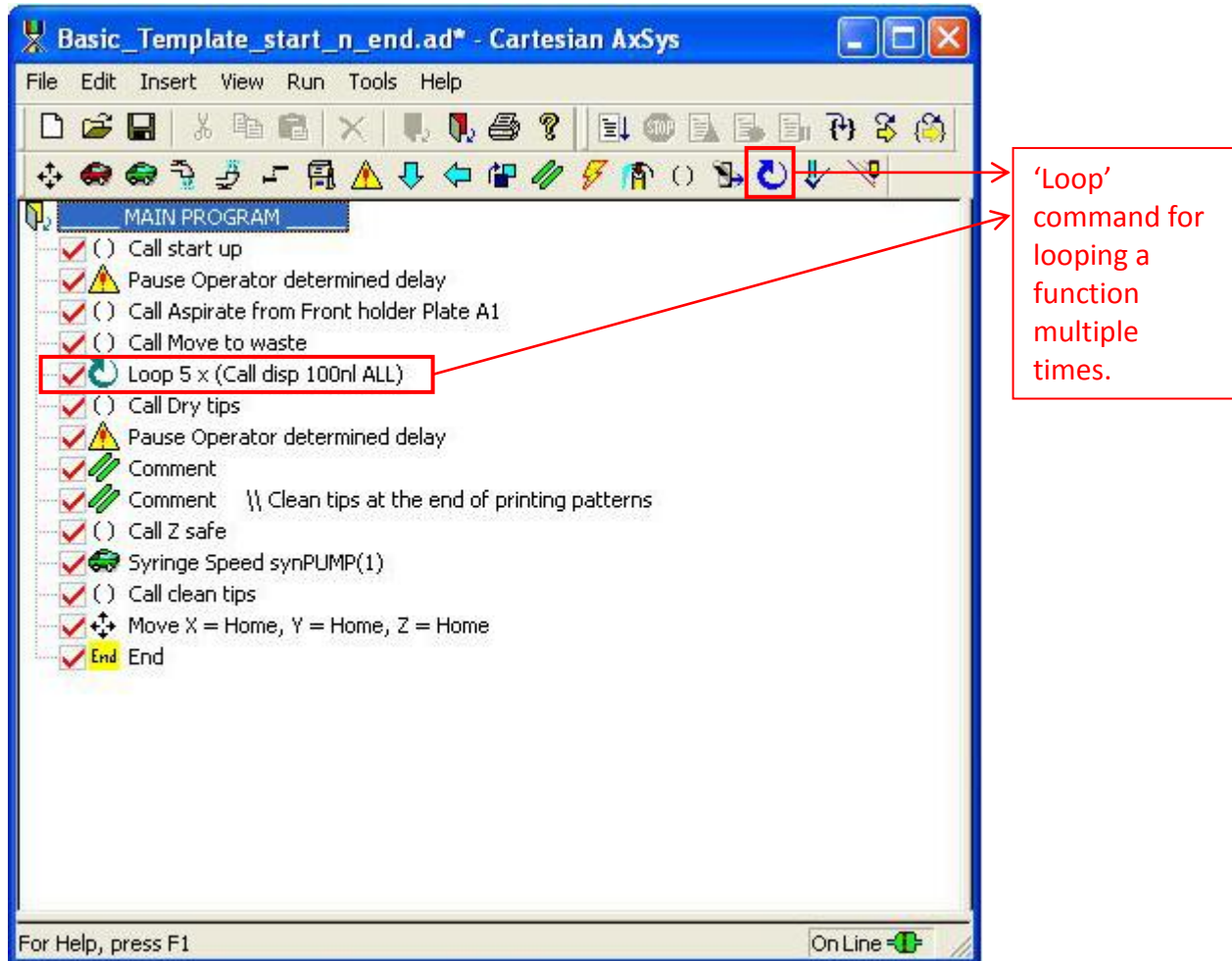
Figure 15: The 'Loop' command in AxSys. The icon boxed in red with a circular arrow pointing at its own tail represents the 'Loop' command. When a function needs to be called repeatedly at one stage in the print program, the 'Loop' command allows the user to loop a function over and over again up to a user-specified number of times, instead of having to use the 'Call' command repeatedly. Along with the nesting feature available in the 'Call' command and the concept of a 'Function' in AxSys, the 'Loop' command is a very powerful feature in the software that allows the user the flexibility to construct fairly complex print programs.

'Wash-pump' and 'Vacuum-pump' commands in AxSys: In addition to the commands described in the figures above, these two commands are also used frequently, but are relatively simple and do not merit detailed description. The 'Wash-pump' command is used to switch on or off a peristaltic pump that circulates a washing or cleansing liquid through wash and waste stations on the printer's deck. At the end of a print program, the dispense tips are wiggled in running flow of a cleansing liquid circulated through the wash station by switching on the wash pump. This cleanses them of any residual active reagents that may be clinging onto them.

The 'Vacuum-pump' command is used to switch on or off the suction pump that connects to the vacuum station on the printer deck. The vacuum station is a hollow closed cuboidal box connected to the suction pump, with holes on its top surface that are just large enough to accommodate the dispense tips. To dry dispense tips from the outside, the dispense head is moved over to the vacuum station and the dispense tips lowered into the station through these holes. The suction pump is switched on momentarily to introduce a negative air pressure around the tips. Any liquid clinging onto the outside of the tips gets sucked into the vacuum station leaving the tips clean.

Residual droplet(s) from wash step or a previous aspirate-dispense action may remain clinging on the outside of a dispense tip near its orifice. In this case, when droplets of minute volume are dispense through that tip, they may not eject cleanly off the tip due to surface tension and charge interactions between the dispensed droplets and the clinging residual droplet(s). The angle at which the droplets leave the tip may also change as a result of these interactions causing inaccurate deposition of droplets. To prevent this, cleaning the dispense tips from outside at the vacuum station is essential before actual dispense steps.

4.1.2.2: General Logical Sequence of a Print Program on the Cell Printer

At the beginning of every program, there are a few steps that need to be implemented for the cell printer to perform optimally:

- The motion control robots that move the head with respect to the printer's deck in all three axes need to be 'homed' i.e. moved to home position. This is because all movements of the printer's head are relative to this home position. Hence, it is vital for the printer's motion control system to identify the home position and remember it before each run.
- The synQUAD pumps that are going to be used in the particular program must be primed after the homing. Priming the pumps 'initializes' them, which is essential before any aspirate or dispense commands can be executed by the pumps, in addition to flushing the channels and the tips of any residual liquids / debris from previous program runs.
- The ceramic tips need to be vacuum dried after the pumps are primed in order to remove any buffer solution that is clinging to the outside of the tip.

After the initial steps, there is generally an aspirate step, wherein the head is moved to a source of the liquid that needs to be dispensed, which in this project for the most part was either cell suspension or cell culture media. The source can be either a handheld source, such as an Eppendorf tube containing cell suspension, or a mounted source, such as a 96-well plate mounted on the deck of the cell printer, with one of the wells filled with the cell suspension. In either case, the head is moved to the source, the tip(s) lowered into the source, followed by multiple aspirate-dispense loops that perform a triturating action re-suspending any cells that may have settled inside the source vial/tube/well. After mixing the cell suspension to uniformly re-suspend the cells, the cell suspension (or media) is aspirated into the coil of tubing above the ceramic tip. (Aspiration reservoir in Figure 5). The tip(s) is/are then raised to a safe height such that they would clear all structures mounted on the printer's deck when the head is moved around.

The aspirated cell suspension (or media) is then deposited onto a target that varies considerably from program to program.

For the cell viability studies performed in this project (described next), human mesenchymal stem cell suspension was aspirated from a well of 96-well plate mounted on the deck and was dispensed into wells of another 96-well plate mounted on the deck.

For seeding fibrin thread bundles with human mesenchymal stem cells, cell suspension was aspirated from a hand-held source (an Eppendorf tube containing cell suspension), and dispensed over the fibrin thread bundles so as to evenly distribute the suspension along the available length of seeding of the bundle.

Similarly, cells are deposited onto various targets depending upon the application for which the cell printer is being used.

4.1.2.3: Steps of Programming the Cell Printer on the AxSys
The concept of programming on AxSys is similar to that in a higher level computer programming language, except that instead of typing logical commands, the commands in AxSys are graphical with both quantitative and qualitative inputs to adjust parameters in each command.

A print program consists of a series of commands written by the user in logical sequence. When executed the program is interpreted and run line by line by the AxSys software which constantly relays these commands to the cell printer, until it reaches the last line in the program or encounters an error.

In order to program successfully on the AxSys (write a program that makes the cell printer do exactly what the user has in mind), the user must first be familiar with each command in appropriate detail so as to know exactly what action that particular command will translate into on the cell printer.

Secondly, the larger picture of a particular program must be clear in the user's mind before s/he begins writing the program. This is because at every line in the program, each command is interpreted and executed by the cell printer in the context of the commands that have been already executed thus far into the program. Only when the user has a clear picture of the program in its entirety can s/he write the correct commands at every step in the program.

A sample program written in the AxSys is depicted in Figure 16. A description of the actions each line of the program would translate into, on the cell printer is given in the caption of the figure.
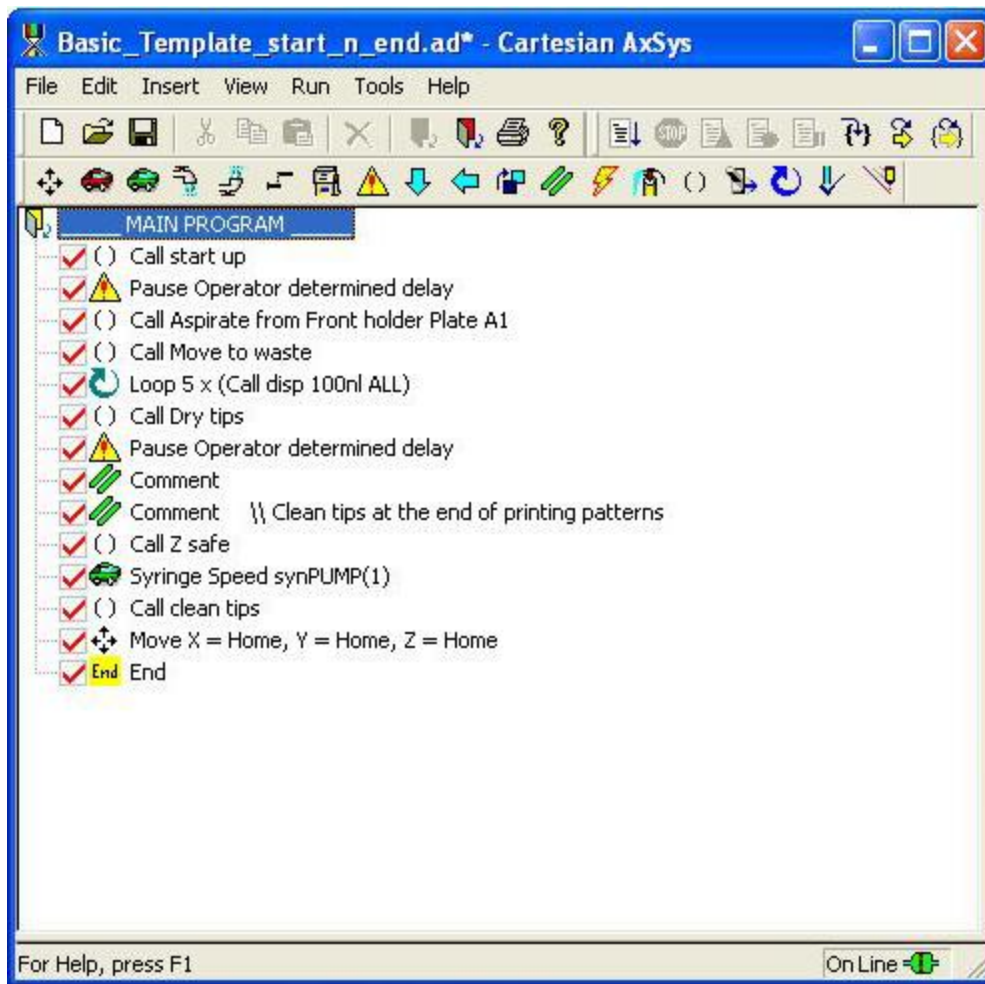
Figure 16: Sample program written on AxSys. This figure depicts the skeleton of a typical program written on the AxSys involving aspirating cells from one source and dispensing them to a destination.

- The first command is a 'Call' command, calling the function named 'start up', which has stored inside it a set of routine actions performed by the cell printer at the start of most programs run by this user (typically – homing the motion control robot in X, Y and Z axes, priming the synQUAD pumps and drying the ceramic tips after priming at the vacuum station).
- Next is a 'Pause' command that would prompt the operator (or user) to perform a check or take an action before proceeding.
- In the third line, 'Aspirate from Front holder A1' function is called, which has stored inside it a set of commands to move to address A1 in 96-well plate mounted in the front holder of the printer's deck and aspirate a required volume of liquid such as cell suspension from the well.
- The fourth line calls a function to move the dispense head to the waste station in order to prepare for the next step, wherein 100 nanoliter droplets of the aspirated liquid are dispensed 5 times (call function looped 5 times), in to the waste station.
- The sixth line calls a function that would move the tips to the vacuum station, lower them into the station, switch on the vacuum pump to dry the tips on the outside, and then raise the tips to a safe height. The steps that follow call functions to clean the tips at the end of the program and reposition the motion control robot to home in all three axes.

4.2: Post-printing Viability of Human Mesenchymal Stem Cells

Before using the cell printer to dispense hMSCs for any purpose, it was necessary to determine whether the printing process would affect the viability of the cells. Because the contemplated use of the cell printer was to dispense hMSCs onto fibrin thread bundles, the time point at which post-printing cell viability was determined was selected as 24 hours - the time period that the current cell seeding method takes to seed hMSCs onto fibrin thread bundles. In order to compare cell seeding efficiency of two methods at 24 hours, it was required to determine first whether the printing process affected cell viability as observed 24 hours post-printing.

For this, hMSCs were dispensed into wells of 96-well plates using either the cell printer or a hand-held micropipette (the current gold standard). After 24 hours of incubation at $37^{o}C$, under atmospheric oxygen, 5% carbon dioxide and 85% relative humidity, cells were stained with Live-Dead Viability/Cytotoxicity kit for mammalian cells (Invitrogen) and Hoechst 33342 dye (Invitrogen).

The Live-Dead Viability/Cytotoxicity kit for mammalian cells (Invitrogen) involves staining cells which are to be tested for viability with two dyes – Calcein AM and Ethidium Homodimer-1. Live cells are distinguished from dead or damaged ones by the presence of ubiquitous intracellular esterase activity, determined by the enzymatic conversion of the virtually non-fluorescent cell-permeant Calcein AM to the intensely fluorescent Calcein. The polyanionic dye Calcein is well retained within live cells, producing an intense uniform green fluorescence in the cytoplasm of live cells (excitation/emission ~495 nm/~515 nm).Ethidium Homodimer-1 only enters cells with damaged membranes and undergoes a40-fold enhancement of fluorescence upon binding to nucleic acids, thereby producing a bright red fluorescence in dead cells (excitation/emission ~495 nm/~635 nm). Ethidium Homodimer-1 is excluded by the intact plasma membrane of live cells. (Product data sheet from Molecular Probes, Invitrogen, Carlsbad, CA).

Even though the Live-Dead viability kit was sufficient to distinguish between live and dead cells, hMSCs were additionally stained with Hoechst 33342 dye (excitation/emission ~350 nm/~461 nm) which stains double stranded DNA present in the nucleus. This was done for the purpose of facilitating software-based image analysis, which requires that the nuclei of all cells in the image to be analyzed be stained and clearly defined, for accurate count results. Calcein AM in the Live-Dead viability kit gets enzymatically converted to brightly fluorescent Calcein in the cytoplasm of live cells, thus clearly defining the cytoplasm; however, it does not stain the nucleus. To complement this cytoplasmic stain, a nuclear dye Hoechst 33342 dye was used. (In case of the dead cells, the Ethidium Homodimer-1 penetrates damaged membranes and binds to nucleic acids inside the cells – mostly the DNA of the nucleus, clearly defining the nucleus and facilitating identification by the software).

4.2.1: Protocol for the hMSCs-viability Comparison Assay:

1. **Programming the cell printer:** Prior to conducting the viability comparison assay, a program was written to aspirate cell suspension from a well of a 96 well plate and dispense twelve aliquots of 10 µL each of the aspirated cell suspension into twelve wells of another 96-well plate mounted on the printer's deck. The program was tested for errors (debugging) using water and corrected as necessary.

2. **Trypsinizing cells and setting up control group:** Human mesenchymal stem cells (passage 9) were trypsinized and re-suspended in DMEM containing 10% fetal bovine serum (FBS), 1% Penicillin and 1% Streptomycin (Lonza, Walkersville, MD). Cells were re-suspended so as to yield a final concentration of 500,000 cells per mL. Aliquots of 10 µL each of cell suspension (equivalent to 5000 cells) were pipetted manually into twelve wells of a sterile 96-well plate pre-filled with 200 µL of cell culture media (indicated by pink colored wells in the control group in the figure below). Provision for appropriate controls for dyes was also made – no cells were added to these wells (Figure 17).
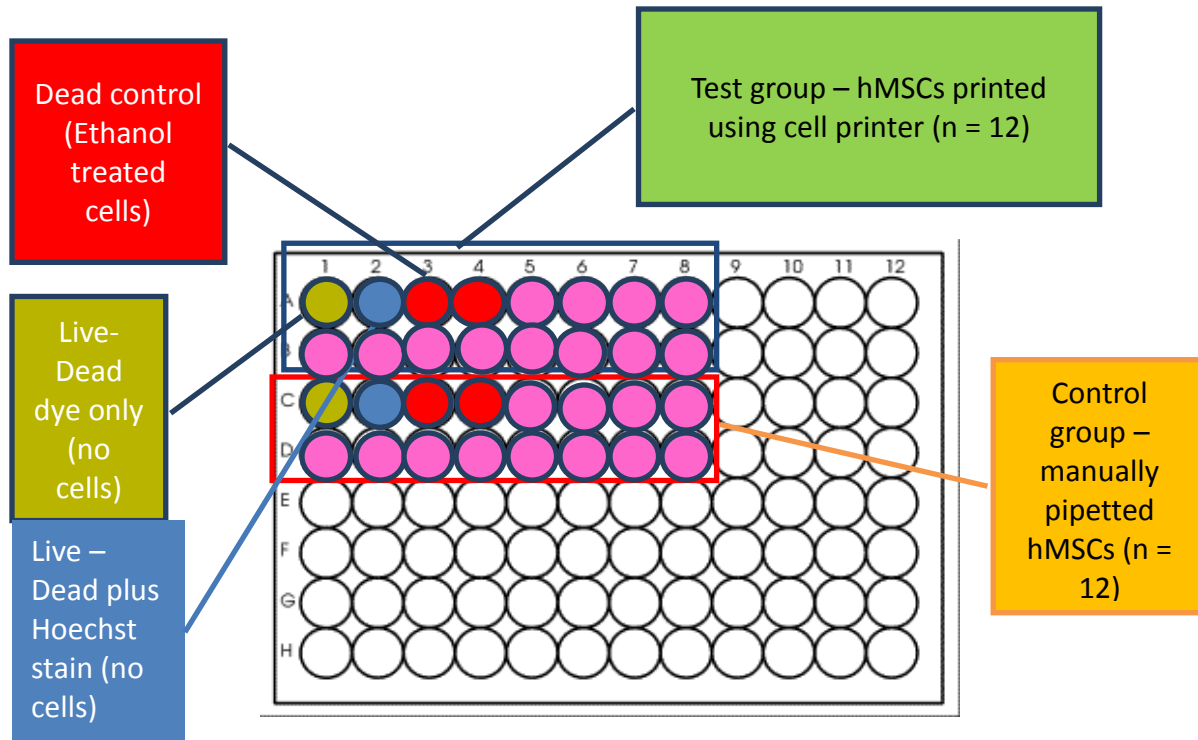
Figure 17: Experimental design for hMSC-viability-comparison assay. A sterile 96-well plate was used for the viability comparison assay. Twelve wells were seeded with hMSCs in each group, 24 in total (A5-A8 and B1-B8 in cell printer group, and C5-C8 and D1-D8 in manual-pipetting group). hMSCs treated with 70% ethanol were used as dead control in both groups (wells A3, A4, C3, C4). Control wells for dyes to test for auto-fluorescence were not seeded with cells (A1, A2, C1, C2).

3. **Dispensing cells using the cell printer:** The remaining cell suspension was transferred to a single well of a fresh sterile 96-well plate, and mounted on the front holder of the cell printer's deck taking sterile precautions. The 96-well plate with twelve wells, already seeded with hMSCs manually using a micropipette, was also mounted on the deck of cell printer on the rear holder. The print program, previously written and tested to aspirate cell suspension from one well of a 96-well in the front holder and dispense twelve aliquots of 10 µL each into twelve wells of 96-well plate in the back holder (in the pattern shown in Figure 17), was then executed. After completion of the print run, the 96-well plate seeded with hMSCs was transferred to an incubator and incubated for 24 hours at 37°C under atmospheric oxygen, 5% carbon dioxide and 85% relative humidity.

4. **Staining cells for viability:** Just prior to completion of the 24-hour incubation period, Calcein AM and Ethidium Homodimer-1 dye solution was prepared fresh in serum free Dubecco's modified Eagle's medium (DMEM) (0.5 µL Calcein AM and 2 µL Ethidium Homodimer-1 in 1 mL of serum-free DMEM). Total 6 mL of dye solution was prepared (200 µL per well for 30 wells in total including controls).

   Note: Calcein AM degrades spontaneously into Calcein in aqueous solutions, therefore it is necessary to prepare the dye solution fresh and use it within an hour. Also, bovine(and human) serum has esterase activity which converts Calcein AM into Calcein. Thus, it is necessary to use serum-free media as solvent for these dyes (product data sheet).

   After the dye solution was prepared, the 96-well plate seeded with hMSCs was removed from the incubator and transferred to a biosafety cabinet. The cell media from all wells in the 96-well plate was suctioned out and 200 µL of freshly prepared Calcein AM and Ethidium Homodimer-1 dye solution was added to each well (as shown in Figure 17). The cells were incubated at 37°C under atmospheric oxygen, 5% carbon dioxide and 85% relative humidity for 15 minutes. While the cells incubated with the dye solution, a second dye solution containing Hoechst and the Live-Dead stains was prepared: 0.5 µL Calcein AM, 2 µL Ethidium Homodimer-1, and 0.5 µL Hoechst 33342 dye in 1 mL of serum-free DMEM. Total 6 mL of dye solution was prepared for 30 wells in both groups, including dye controls.

   After 15 minutes, the 96-well plate was transferred from the incubator to the biosafety cabinet; the first dye solution was suctioned out of all wells, and second dye solution containing Hoechst in addition to Live-Dead stains was added to all wells (200 µL per well). The cells were incubated for another 15 minutes with the second dye solution and then visualized with fluorescence microscopy (Leica DM IL microscope) (Figure 18).
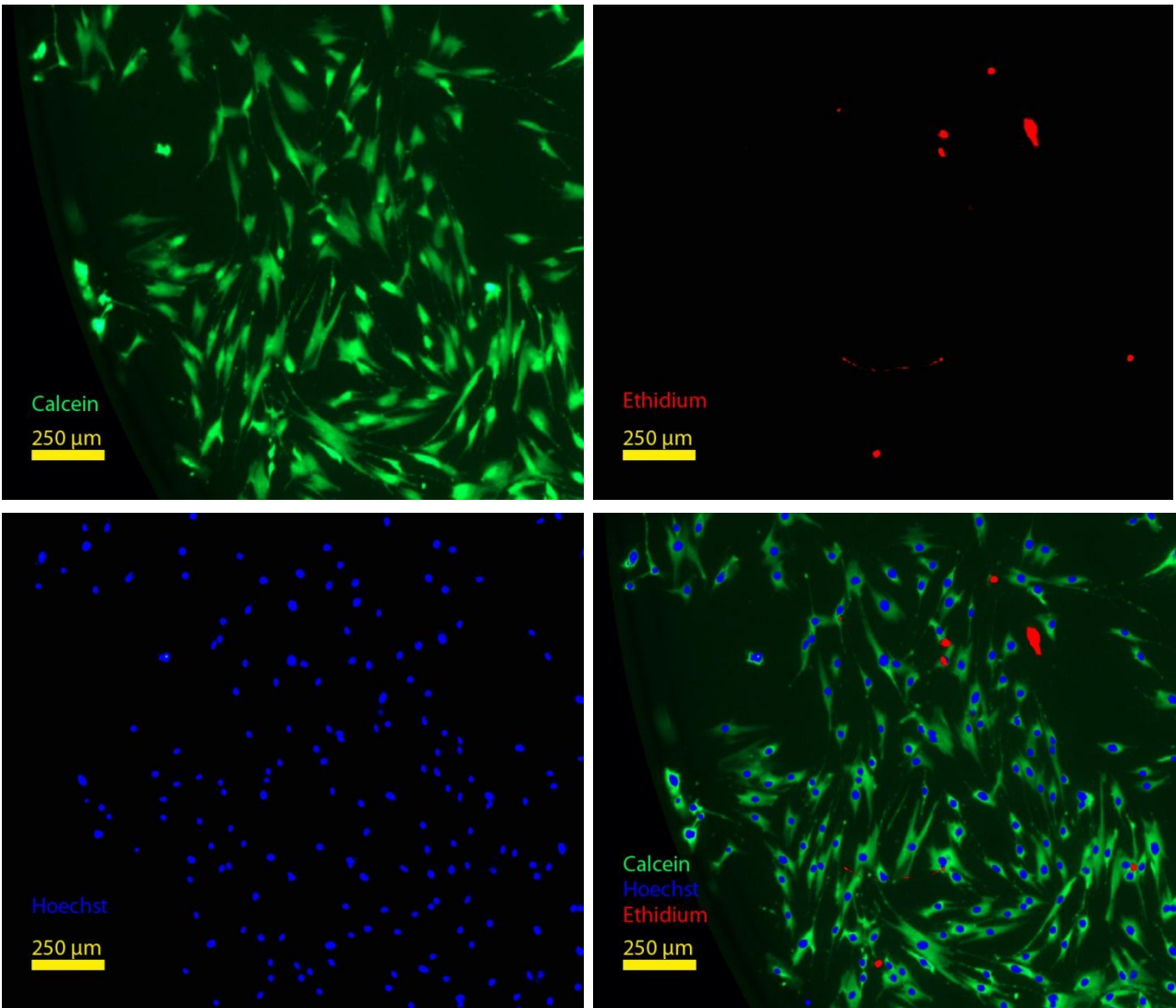
Figure 18: Fluorescence microscopy for hMSC-viability comparison assay. Cytoplasm of live cells fluoresce bright green with Calcein (top left), nucleic acids (mostly DNA in the nucleus) of dead cells take up Ethidium that fluoresces red (top right). Hoechst (bottom left) was used as a counter stain for the cytoplasmic dye Calcein. Overlay of all three images is shown on the bottom right.

5. **Imaging using fluorescence microscopy and post-processing:** All wells seeded with cells were imaged with fluorescence microscopy (Leica DM IL inverted microscope). Imaging each well in its entirety was essential to obtain total number of cells and percentage of viable cells in each well. For this, a 'tiling' technique was used in which images of different but slightly overlapping regions of the wells were taken, to cover the entire well region by region. Three images were taken for each region, using three optical filters - one each of the three dyes – Calcein, Ethidium and Hoechst. These three images for each region were then overlaid using software (Adobe Photoshop) to obtain a single image showing objects stained by all three dyes for that region. All regions of a well imaged and processed similarly were then stitched using software (Adobe Photoshop) to

obtain a single image of the entire well showing all objects in the well stained with all three dyes. (Figure 19)
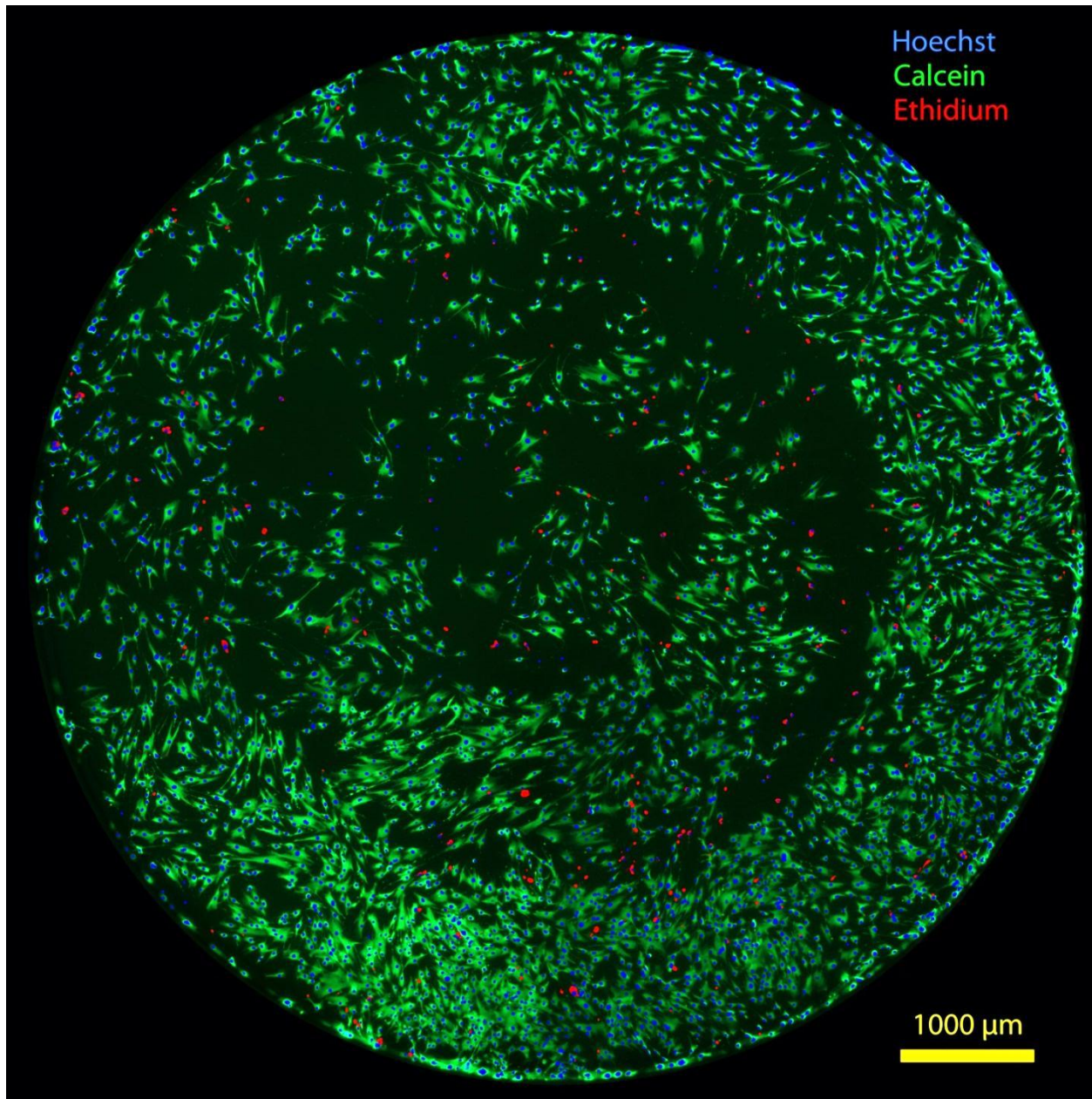
Figure 19: Stitched image showing an entire 96-well plate well seeded with hMSCs. 'Tiling' (imaging different but slightly overlapping areas of the well) was done to image an entire well, using three fluorescent filters for each region – one for each dye. Images of separate regions (or 'tiles') were then stitched together to form a single image of the entire well as shown in this figure. The same procedure was followed to image all wells seeded with hMSCs and dye controls in both groups.

6. **Image Analysis using Cell Profiler:** Images of all wells were analyzed using an open source image analysis software – Cell Profiler (Broad Institute, Cambridge, MA) – www.cellprofiler.org.

4.2.1.1: Obtaining Accurate Counts of Viable hMSCs from Image Analysis:

Initial attempts at identifying the live-cells based on the cytoplasmic staining (Calcein) yielded inaccurate results because all object identification algorithms in Cell Profiler (and other equivalent open source software) are designed to identify fairly round objects, not irregularly shaped ones. hMSCs are stellate, triangular or spindle shaped when in tissue culture in vitro and the bright green Calcein cytoplasmic signal in viable hMSCs follows the same contour in images taken by fluorescence microscopy. These were not conducive to being identified accurately by any of the algorithms in the software. Attempts were also made to design custom algorithms on MatLab (Mathworks, Inc.) but were unsuccessful. The algorithms of the software are most accurate at identifying nuclei of cells due to their round morphology. Thus, it was decided to add an additional counter-staining for the nuclei - Hoechst 33342, using the count of the nuclei as a representation of the count of cells.

However, with Hoechst staining, not all objects that showed the Hoechst signal showed cytoplasmic Calcein signal around them. The reasons for this observation are not known, but it is speculated that these objects were nuclei of cells that were damaged or had weak esterase activity; not enough to catalyze conversion of Calcein AM into fluorescent Calcein. A few of these round objects (probably nuclei) showed an Ethidium signal, while the rest did not. Due to such non-uniformity of co-localization of nucleic Hoechst signal, cytoplasmic Calcein signal and nucleic Ethidium signal, defining a uniform rule to classify all Hoechst stained objects as belonging to the class of either viable or non-viable cells was not possible in the raw images without further post-processing.

To circumvent this problem, images of entire wells were scanned by eye for round objects that showed a Hoechst signal (nuclei) but did not co-localize with either Calcein cytoplasmic signal, or nucleic Ethidium signal. Under the reasonable assumption that such nuclei could not be conclusively considered as belonging to viable or non-viable cells, these objects were excluded from the images by manually masking them with black color (same as background color) using the paintbrush tool in Adobe Photoshop. These modified images were then used for image analysis in Cell Profiler. This post-processing prior to analysis was done for images obtained from all wells in both groups (Figure 20).

Also, nuclei that stained with both Hoechst and Ethidium Homodimer-1 (i.e. round objects where the red and blue color co-localized) were considered as those belonging to dead cells. (Recall that Ethidium Homodimer-1 can permeate only damaged cell membranes, not intact ones in viable cells). To account for these, objects that showed both Hoechst and Ethidium signal were counted manually in all images. The count of such objects was subtracted from the total count of objects that stain with Hoechst obtained from the modified images using Cell Profiler. Recalling that the modified images contained only those objects that showed a Hoechst signal co-localized with Calcein or Ethidium, subtracting the count of objects that showed a Hoechst signal co-localized with an Ethidium signal yielded the count of only those objects that showed a Hoechst signal co-localized with or surrounded by a Calcein signal i.e. viable cells.
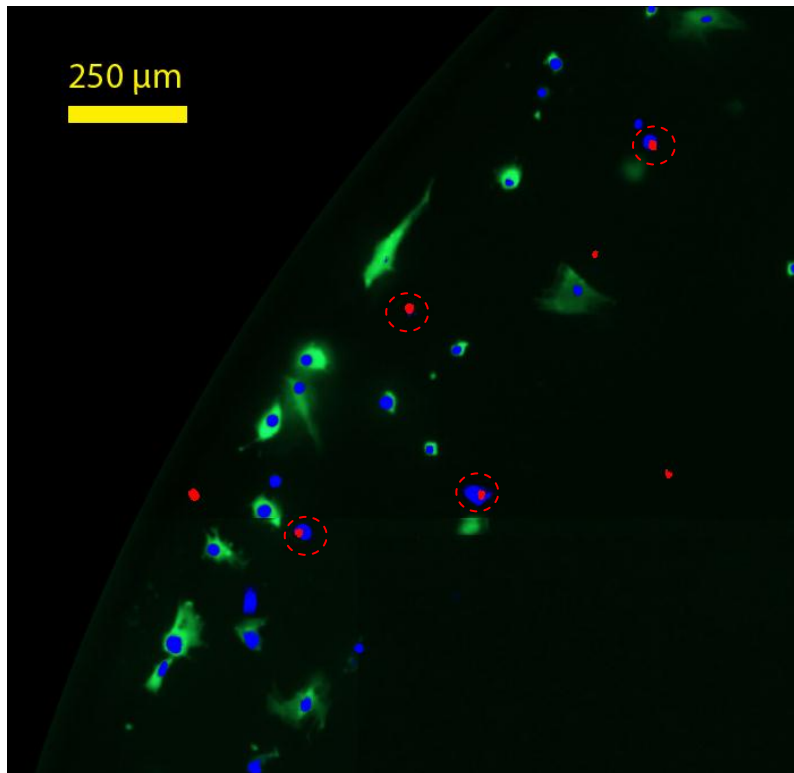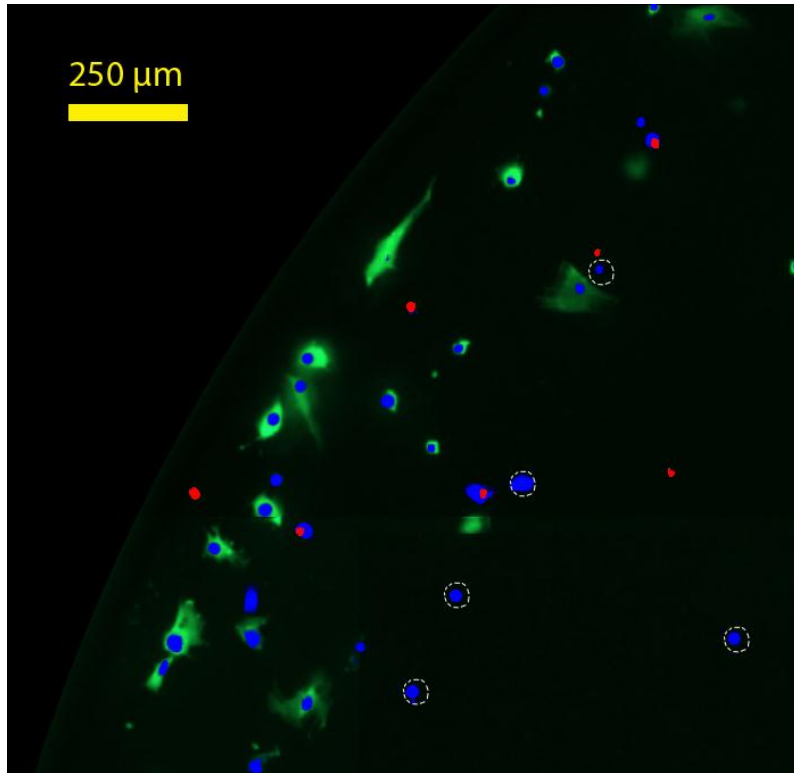
Figure 20: Image correction for objects stained with Hoechst but not with Caclein or Ethidium. Objects that showed a Hoechst signal and a Calcein signal around it were considered as live cells. Those that showed a Hoechst signal and an Ethidium Homodimer-1 signal or Ethidium Homodimer-1 signal alone, were considered as dead cells. Those that showed Hoechst signal but did not co-localize with a Calcein signal or an Ethidium Homodimer-1 signal were identified manually in all images (depicted in the top image by broken white circles). Such objects were masked using the paintbrush tool in Adobe Photoshop to yield a modified image as shown in the bottom image, lacking only these objects but preserving all others. These modifed images were used for analysis in Cell Profiler software, to obtain a count of the total number of objects that showed a Hoechst signal. Additionally, objects that showed both Hoechst and Ethidium Homodimer-1 signal were also identified and counted manually in each image (depicted by broken red circle in bottom image). The count of such objects was subtracted from the count of total number of Hoechst stained objects (nuclei) obtained from in the modified images using Cell Profiler to correct for dead cells that picked up both Hoechst and Ethidium. This entire process yielded the count of only those objects that picked up Hoechst signal (nuclei), co-localized with a Calcein signal, and did not co-localize with an Ethidium signal, i.e. viable cells.

Detailed description of how the image analysis software Cell Profiler works is beyond the scope of this work. However, the basic steps that were followed in the algorithms to obtain a count of Hoechst and Ethidium stained objects in the modified (post-processed) images are described.

Identification of Hoechst-stained nuclei: (Figure 21)

i. The images to be analyzed were first 'loaded' onto the analysis software, by specifying a folder location where the images were located on a local drive on the computer.

ii. The intensity of blue color (Hoechst signal) at each pixel in the image was displayed on a grey scale i.e. the blue channel was converted to grey scale. Based on the intensity of the background in immediate surroundings of each object, a local threshold for minimum acceptable intensity for foreground objects was calculated by the software for that region (Otsu-adaptive algorithm). Pixels in the image having intensity higher than this calculated threshold were considered as belonging to the foreground.

iii. Foreground pixels were then grouped into 'objects' based on shape; objects with elliptical shape were sought for by the software algorithm (assuming the objects are all nuclei which are more or less round). The number of such individual objects identified (object count representing number of Hoechst-stained nuclei) was exported to a MS Excel sheet. To obtain the total number of Hoechst-stained nuclei in each well, individual counts of Hoechst-stained nuclei obtained from images representing all sub-regions of each well were summed. This gave the total number of nuclei in each well, most of which belonged to live cells and a few to dead cells (showing Ethidium signal as well). The exact number of nuclei belonging to live cells was obtained after manually correcting for those that stained with Ethidium Homodimer-1 as well; as described in Figure 20.

Identification of Ethidium-stained nuclei: (Figure 22)

A similar algorithm was used to identify Ethidium-stained nuclei, with the exception that the red channel was converted to grey scale. A threshold was similarly calculated to differentiate pixels into foreground and background based on the intensity of the red color at each pixel. Pixels were grouped into 'objects' and the number of objects identified in each image was exported to an excel sheet. This represented the number of Ethidium-stained nuclei in the image, i.e. number of dead cells. To obtain the count of total number of dead cells in each well, individual counts of Ethidium-stained objects obtained from images representing all sub-regions of each well were summed.
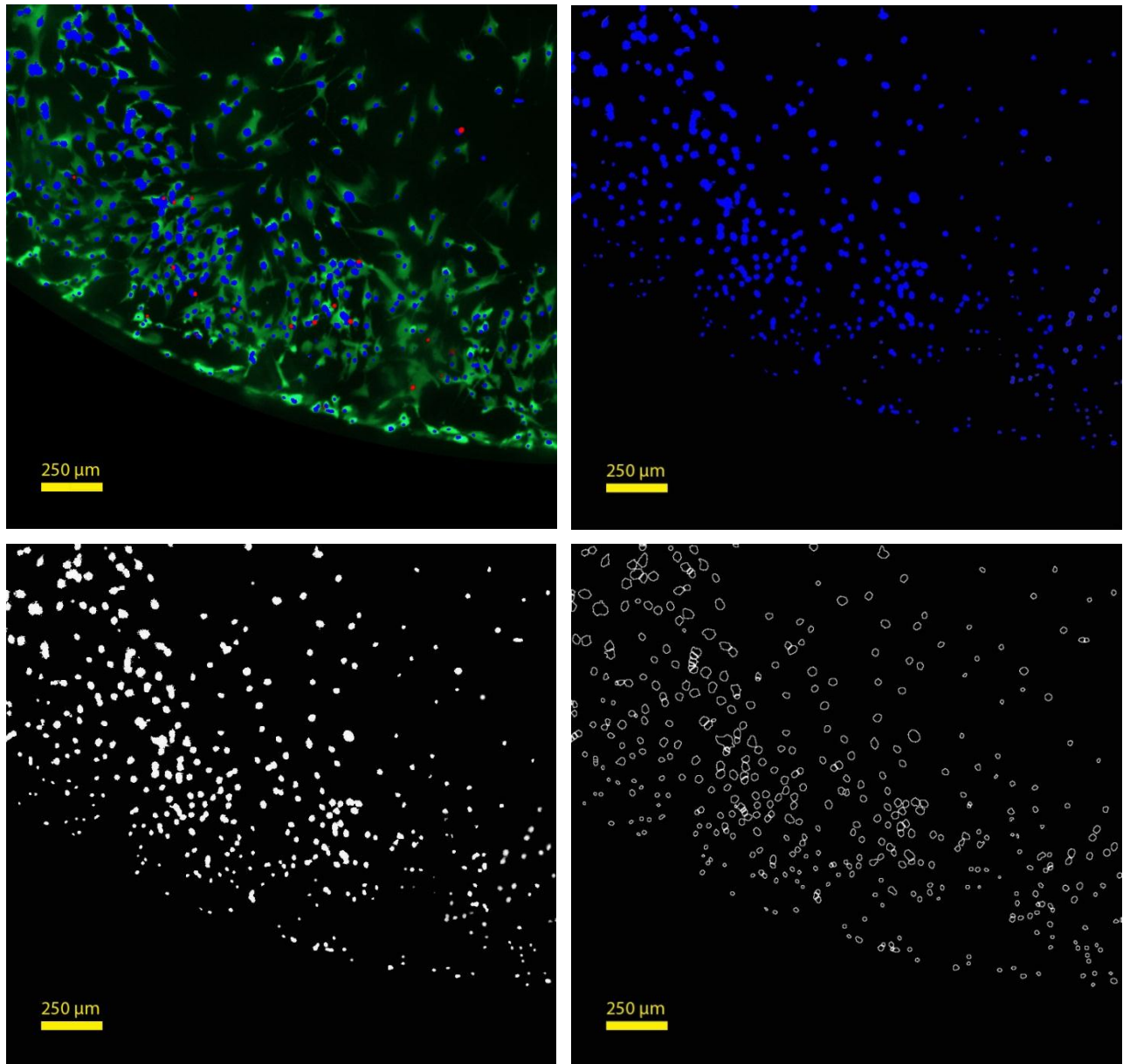
Figure 21: Identification and counting of Hoechst-stained nuclei using Cell Profiler. The original image depicting an overlay of the Calcein, Hoechst and Ethidium signals in $1/16^{th}$ of a well is shown on the top left. From this, only the Hoechst signal (blue channel) was used for analysis after post processing. In the first step, the software converted the input image (top-right) into a grey scale image based on the intensity of blue color at every pixel in the image (bottom-left). A threshold for minimum intensity to segregate foreground objects from the background was calculated by the software based on the background color and intensity. All pixels in the image that had intensity higher than this minimum threshold intensity in the blue color were assigned to foreground, while the rest were assigned to background. The foreground pixels were then grouped into individual 'objects' based on the shape of adjoining foreground pixels (bottom right). The count of individual objects identified was exported to an MS Excel sheet.

50
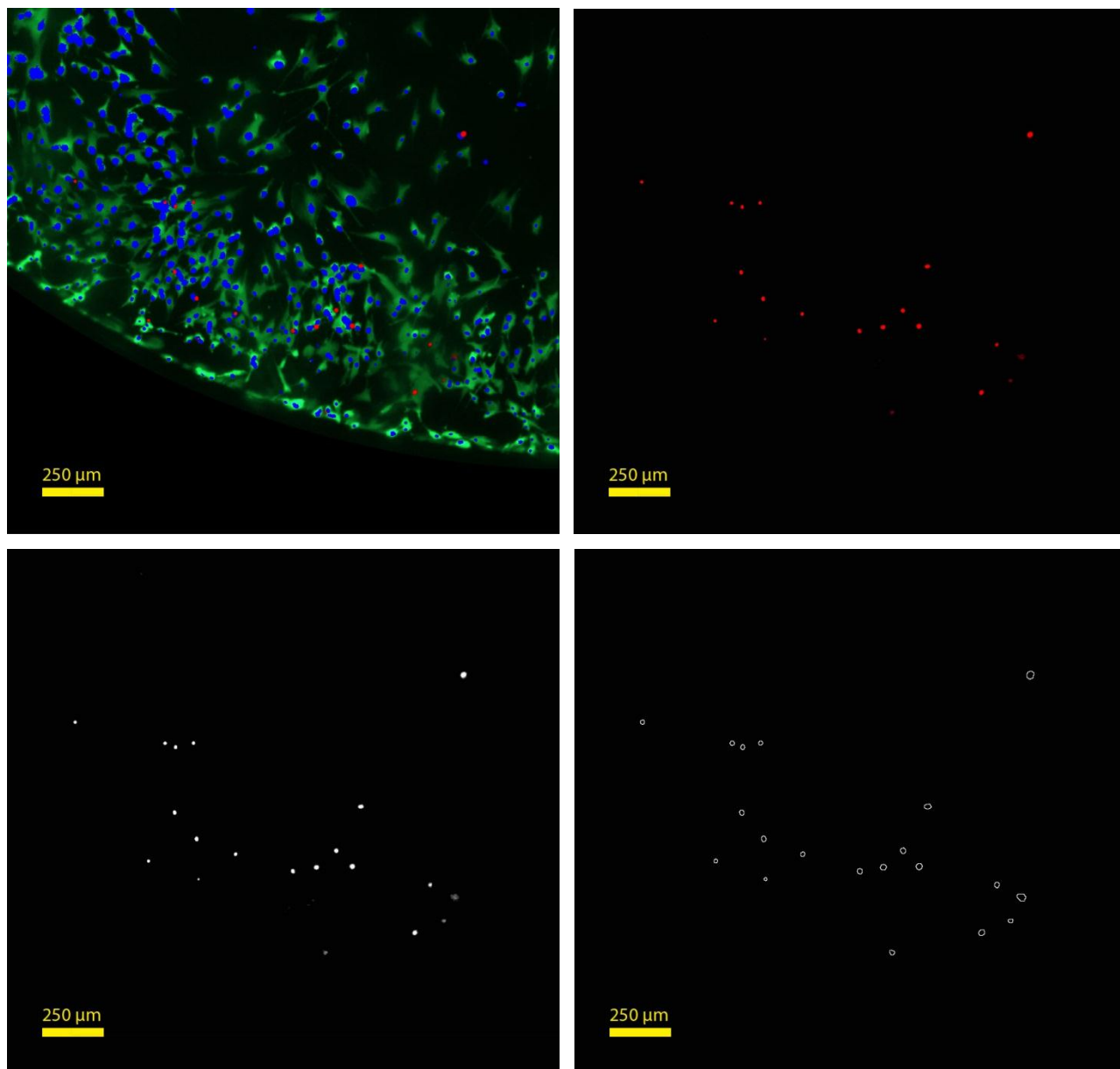
Figure 22: Identification and counting of Ethidium-stained nuclei using Cell Profiler. The original image depicting an overlay of the Calcein, Hoechst and Ethidium signals in $1/16^{th}$ of a well is shown on the top left. From this, only the Ethidium signal (red channel) was used for analysis. In the first step, the software converted the input image (top-right) into a grey scale image based on the intensity of red color at every pixel in the image (bottom-left). A threshold for minimum intensity to segregate foreground objects from the background was calculated by the software based on the background color and intensity. All pixels in the image that had intensity higher than this minimum threshold intensity in the red color were assigned to foreground, while the rest were assigned to background. The foreground pixels were then grouped into individual 'objects' based on the shape of adjoining foreground pixels (bottom-right).

4.2.1.3: Calculation of percentage of viable cells:

Nuclei that showed both Hoechst and Ethidium signal as shown in the bottom image in Figure 20 (i.e. nuclei of cells with damaged membranes) were counted manually in the post-processed image of the entire well, for all wells. The count of such nuclei was subtracted from the total number of nuclei that stained with Hoechst for the respective well obtained using Cell Profiler, for all wells. Recalling that image post-processing allowed only those objects that showed a Hoechst signal co-localizing with either Ethidium or Calcein signal to remain, this subtraction yielded the count of objects (nuclei) that showed a Hoechst signal co-localizing with a cytoplasmic Calcein signal i.e. count of viable cells. Such a count of viable cells was obtained for all wells seeded with hMSCs in both groups.

The count of objects that stained with Ethidium Homodimer-1 in a well was used as the count of non-viable cells in that well. As for the viable cell count, the count of non-viable cells was also obtained for all wells.

The sum of viable and non-viable cells of respective wells gave the total number of cells for all wells. Percentage of viable cells was obtained by dividing the number of viable cells by the total number of cells for all wells.

4.2.1.4: Comparison of cell viability

Mean cell viability was calculated for both groups - wells seeded with hMSCs using the cell printer or by manual pipetting, and used for comparison. The hypothesis that there was no difference between the viability of hMSCs between the two groups was tested statistically.

4.3: Fibrin Microthread Production and Bundling

Fibrin microthreads were extruded using a previously established protocol (61). Two separate 1 mL syringes were each filled with thrombin and fibrinogen taken from bovine plasma (Sigma Aldrich, St. Louis, MO). A blending application tip was used to combine the thrombin and fibrinogen and the combined solution was extruded through 0.38 mm inner diameter polyethylene tubing (Beckton Dickinson, Franklin Lakes, NJ) (drawn by hand) into a 10 mM HEPES, 7.4 pH bath that was kept at room temperature (Figure 24). After 15 minutes in the bath, the microthreads were taken out and air dried (Figure 23). Dry microthreads have an average diameter of about 35 μm (Figure 25).
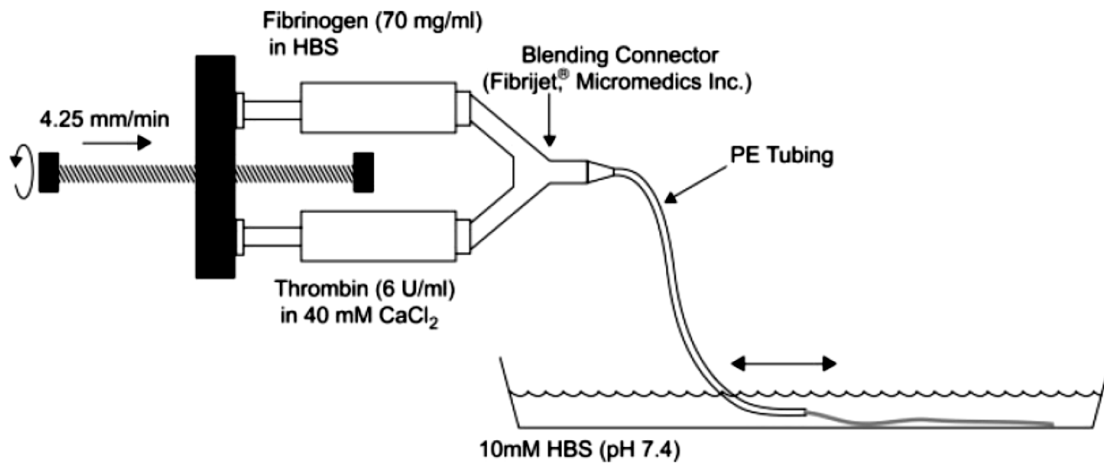
Figure 24: Diagram depicting extrusion of fibrin microthreads (61)

Figure 23: Fibrin microthreads - gross appearance. Fibrin microthreads are stretched and hung to be dried at room temperature on the lab bench top, usually overnight. Dry fibrin microthreads are thin, long, hair-like, shiny greyish white in appearance. Red arrows to the left of the image mark one end of the microthreads in this image.
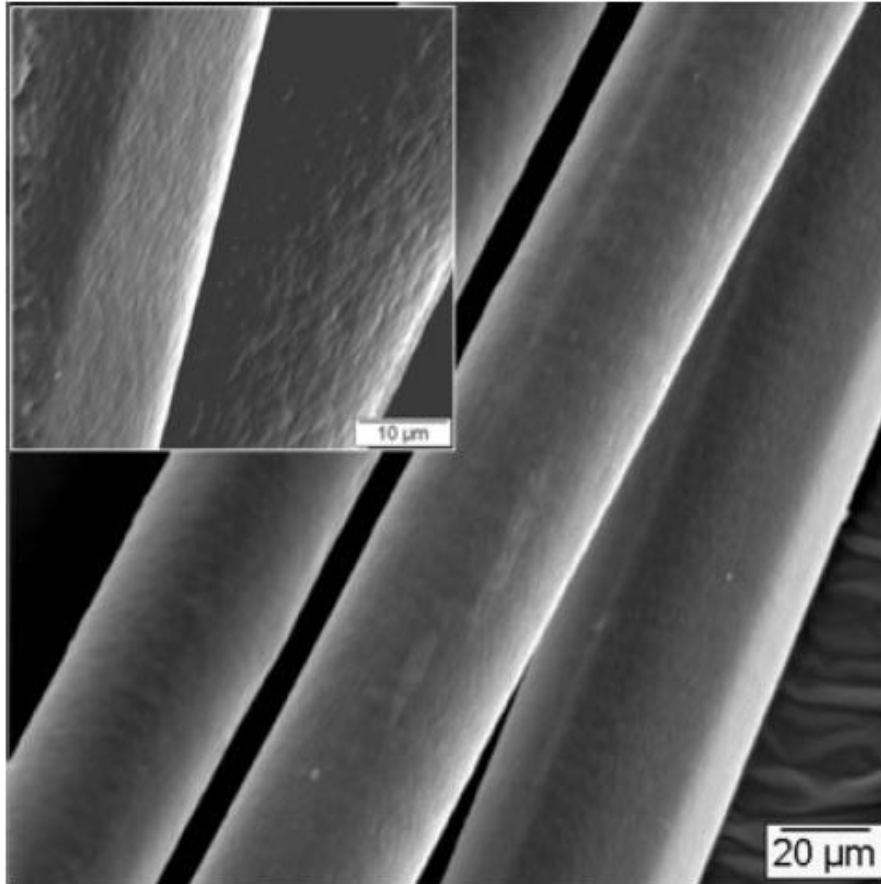
Figure 25: Scanning electron micrograph of fibrin microthreads (61)

Individual dry fibrin microthreads have a diameter ranging from 20 to 50 µm (61). They are quite delicate and do not have sufficient mechanical strength to be used as sutures on a needle. They also do not have sufficient surface area to allow attachment of hMSCs. To circumvent this problem, individual fibrin microthreads were 'bundled' to form a thicker, stronger suture-like structure, having sufficient mechanical strength to be used as a suture and having enough surface area to allow cellular attachment.

Each fibrin thread bundle used for this work consisted of 12 fibrin microthreads. For bundling, 12 fibrin microthreads were placed adjacent to each other and bunched together at one end, held in place by using adhesive tape. Droplets of de-ionized water were slowly 'dragged' along the length of the bunched thread from the taped end to the other end, to wet all the bundles end to end. As the microthreads hydrate, they aggregate spontaneously and stick to each other when sufficiently wet. Once aggregation was observed after repeated wetting of the bunched microthreads, they were suspended freely; vertically held at their taped end and hanging freely at the other end (Figure 26). The microthread bundle was then twisted repeatedly by hand at its free end in a clockwise direction (when looking at the cross-section of the thread bundle from its free

end). Twisting of the bundle has been observed to help the individual threads adhere better and prevents fraying. To make sure the entire length of the bundle was twisted uniformly, the bundle was twisted repeatedly from the free end until the twists on the bundle 'traveled' all the way along the length of the bundle from the free end to the taped end. The twisted bundle was then secured at the free end with adhesive tape and allowed to dry in the air.

|← 18 cm →|
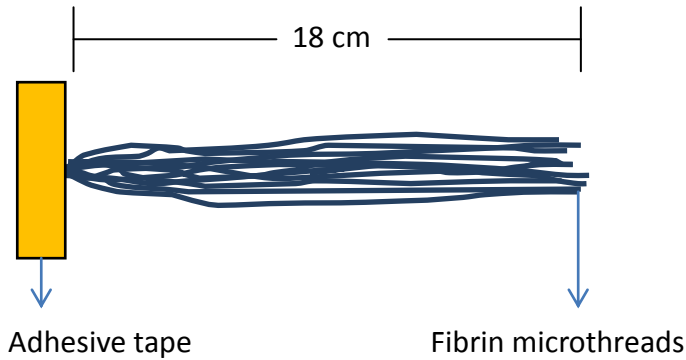
Step 1: Twelve individual microthreads were anchored in a bunch at one end using tape

Adhesive tape   Fibrin microthreads
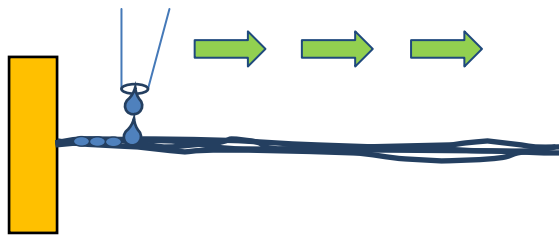
Step 2: The bunched microthreads were wet from one end to the other with de-ionized water in order to hydrate them. Wetting causes them to aggregate into a bundle spontaneously.
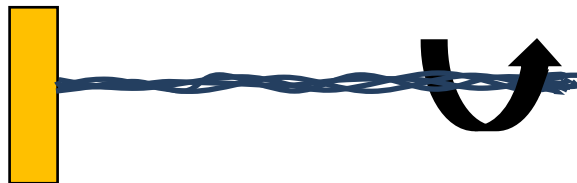
Step 3: The hydrated bundle was twisted by hand at its free end in the clockwise direction, repeatedly, until the twists traveled the entire length of the bundle.
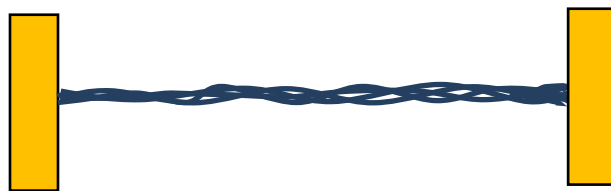
Step 4: After twisting, the bundle was secured at the free end with adhesive tape and was allowed to air dry.

Figure 26: Schematic depicting steps of making a bundle of twelve fibrin microthreads

Air dried bundles prepared in this manner were then incorporated into the bioreactor assemblies used in the two seeding methods - the cell printer and the tube rotator method for seeding hMSCs onto the thread bundles.

4.4: Comparison of Seeding efficiency

4.4.1: Overview
In order to compare the efficiency of the two methods – the current method (tube rotator method) and the cell printer method – for seeding of hMSCs onto fibrin thread bundles, special bioreactors were designed for both methods. These were designed so as to allow hMSCs in cell suspension to come in contact with fibrin thread bundles for a sufficient period of time and to provide an environment conducive to cell survival and seeding. Cell seeding onto thread bundles was carried out simultaneously with both methods using the same cell suspension, for comparability. The bioreactors freshly seeded with cell suspension were then incubated for 24 hours at $37^{\circ}C$ under atmospheric oxygen, 5% carbon dioxide and 85% relative humidity. Visualizing the threads by confocal microscopy after staining with fluorescent dyes was selected as method of choice to count the number of cells on each thread bundle over other methods due to reasons detailed in the discussions chapter. For this, seeded threads were then fixed, stained and mounted on cover-slips for examination using confocal microscopy. The entire length of each bundle was imaged on the confocal scope in serial segments from one end to the other end. Maximum projections were generated for each segment of the bundle, which were then stitched using Adobe Photoshop into a single image showing one side of the entire length of the seeded thread bundle. The number of cells visible in this image (on one side of the bundle) on each thread was counted manually at least twice by different individuals to account for subjectivity. The counts were then averaged to obtain the count of cells on one side of the bundle. Under the reasonable assumption that the bundles seeded uniformly on both sides, this count was multiplied by two to obtain the total number hMSCs seeded on the entire thread bundle. The count was then normalized to the length of the thread bundle (for comparability across threads with minor variations in length) and used for calculation of seeding efficiency. The mean seeding efficiency of three experiments using one thread bundle each was used for comparison of the two methods.

Bioreactors used in the two methods, the protocol followed for seeding the threads, fixation and staining, imaging using confocal microscopy, image post-processing to obtain images of entire length of thread bundles, counting the number of cells on each bundle, and calculation of seeding efficiency are described in this section.

4.4.2: Bioreactor assembly for tube rotator method and the seeding process
Twelve fibrin microthreads, each of approximately 18 cm length, were bundled using the above described method to form a single bundle of the same length. This bundle was air-dried and cut into two halves of 9 cm each. One half was used for making the bioreactor assembly for the tube-rotator method (the current method for seeding hMSCs onto fibrin microthread bundles), while the other half was incorporated in the bioreactor assembly for seeding cells onto the bundle using the cell printer.

Because fibrin microthreads are extruded and bundled by hand, there is inherent variation in the diameter and number of twists from bundle to bundle. By using two halves of the same bundle as a set, one half being used in assembly for the current method and the other half being used for the assembly for the cell printer method, the effect of variability in the bundle dimensions on cell seeding was minimized, thus allowing fair comparison between the two seeding methods.

For making the bioreactor assembly for the tube-rotator method (Figure 27), the fibrin microthread bundle was cut to a length of 2 cm and placed inside a 4-cm length of 1.98 mm inner-diameter Silastic tubing (Dow Corning, Midland, MI). Slide clamps (Qosina, Edgewood, NY) were applied at both ends of the tubing making the compartment containing the thread bundle water-tight. The tubing was gas permeable allowing for gas exchange when the cell suspension was injected into the assembly.

The bioreactor assembly was then sterilized with Ethylene Oxide gas. One end of the bioreactor was kept open by sliding out one of the slide clamps, in order to allow proper permeation of Ethylene Oxide gas into the Silastic tubing and around the thread bundle (Figure 28).

At the time of seeding, the bioreactor assembly in sterile packing was transferred to a biosafety cabinet along with the cell suspension that was going to be used to seed the thread bundle in the assembly. The single slide clamp closing one end of the tubing was removed leaving the tubing containing the thread bundle open at both ends. After hydrating the thread bundle with deionized water for 30 minutes, 100 µL of cell suspension containing 500,000 hMSCs was pipetted into the tubing and slide clamps were replaced at both ends to make the assembly water-tight. The bioreactor assembly freshly loaded with cell suspension was then placed inside a 50 mL conical tube with apertures to allow gas exchange. The conical tube was then placed on a tube rotator (MACSmix™ rotisserie (MiltenyiBiotec, BergischGladbach, Germany, see **Figure 29**).
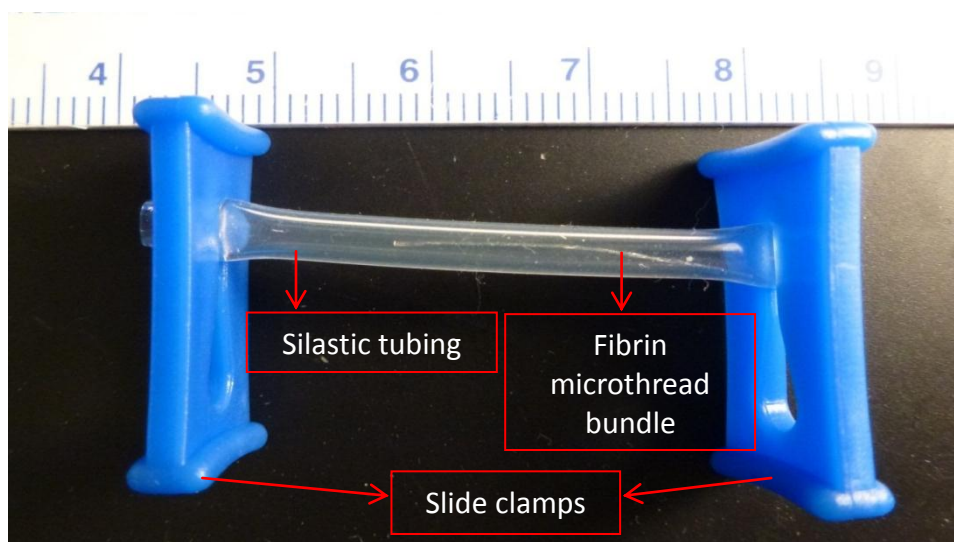
Figure 27: Tube-rotator assembly for seeding fibrin microthread bundles with hMSCs.
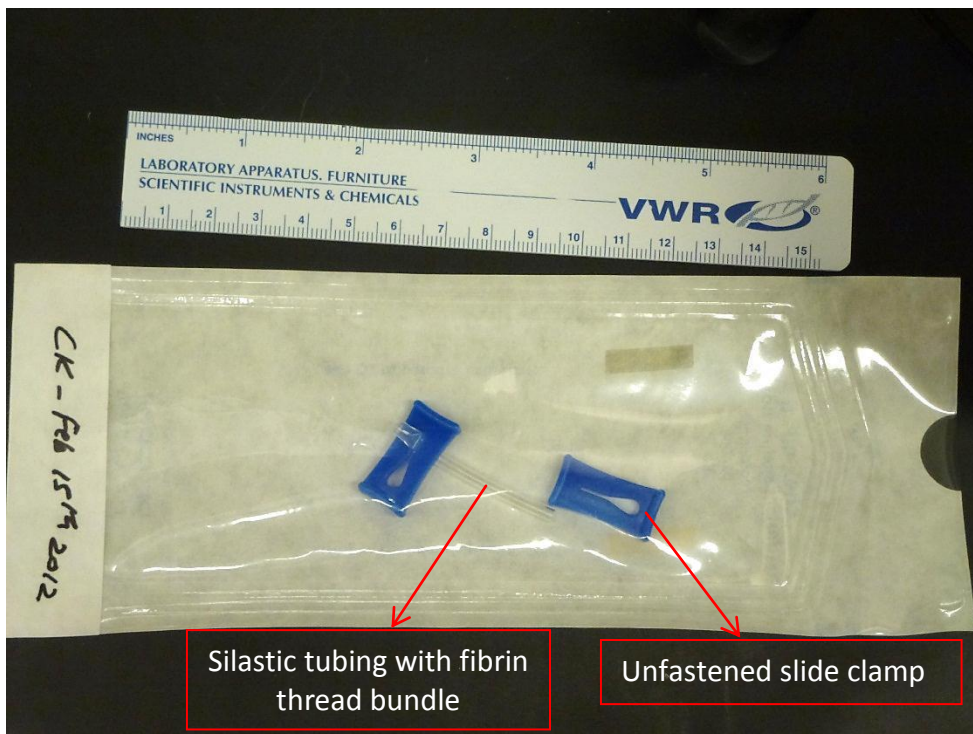
Figure 28: Bioreactor assembly for tube-rotator method in sterile packing after ethylene oxide gas sterilization. Note that one end of the silastic tubing containing the fibrin thread bundle was left open (the slide clamp was taken off to allow better gas penetration).


Figure 29: Seeding bioreactor assembles in 50 mL conical tubes mounted on a tube rotator.

The tube rotator is a battery operated device with a rechargeable battery and can rotate at speeds of 4, 8 or 12 rotations per minute. After the bioreactor assembly was mounted onto the tube rotator, it was set to its lowest rotation speed setting of 4 rpm and placed inside the incubator to allow hMSCs to attach to the fibrin thread bundles for 24 hours at 37°C under atmospheric oxygen, 5% carbon dioxide and 85% relative humidity. After 24 hours, the bundles were removed, fixed, stained and prepared for examination using confocal microscopy.

The rationale behind this dynamic method of seeding versus a static method is that the gentle rotation of the bioreactor containing the cell suspension with hMSCs around the fibrin thread bundle along the axis of the bundle would cause the hMSCs to come in contact with all sides of the thread bundle, aiding uniform seeding on the entire circumference of the bundle. Because this current method of seeding relies mainly on the tube rotator, it is referred to as the 'tube rotator method' in this work, against which the 'cell printer method' of seeding is compared.

It should be mentioned that the bioreactor assembly used for the tube rotator method in this study had minor modifications from the one currently used for seeding thread bundles with hMSCs. The current assembly uses a thread bundle attached to a suture needle because these bundles are meant to be sutured into a rat heart by surgery (18). For this reason, the assembly uses a 27G-hypodermic injection needle fixed at one end of the Silastic tubing with the slide clamp, which is used as a port to inject cell suspension into the tubing containing the thread bundle. Because this study does not involve surgical implantation of seeded thread bundles, suture needles were not used in the bioreactor assembly. This eliminated the need for using a hypodermic injection needle as a port for injecting cell suspension into the tubing, because the same could now be achieved using a 200 μL micropipette. Thus, hypodermic injection needles were not used as a part of this bioreactor assembly to seed threads using the tube rotator method.

4.4.3: Bioreactor assembly for seeding thread bundles with hMSCs using cell printer and the seeding process

It is most convenient to generate print programs containing linear print paths on the cell printer. Therefore, the main criterion for designing a bioreactor assembly was one that could hold a fibrin thread bundle straight and parallel to the deck of the printer to allow the cell suspension to be printed onto it in a linear path. It was also necessary that the assembly be able to mount at least 2-cm length of fibrin thread bundle (same length of thread used in the tube-rotator assembly) when held straight, and that the assembly be able to fit in a microtiter plate well format that was commonly available in sterile packaging. Six-well plates were chosen as the platform for the bioreactor assembly as they offered enough room to accommodate the required length of the fibrin thread bundle. A 3D model of a circular ring with dimensions designed to fit a six well plate was designed in a 3D modeling software - Solidworks (Dassault Systèmes SolidWorks Corp., Waltham, Massachusetts, USA).

Delrin plastic (McMaster Carr, CA) was selected as the material to make the ring due to its biocompatibility, compatibility with all sterilization techniques, ready availability, low-cost and easy machinability. Twelve rings were machined according to the drawings, so that multiple bundles (up to 6) could be seeded in a single experiment. Each ring was designed with holes to fit 2 dowel pins at diametrically opposite ends of the ring to act as anchoring posts for the fibrin thread bundle. The ring assembly before and after fibrin thread bundle was mounted on it is shown in Figure 30. Ring assemblies fit into six well plates as shown in Figure 31.
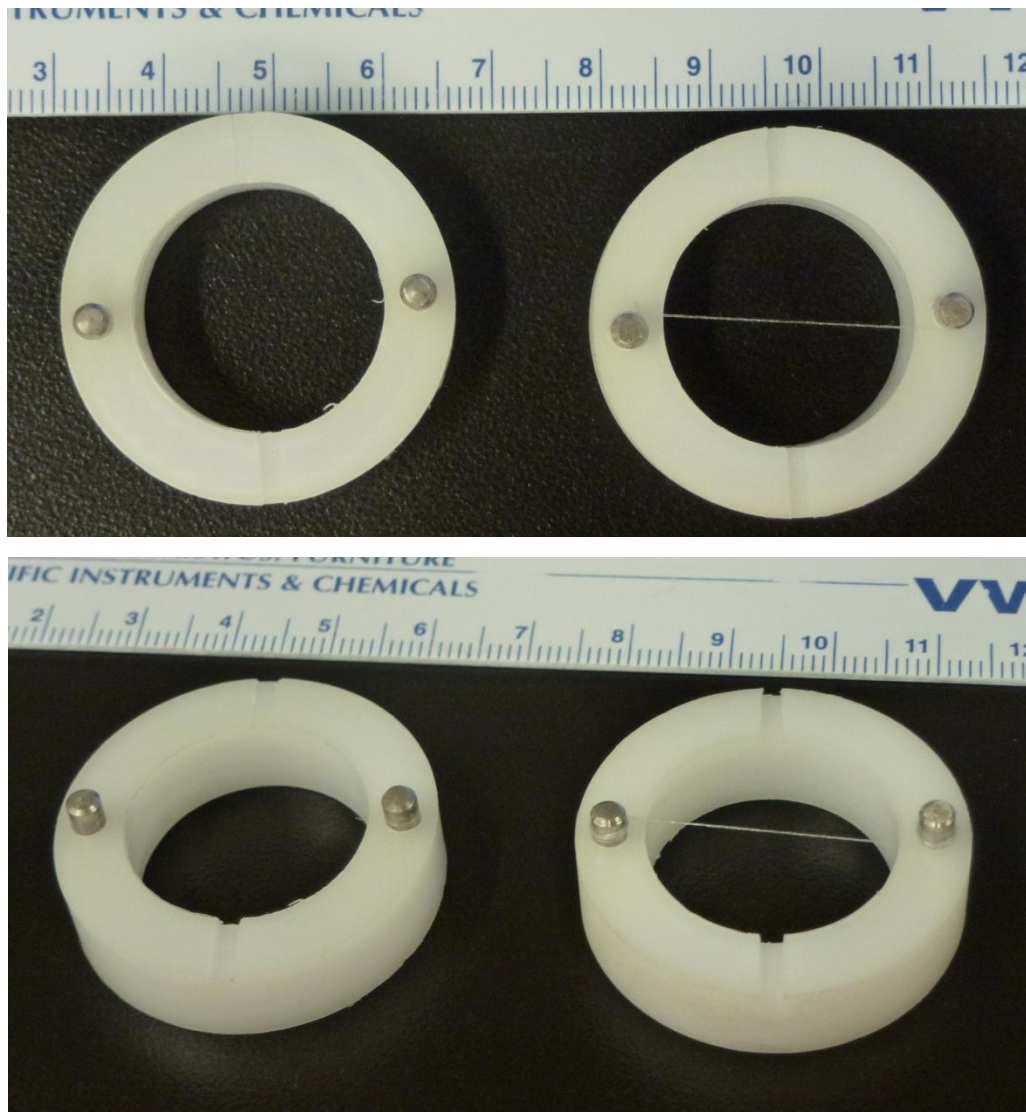
Figure 30: Delrin ring assembly to mount fibrin thread bundles. Top image – top view: left – ring without the thread bundle, right – ring with the thread bundle mounted on it. Bottom image – angled view of the same rings. In the ring assembly on the right, the bundle is wound twice around the dowel pins at both ends to keep it positioned horizontal and straight. The scale in both images is in centimeters.
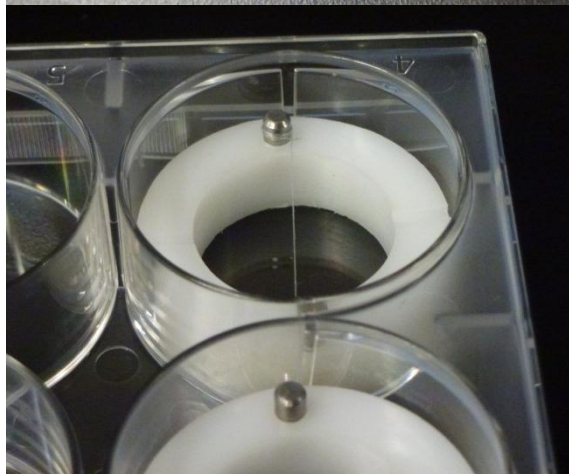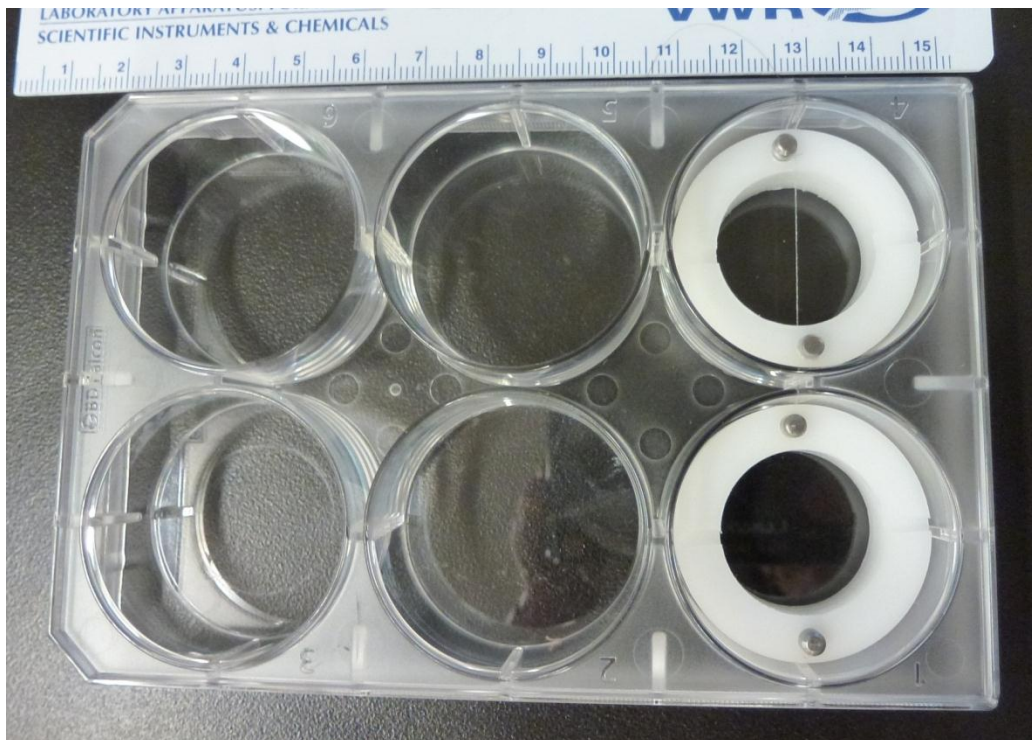
Figure 31: Delrin ring assembly inside wells of a six well plate. The top image shows 2 assemblies placed in wells of a six well plate, one with the thread bundle mounted (top well), and one without the thread bundle. The image to the left shows an angled view of the assembly inside the top well for better depth perception.

4.4.4: Protocol for seeding fibrin thread bundles using the cell printer

Preparing the bioreactor assembly for seeding

Recalling from the section describing the tube rotator assembly, 12 fibrin microthreads, each of approximately 18 cm length, were bundled to form a single bundle of the same length. The bundle was air-dried and cut into two halves of 9 cm each. One half was used for making the bioreactor assembly for the tube-rotator method, while the other half was incorporated in the bioreactor assembly for seeding cells onto the fibrin thread bundle using the cell printer i.e. the Delrin ring assembly.

The 9-cm length of the fibrin thread bundle was first hydrated by immersing in de-ionized water for 15 minutes. Because dry fibrin thread bundles are stiff and brittle, a fibrin bundle could be wound around the dowel pins of the delrin plastic ring assembly only when hydrated, which is when they become quite flexible and compliant. After hydration, the two ends of the 9-cm length of the bundle were held with 2 pairs of forceps. Using the two forceps, the bundle was wound twice around the dowel pins on the bioreactor assembly to position the thread straight and parallel to the plane of the top-surface of the ring.

The mounted bundle was then air-dried for 15 minutes and then placed in a sterilizing packaging. After sterilizing the assembly with the mounted thread with Ethylene oxide gas, this assembly was kept in a moisture free environment until the seeding experiment was conducted.

Writing a Print Program on the Cell Printer for seeding

A print program on the cell printer was written and tested well before the seeding experiment. A delrin ring bioreactor assembly with a fibrin thread bundle mounted onto it was placed in a well of a six well plate which in turn was mounted onto the cell printer's deck in the plate holder. This assembly was used to identify X, Y, Z co-ordinates of important landmarks to write a print program on the cell printer to dispense 10 µL of cell suspension onto the thread bundle. The program was written so as to evenly distribute the 10 µL of cell suspension onto 2 cm length of the thread bundle presented to the printer, with a total run time duration of about 10 minutes.

A brief outline of the print program for seeding was as follows:

- A 6-well plate the delrin ring assembly with the fibrin thread bundle was mounted on the rear plate holder on the printer's deck. The thread bundle was aligned along the X-axis of the cell printer.
- The motion control of the dispense head was homed in X, Y and Z axes.
- One motorized syringe pump (synQUAD pump) (one channel) was used for this print program; this pump was initialized and primed.
- The dispense tip (ceramic tip mounted on the dispense head) was cleaned of any residual liquid post-priming by vacuum suctioning.
- The dispense head was moved towards the front of the deck and positioned in a manner that would be convenient to present a hand-held Eppendorf to the dispense tip. The operator was then prompted to present a source tube (typically an Eppendorf tube containing the cell suspension). 'Presenting' the tube implies holding the Eppendorf tube by hand inside the biosafety cabinet housing the cell printer in front of the printer's dispense tip such that the tip is immersed in the suspension as deep as possible, without touching the bottom of the Eppendorf tube. (Figure 32)
- 10 µL of cell suspension was aspirated from the Eppendorf tube, after which the operator was prompted to remove the tube from the Biosafety cabinet.
- The dispense head was programmed to move so as to position the dispense tip exactly over the thread bundle mounted on the delrin ring in the 6-well plate. (Figure 33)

- The tip was then moved to one end of the bundle to begin dispensing the cell suspension. The hMSC-suspension was gently dispensed over 2 cm-length of the thread bundle in 100 nL droplets spaced 100 µm apart as the tip moved slowly (at 5 mm/sec) over the bundle towards the other end. 2 µL of cell suspension was dispensed in a single pass over the thread bundle. Four more such passes were made from end to end to distribute 10 µL of cell suspension along the length of the thread bundle.
- End to end sweeping movements over the length of the bundle with the tip positioned at the same Z-height as for dispensing (close to the thread bundle) were repeated a few more times to further even the distribution by capillary action.
- The tip was then raised and moved over to the wash and waste station, the channel was flushed by priming a few times and the motion control repositioned back to home in X, Y and Z to end the print program.
- At this point, the operator was expected to unmount the 6-well plate with the freshly seeded thread bundle from the printer's deck by hand, and transfer it to the incubator.

The print program was tested for errors over multiple iterations until satisfactory results were achieved and the final version then saved on the hard-drive of the controlling computer. Prior to the seeding experiment, this tester version of the print program was loaded from memory.
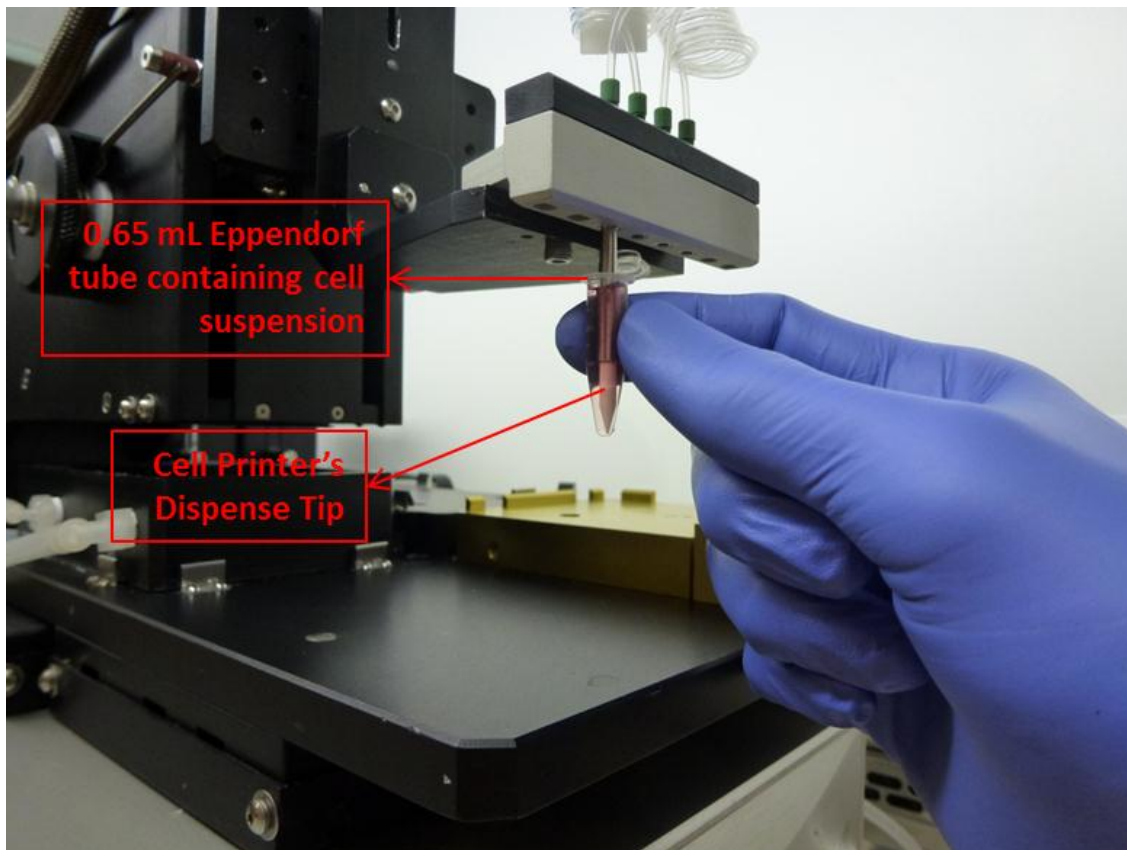
Figure 32: Presenting cell suspension to the cell printer's dispense tip for aspiration

Figure 33: Cell printer's tip positioned over the thread bundle ready to begin dispensing hMSC-suspension

Seeding Procedure

Human mesenchymal stem cells (passage 9 or lower passage), were expanded until an approximate sufficient number of cells for seeding were available (at least 100,000 cells per thread). At a time, usually a pair of thread bundles was seeded with hMSCs, one bundle with each of the two comparison methods.

On the day prior to the seeding experiment, articles necessary for the seeding experiment were sterilized by ethylene oxide gas sterilization or by autoclaving.

Just prior to the start of the seeding experiment, the cell printer was then turned on and the print program previously written and saved for seeding thread bundles with cells was loaded. The printer was kept in a ready-to-go condition as soon as cells were trypsinized and available for seeding onto the bundle.

At the start of the seeding experiment, a sterile delrin ring assembly with the thread bundle mounted on it inside its sterile packaging was transferred to a biosafety cabinet along with a sterile 6-well plate, pre-warmed cell media and other materials necessary for the experiment following necessary sterile procedure. The delrin ring assembly was transferred to a well of the

6-well plate using sterile procedure. 4 mL of sterile cell culture media – DMEM + 10% FBS + Penicillin/Streptomycin – pre-warmed to 37°C was added to the well containing the delrin ring assembly with the thread. The amount of media added was enough to submerge the thread bundle which was necessary for hydrating the thread bundle prior to seeding it with hMSCs. The lid of the 6-well plate was replaced and the plate was transferred to an oven to be warmed at 60°C until the cells were trypsinized and the cell printer prepared for seeding.

A T75 flask of hMSCs at near cent per cent confluence was transferred to the biosafety cabinet, and the cells trypsinized following standard Trypsinization procedure. The suspension was centrifuged and supernatant media containing trypsin suctioned out. The cell pellet was re-suspended at a concentration of 500,000 cells/mL (equivalent to 50,000 cells per 100 µL).

100 µL of cell suspension was added to a sterile bioreactor assembly for the tube-rotator method (described previously) containing a 2 cm long fibrin thread bundle composed of 12 individual microthreads. Slide clamps were attached at both ends of the tubing to make it water-tight. The assembly was then placed in a 50 mL conical tube which was then mounted on the tube rotator (Figure 29), while the awaiting the other bundle to be seeded using the cell printer.

A much smaller volume of cell suspension could be accommodated on the thread bundle mounted on the bioreactor assembly for the cell printer. It was determined by empirical testing, that 10 µL of cell suspension could be accommodated on 2 cm length of the fibrin thread bundle. In order to deliver 50,000 cells in 10 µL to the thread bundle (instead of 100 µL in the tube rotator method), the cell suspension had to be concentrated 10 times. For this, the remaining cell suspension was centrifuged at 1000 rpm for 3 minutes. The supernatant media was suctioned out and the cell pellet was re-suspended in fresh pre-warmed cell culture media at a concentration of 5,000,000 cells/mL (equivalent to 50,000 cells per 10 µL). This cell suspension (which was usually no more than 100 µL total) was transferred to a sterile 0.65 mL Eppendorf tube.

The 6-well plate containing the bioreactor assembly for the cell printer placed in the oven for warming was removed and transferred to the biosafety cabinet housing the cell printer, along with the Eppendorf tube containing the cell suspension. The 6-well plate was then mounted on the rear plate-holder of the cell printer's deck and the media inside the well containing the delrin ring assembly suctioned out leaving the hydrated thread bundle suspended in mid-air, held horizontal, parallel to the printer's deck. The thread bundle was then aligned along the X-axis of the printer (to follow the print pattern of the print program).

The seeding program on the cell printer which was kept ready at the start of the experiment was then executed, and the cell suspension seeded onto the thread bundle, following the procedure described in the previous section, over a run-time duration of ten minutes. Note that the hydrated thread bundle was suspended in mid-air and was not in contact with any culture medium.

Because of this, all the cell suspension that was dispensed onto the thread bundle remained on the bundle due to hygroscopic properties of the fibrin thread bundle and surface tension of the cell suspension, not allowing it to fall off.

The 6-well plate containing the thread bundle freshly seeded with hMSCs was then unmounted from the printer's deck and transferred to the incubator to be incubated at 37°C under atmospheric oxygen, 5% carbon dioxide and 85% relative humidity for twenty minutes.

The thought behind this short incubation was to allow some initial attachment of the hMSCs on the fibrin thread bundle, while at the same time not causing cell damage due to dehydration. If the freshly seeded thread bundle would be immersed in media immediately, the cells would disperse and the advantage of using the cell printer to target the thread bundle would be lost. However, preventing dehydration was also important. Immediately after the cell suspension was dispensed onto the thread bundle using the cell printer, the little amount of media (10 µL) was the only source of hydration for the cells and the thread bundle. At room temperature and moisture conditions, this amount of media would evaporate within minutes. So it was also necessary to hydrate the seeded thread bundle with media soon, at the same time allow some time to initiate the process of cell attachment to the threads.

It was empirically determined that twenty minutes inside the incubator was the 'sweet spot' where the media was be evaporated enough so as to not leave any visible liquid on the thread bundle, at the same time, not so much that the thread would be visibly dehydrated. Whether this twenty minute incubation period inside the incubator was enough time to allow any cell attachment at all, or if a different approach can be employed to facilitate targeted attachment on the bundle, will require further work, but for now, the assumption was some cell attachment was occurring.

After this twenty minute initial incubator period, the 6-well plate with the seeded fibrin thread bundle was transferred to a biosafety cabinet. The thread bundle was cut at both ends (beyond the region of where the cells were seeded) to separate the seeded thread from the delrin ring assembly. The bundle was then carefully transferred to a bioreactor assembly similar to the one used for the tube-rotator method: into a sterile 4 cm long silastic tubing. (Figure 27) (The twenty minute incubation period would cause the bundle to stiffen just enough so that it would hold its linear shape when held at one end with a small vascular clamp. This made it possible to insert the bundle into the silastic tubing without scraping their surfaces).

After transferring the bundle into the silastic tubing, 100 µL of media was added to the tubing using a pipette, and slide clamps were attached at both ends of the tubing to make the bioreactor compartment containing the thread bundle water-tight. The bioreactor was then labeled and

placed inside a 50 mL conical tube and mounted on the tube rotator alongside the bioreactor seeded previously with cell suspension (tube-rotator method). (Figure 29)

The tube rotator was set to its lowest rotation speed setting (4 rpm) and placed inside the incubator at 37°C under atmospheric oxygen, 5% carbon dioxide and 85% relative humidity for 24 hours.

4.4.5: Protocol for staining thread bundles for microscopy

After 24 hours, the tube rotator with the conical tubes containing the bioreactor assemblies with seeded fibrin thread bundles was removed from the incubator. The thread bundles were removed from their respective bioreactor assemblies and were rinsed with phosphate-buffered saline to prepare them for fixation.

The bundles were then immersed in 4% paraformaldehyde (Boston Bioproducts, Worcester, MA) for ten minute to fix the thread bundle and the cells attached to it.

Two stains were used to stain the threads for confocal microscopy – Phalloidin and Ethidium Homodimer-1.

Phalloidin (Alexa Fluor 488 conjugated Phalloidin, Molecular probes, Invitrogen, Carlsbad, CA) stains F-actin filaments which constitute the cytoskeleton of cells. F-actin filaments are present in the cytoplasm. Their orientation indicates the alignment and morphology of a cell. Phalloidin staining not only helps identify the cytoplasm but also helps identify cell alignment and orientation. Phalloidin fluoresces bright green (excitation∕emission: 495nm∕518 nm).

Ethidium Homodimer-1 (part of Live/Dead Viability/Cytotoxicity kit, Molecular probes, Invitrogen, Carlsbad, CA), stains nucleic acids – both DNA and RNA, in cells whose cell membranes have been compromised (fixation by paraformaldehyde was sufficient to allow penetration of Ethidium in cells). DNA present in the nucleus takes up the dye strongly fluorescing bright red (excitation/emission ~495 nm/~635 nm). Ethidium Homodimer-1 was selected as a nuclear dye for this project because of its resistance to bleaching over time with exposure to laser light (used in confocal microscopy), compared to other nuclear stains such as Hoechst 33342.

While awaiting the bundles to be fixed by 4% paraformaldehyde, fresh dye solutions of the dyes were prepared: 25 µL if Phalloidin added to 975 µL of phosphate buffered saline (PBS) and 2 µL of Ethidium Homodimer-1 in 998 µL of PBS. (Concentrations were selected as per the recommendations by the manufacturer).

The fixed thread bundles were transferred onto a 24x50 mm rectangular cover slip (VWR, Radnor, PA) and washed twice with PBS to remove residual paraformaldehyde before adding dyes. (Cover slips were used instead of regular microscope slides to facilitate viewing of deeper fields on confocal microscopy).

The microthread bundles were permeabilized with 0.25% Triton X-100 (Sigma Aldrich, St. Louis, MO) in PBS for 10 minutes, followed by rinsing with PBS. The bundles were then treated with 1% bovine serum albumin (Sigma Aldrich, St. Louis, MO) in PBS for 30 minutes to reduce non-specific binding of the dyes.

The bundles were then stained with Phalloidin for 30 minutes, washed with PBS thrice, and treated again with 1% bovine serum albumin again thrice for 5 minutes each, to wash off any residual Phalloidin that did not bind to the thread bundles.

Thereafter, Ethidium Homodimer-1 dye solution was added to the bundles for 15 minutes, followed by two washes of PBS.

Finally, spacers for were placed around the thread bundles on the coverslips to prevent the threads from being flattened under the weight or pressure of the opposite coverslip. Another coverslip of the same size (24x50 mm) was used for sealing each mounted thread bundle, with a sealing solution – Cytoseal 60 (Thermo Scientific, Waltham, MA) being used to seal two coverslips together(Figure 34). The sealant was allowed to cure for 4 hours before any imaging was done.
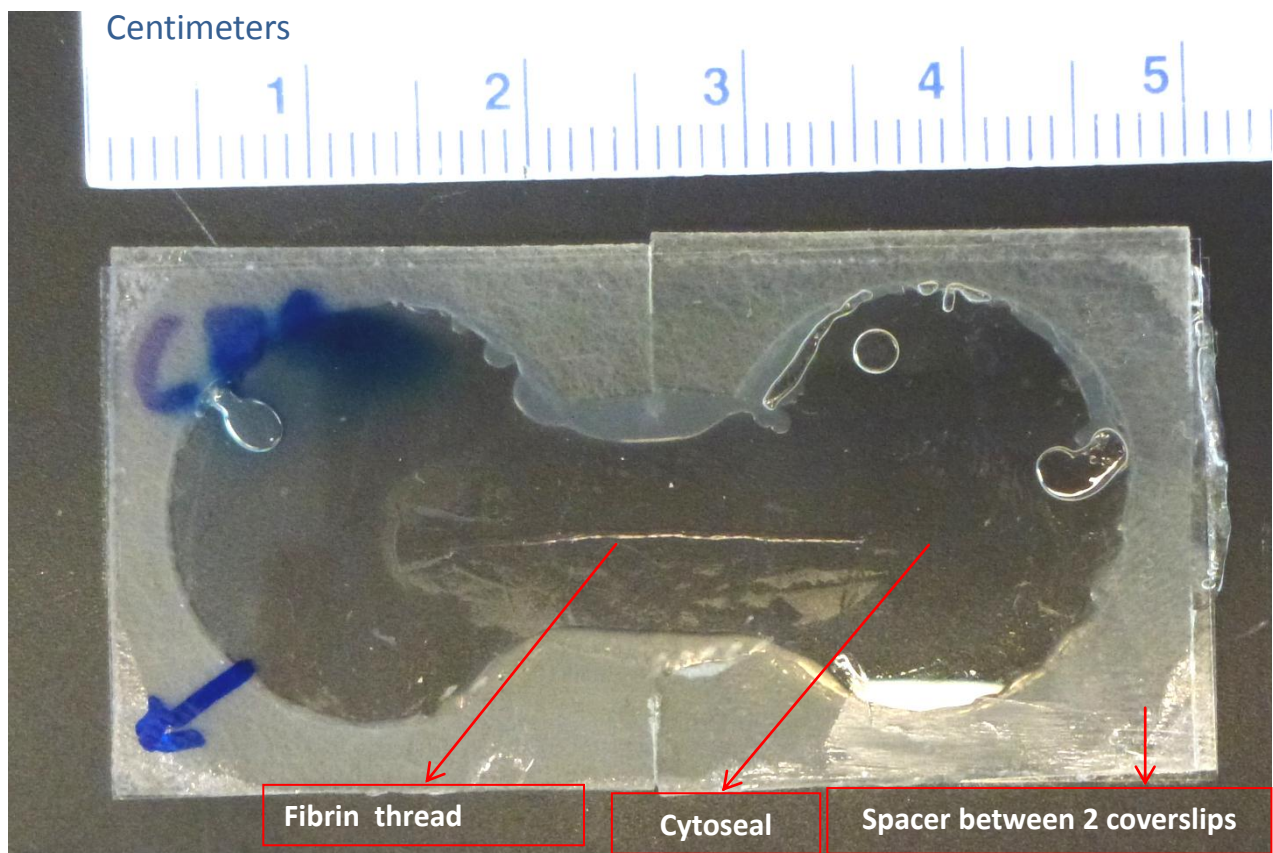

Figure 34: Stained fibrin thread bundle mounted in between two 24x50 mm coverslips.

4.4.6: Confocal Imaging

Fluorescent microscopy was good enough to qualitatively assess if a particular fibrin thread seeded with hMSCs and if so, how well. However, because of the 3 dimensional shape of the thread bundle, the cells attached on the entire semi-cylindrical circumference of the bundle and the groves in between individual microthreads, cells were situated in different planes. Capturing cells situated in different focal planes ordinary fluorescent microscopy was proving to be extremely time consuming and tedious.

With confocal microscopy, light from different focal planes of the object to be visualized can be captured separately. This way a separate image can be constructed for each focal plane. Images of different focal planes of the same region of the object can then be overlaid to generate a 'Maximum Projection' of that region, revealing objects spanning different focal planes in a single image. This was ideal to visualize a thread bundle seeded with hMSCs situated in different focal planes along the contours of its semi-cylindrical surface, complicated by twisting of the fibrin microthreads on each other.

Seeded thread bundles were visualized using confocal microscopy (Leica TCS SPS II point scanning confocal microscope) from end-to-end in partly overlapping segments at 20x magnification using laser-lights of specific wavelengths to excite the fluorescent dyes and appropriate filters with photomultiplier tubes used to capture emitted light in specific wavelengths.

Two lasers were utilized to excite the fluorescent molecules in the sample: an Argon laser emitting at 488 nm for Alexa Fluor 488 conjugated Phalloidin, and a Diode-pumped solid state (DPSS) laser emitting at 561 nm for Ethidium Homodimer-1 (which is excited over a wide range of wavelengths around 495 nm). Two photomultiplier tubes were used to collect and amplify the signal from the two fluorophores: one capturing a bandwidth of 499 to 545 nm for Phalloidin, and another capturing a bandwidth of 595 to 647 nm for Ethidium Homodimer-1.

For the actual imaging process, the thread bundle mounted in between two coverslips was mounted on the stage of the confocal microscope. The stage was moved to locate one end of the thread bundle, which was then positioned in the center of the viewing field of the confocal microscope. Serial Z-sections of the thread bundle (known as a 'Z-stack') were taken at 2 µm intervals to a depth of about half of its circumference, starting from the most superficial plane, visualizing progressively deeper planes until approximately half thickness of the thread bundle was reached (a total depth of about 250 µm, varying slightly from bundle to bundle). A maximum projection was generated to visualize all focal planes of that segment of bundle in a single image. The microscope stage was then moved to bring the adjacent segment of the thread bundle in the microscope's view, followed by Z-stack of that section, and a maximum projection. This process was repeated until the other end of the thread bundle was reached. (Figure 35)

A slight overlap between two adjacent segments of the bundle was maintained while imaging all segments, to facilitate 'stitching' of the images together.
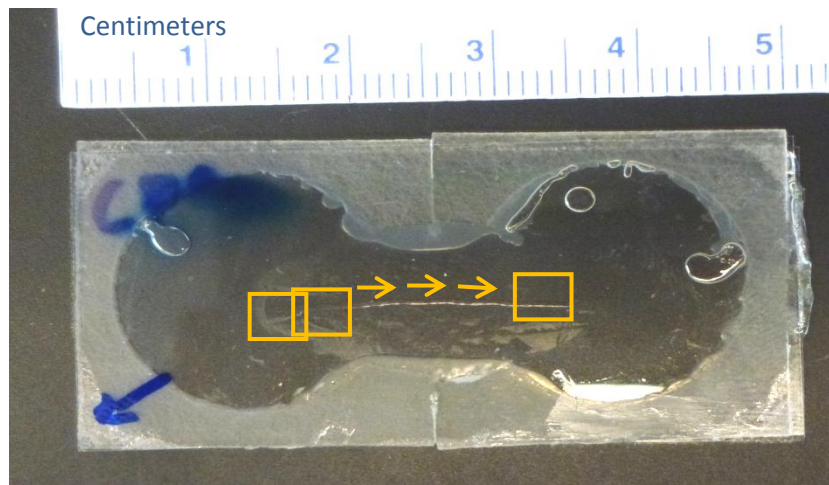

Figure 35: Confocal imaging of a seeded fibrin thread bundle from end to end in partially overlapping segments

4.4.7: Post-processing of images – Stitching using Adobe Photoshop

Maximum projections of all segments of the thread were stitched together using software (Adobe Photoshop) to generate a single image of one half of the circumference of the entire length of the thread. This image was effectively a 2-dimensional projection of one side (semi-cylindrical half) of the thread bundle. (Figure 36, Figure 37)
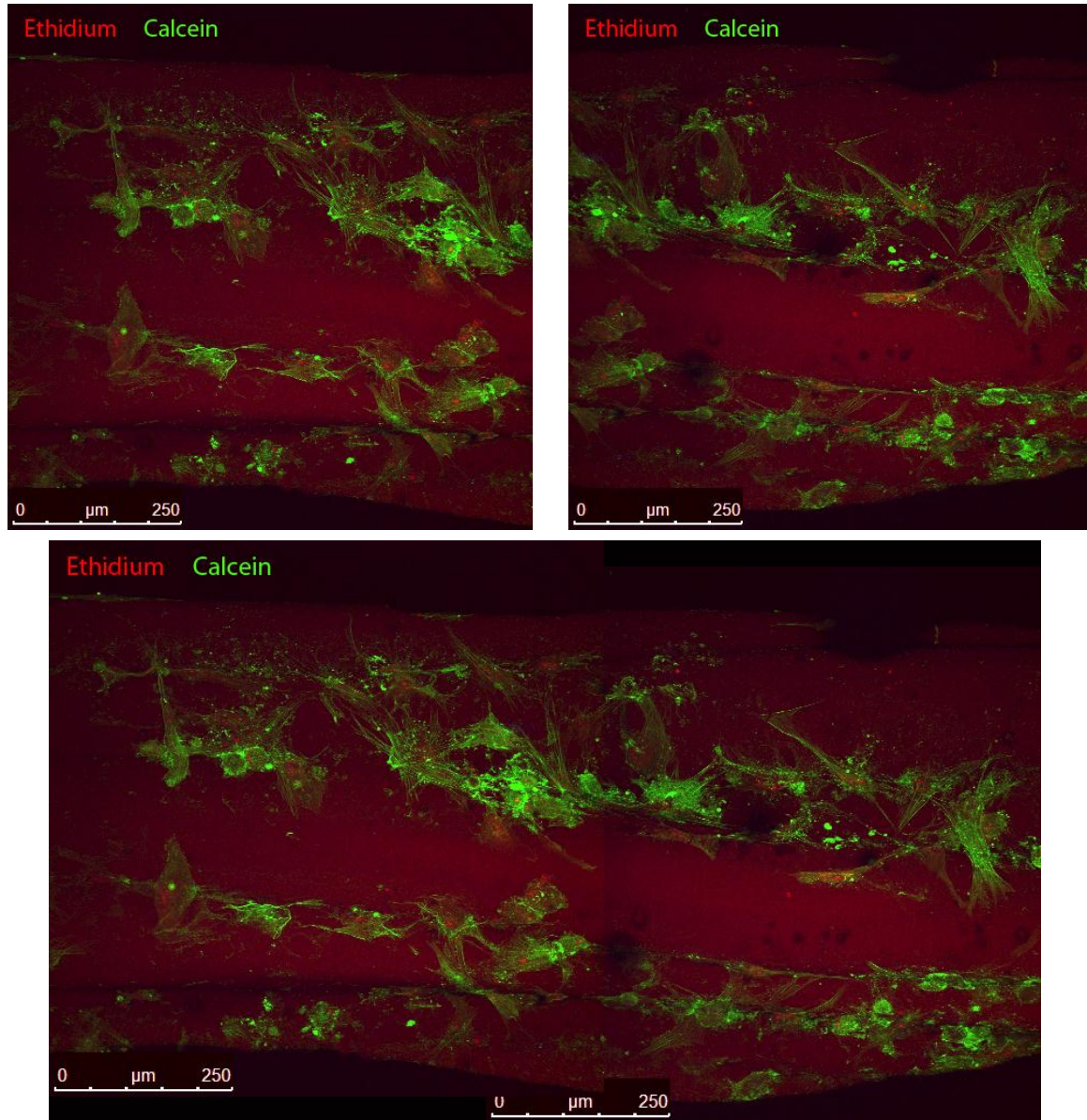
Figure 36: Stitching images of adjacent segments of a fibrin thread bundle. Individual segments of the seeded fibrin thread bundle were imaged in different planes of depth starting from the most superficial to the deep, covering about half the diameter of the bundle, creating a 'Z-stack'. Maximum projections of these yielded a 2D projection of one half of the circumference of that segment of the bundle. Such maximum projections of two adjacent segments are shown here in the top two images. These images were then stitched together using Adobe Photoshop to yield a single image depicting the segment of the thread covered by the individual images (bottom image). Similar, images of adjacent segments of the entire bundle were stitched together to yield a single image of the bundle from end to end.
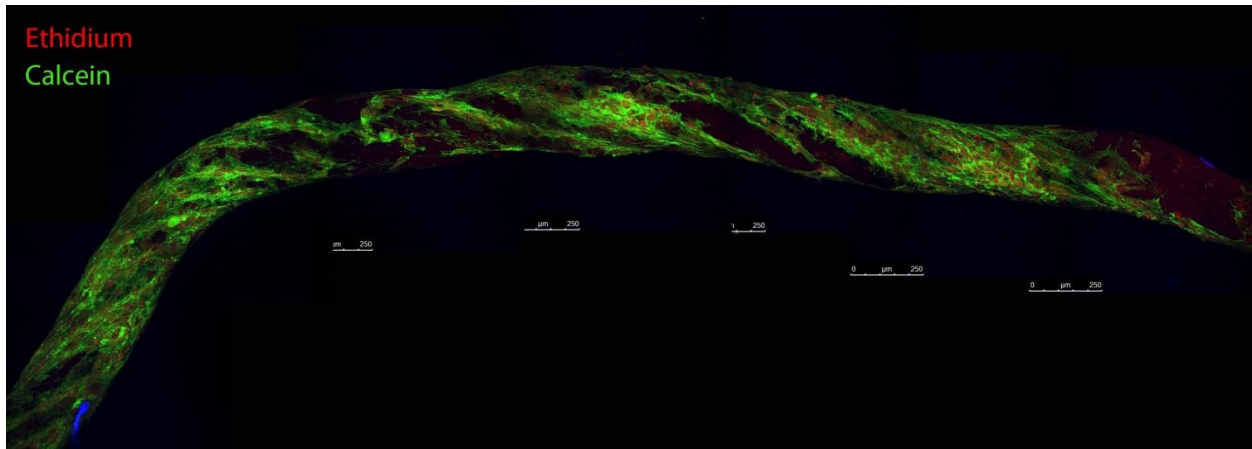
Figure 37: Image of a thread bundle obtained by stitching images of segments of the bundle together. Note the characteristic twisting appearance of the individual microthreads on each other in the bundle. Green = Phalloidin (F-actin filaments of cytoplasm of seeded hMSCs). Red = Ethidium Homodimer-1 (Nucleic acids, predominantly DNA of nuclei of cells).

4.4.8: Counting cells seeded on thread bundles and calculation of seeding efficiency

Phalloidin and Ethidium stained hMSCs seeded on thread bundles were counted manually by eye from the image of the entire bundle obtained by stitching images of individual segments of the bundle from end to end. Counting was done by at least two individuals for each thread bundle to account for variability in counts due to subjectivity, and the average of all counts was considered for calculations of seeding efficiency.

The count was obtained from the image of half the circumference of the thread bundle. Under the fair assumption that cells seeded evenly on both sides of the fibrin thread bundle, this count was considered as representing half the number of cells seeded on the entire bundle. Thus, the total count of number of cells seeded was obtained by multiplying this count by 2.

Calculation of seeding efficiency

Because fibrin thread bundles were bundled and cut manually, there was some variation in length and diameter from bundle to bundle.

To account for the variations in diameter from bundle to bundle, full length bundle of 18 cm was cut into two halves, with one half being used in the bioreactor assembly to seed with the cell printer while the other half being used in the bioreactor assembly for the tube rotator method. These were always used in pairs for comparison of seeding efficiency, to make sure that the diameter of the seeded bundles being compared was similar.

To account for the variations in the length of the bundles, the number of seeded cells counted for each bundle was normalized to the length of the bundle, i.e. the number of cells seeded per millimeter length of the bundle was calculated for each bundle.

For this, first the total number of cells seeded on the bundle was manually counted as described previously. The length of each bundle was measured using software from the image of the entire bundle generated after stitching using software (Adobe Photoshop). The number of cells seeded per millimeter length of the bundle was then calculated by dividing the total number of cells seeded by the length of the bundle in millimeters.

The number of cells available for seeding each millimeter length of the bundle was calculated by dividing the total number of cells used for seeding the bundle (50,000) by the length of the bundle in millimeters.

The efficiency of seeding was calculated per millimeter length of the bundle by dividing the number of cells that seeded per millimeter by the number of cells that were available for seeding per millimeter length of that bundle.

For example, if the count of cells obtained from the image of a bundle was 2500, the total count of cells seeded on the bundle would be 2500 x 2 = 5000 cells. Suppose the length of this particular bundle was 20 mm. The number of cells seeded per mm =5000/20 = 250 cells per mm.

The number of cells available for seeding each millimeter of the bundle = Number of cells used to seed the bundle (50,000) divided by the length of the bundle in millimeters (20) = 50000/20 = 2,500 cells per mm

Efficiency of seeding = (Number of cells seeded per mm) / (Number of cells available for seeding per mm) *100

$$= (2,500/25,000)*100 = 10 \%$$

4.4.9: Comparison of seeding efficiency
The mean seeding efficiency per millimeter length of bundle was calculated for each group, and was used for comparison between the groups. The hypothesis that there is no difference in the efficiency of seeding hMSCs onto the bundles using the two methods – the tube rotator method and the cell printer – was tested statistically.

4.5: Statistical Analysis
Statistical analyses were performed using a combination of manual calculations and Analysis ToolPak in Microsoft Excel 2010. Statistical differences were determined using unpaired, two-tailed T tests assuming that the two comparison groups had unequal and unknown population variances. All data was reported in the following format unless otherwise noted: mean ± standard deviation. All experiments had a minimum of n = 3. A p-value < 0.05 was considered as a statistically significant difference between groups.

Chapter 5: Results

5.1: Post-printing Viability of Human Mesenchymal Stem Cells:

For each well of the 96-well plate seeded with hMSCs, an image of the entire well was constructed by stitching images of different regions of the well using Adobe Photoshop. Representative images of wells seeded using the cell printer and a hand-held pipette are shown in respectively.
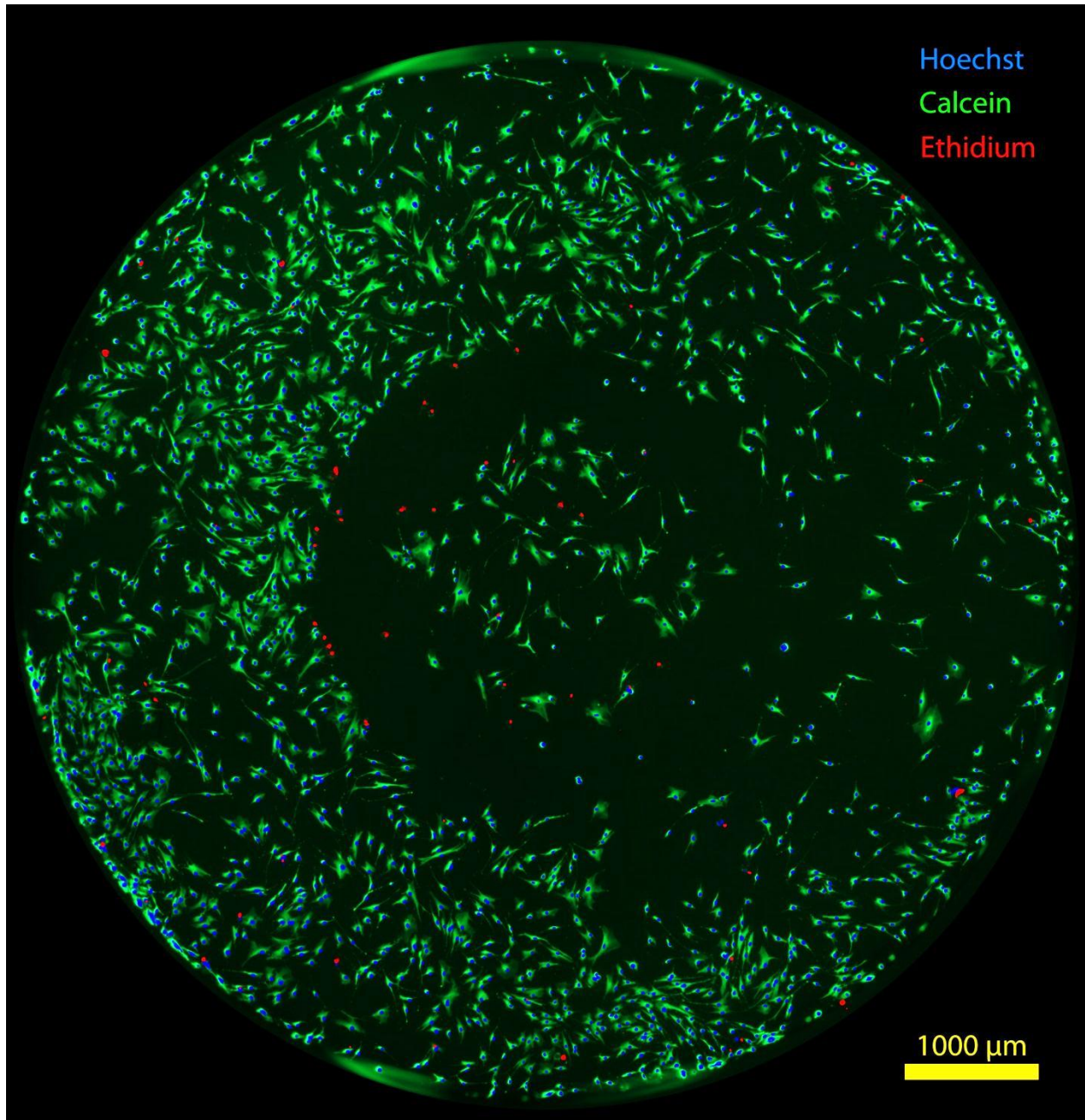
Figure 38: Representative image of a well of a 96-well plate seeded with hMSCs using the cell printer. Cytoplasms of live cells show a bright green Calcein signal. Nuclei of dead cells show a red Ethidium Homodimer-1 signal. All nuclei show a blue Hoechst 33342 signal.
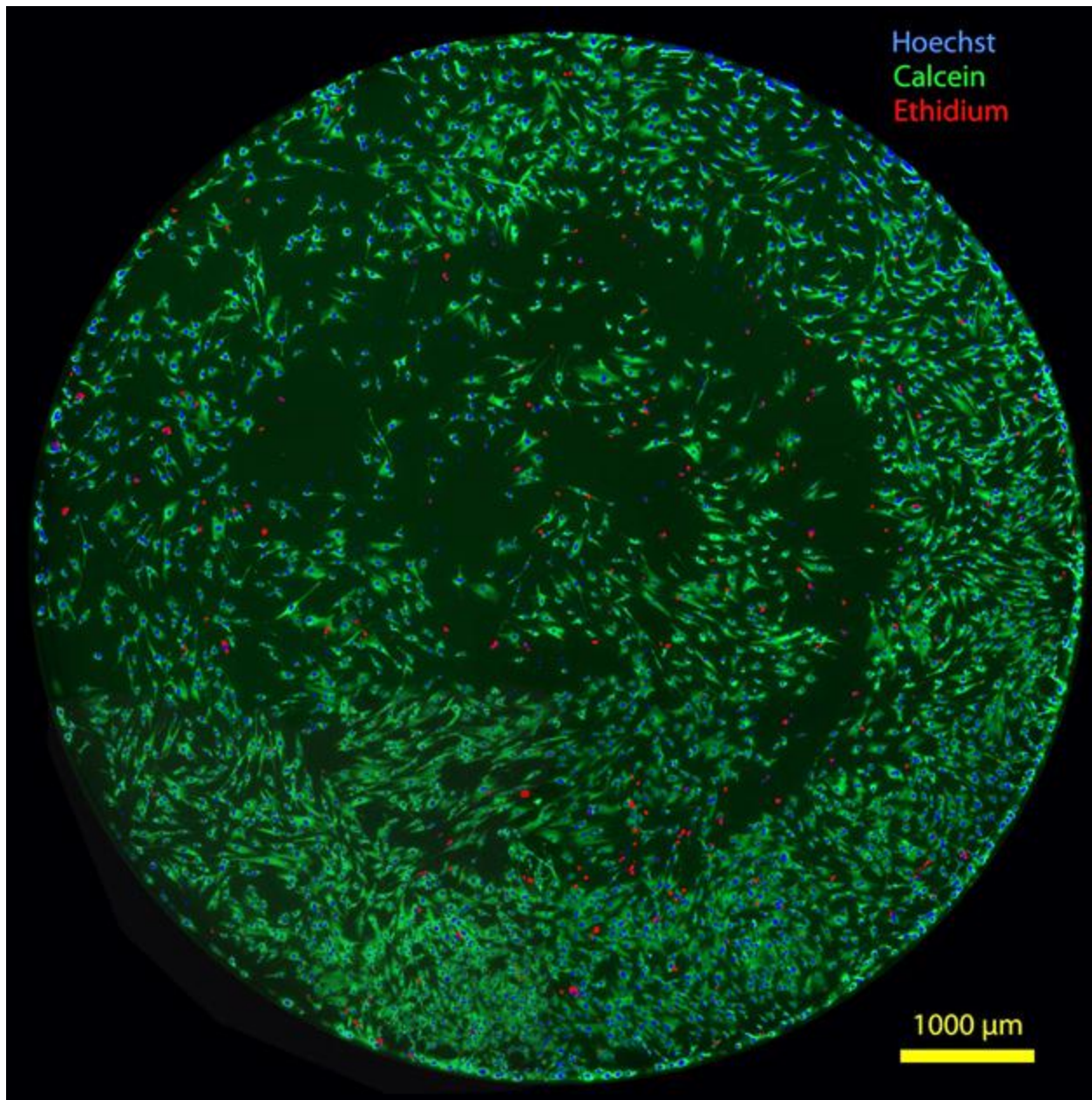
Figure 39: Representative image of a well of a 96-well plate seeded manually with hMSCs using a hand-held pipette. Cytoplasms of live cells show a bright green Calcein signal. Nuclei of dead cells show a red Ethidium Homodimer-1 signal. All nuclei show a blue Hoechst 33342 signal.

Images of all wells were analyzed using CellProfiler as described earlier in order to obtain the percentage of viable cells in all wells seeded either using the cell printer or a handheld pipette. The mean percentage of viable cells in the two groups – cell-printer dispensed and manually pipetted is shown in Figure 40. The viability of hMSCs 24 hours post-dispensing using the cell printer was found to be 90.9 ± 4.0 % and by manual pipetting was 90.6 ± 8.2 % (mean ± standard deviation) with an n of 12 in both groups (Figure 40). P-value obtained by applying a Students' T-test assuming the samples in two groups are derived from independent populations with unequal and unknown variances was 0.90 (not significant).

The number of cells counted in individual wells - live, dead and total, and the percent viability for each well for the cell printer group are listed in

Table 1, and the same for the manually pipetted group are listed in Table 2.
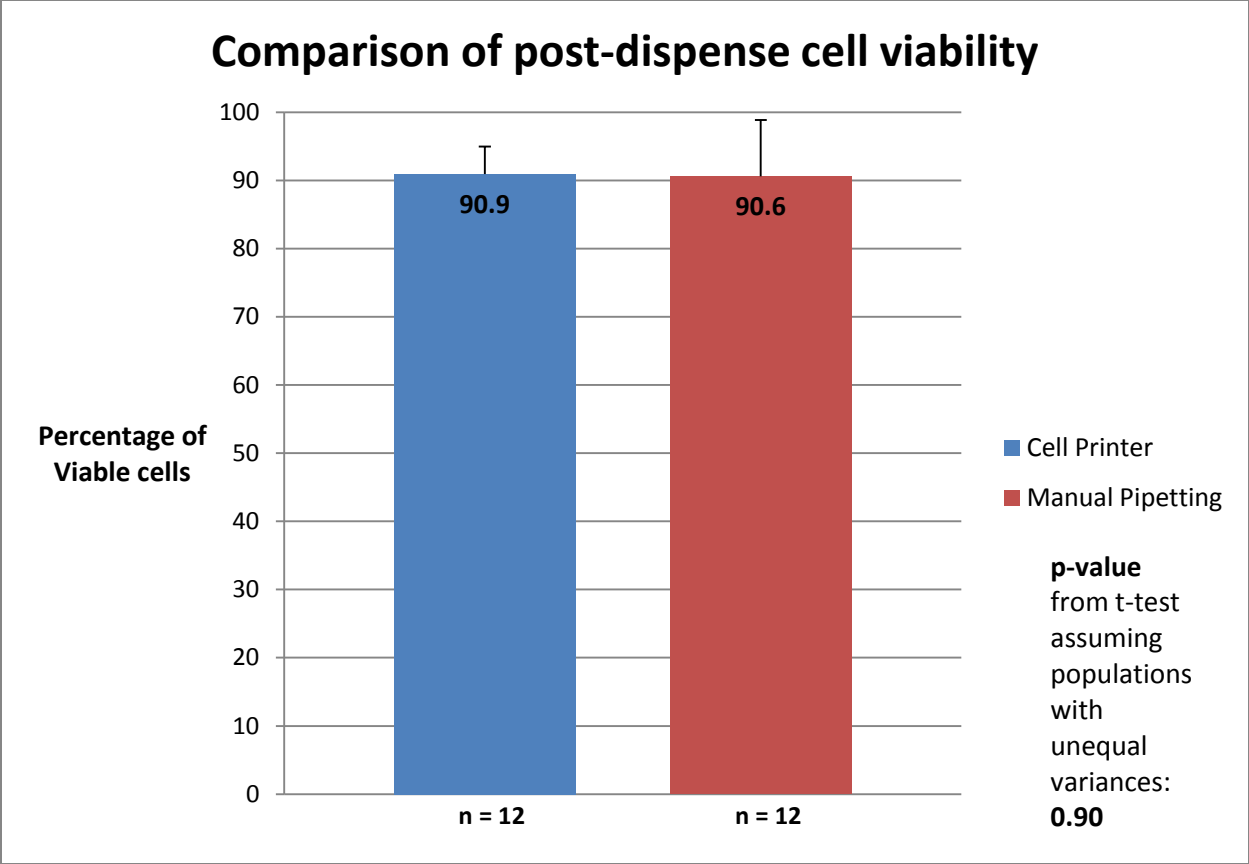
Figure 40: Viability of hMSCs 24 hours post dispensing. Mean viability for all wells containing cells dispensed using the cell printer is depicted in blue, and for wells with cells dispensed manually using a hand-held pipette is depicted in maroon.

Table 1: Viability of cell dispensed using the cell printer

Well no.	Live cell count	Dead cell count	Total cell count	Percentage of live cells
1	2364	247	2611	90.54
2	1988	119	2107	94.35
3	1792	351	2143	83.62
4	1836	167	2003	91.66
5	1800	70	1870	96.26
6	2158	161	2319	93.06
7	2477	120	2597	95.38
8	2728	318	3046	89.56
9	3000	197	3197	93.84
10	1879	302	2181	86.15
11	2702	270	2972	90.92
12	2095	342	2437	85.97
Average	2235	222	2457	**90.94 %**
Standard dev.	413	96	434	**4.00 %**

Table 2: Viability of cells dispensed manually using a handheld pipette

Well no.	Live cell count	Dead cell count	Total cell count	Percentage of live cells
1	4288	190	4478	95.76
2	4616	235	4851	95.16
3	3299	196	3495	94.39
4	3174	323	3497	90.76
5	1595	746	2341	68.13
6	3355	804	4159	80.67
7	3304	230	3534	93.49
8	3612	191	3803	94.98
9	3593	177	3770	95.31
10	4091	342	4433	92.29
11	3635	152	3787	95.99
12	4123	439	4562	90.38
Average	3357	335	3893	**90.61 %**
Standard dev.	765	222	671	**8.24 %**

Counts of nuclei of live and dead cells from the data obtained by analyzing images of entire wells using Cell Profiler image analysis software for individual wells in both groups based on the protocol described in section 4.2.1.1: Obtaining Accurate Counts of Viable hMSCs from Image Analysis: is listed in tables in Appendix A: Post-Printing Cell Viability Measurements.

There is a noticeable difference in the average live, dead and total cell count per well in the two groups. Upon statistical analysis, this difference was found to be significant ($p<0.05$) with the number of live and total cells per well in the cell printer group significantly less than the number of live and total cells per well in the handheld pipetted group.

The reason for this observation is unclear. A possible scenario that explains the observed difference is non-uniform splitting of cell suspension: when the cell suspension was split into two halves of equal volume (into two 0.65 mL Eppendorf tubes), each half to be used for dispensing cells for each of the two methods, it is possible that more cells were transferred in the aliquot used for dispensing using a hand-held pipette than in the aliquot used for dispensing using the cell printer. This could be due to non-uniform distribution of cells in suspension because of cell settling or otherwise. Alternatively, in a less likely scenario, the cell printer was dispensing less cell suspension than it was programmed to, and thus correspondingly less number of cells were dispensed per well.

In view of this, another experiment was performed to determine whether the observed difference was due to accidental non-uniform splitting of the cell suspension or due to an actual defect in the dispensing mechanism of the cell printer. A fixed volume (10 µL) of suspension of human fibroblasts (P14) (Lonza, Walkersville, MD) in Dubecco's modified Eagle's medium having a concentration of 600,000 cells/mL was dispensed using the cell printer in ten 0.65 mL Eppendorf tubes. Ten µL of the same cell suspension was dispensed into another ten 0.65 mL Eppendorf tubes using a handheld pipette, in parallel.

Ten µL of 0.04% Trypan Blue (Invitrogen, Carlsbad, CA) was added to all Eppendorf tubes containing 10 µL of cell suspension. The number of live, dead and total cells was counted using the Trypan Blue exclusion principle on a hemocytometer (Hausser Scientific, Horsham, PA) using an inverted light microscope (Nikon TMS, Tokyo, Japan) in all ten samples in both groups.

The counts of live, dead and total cells per 10 µL of suspension dispensed using the cell printer are given in Table 3, while the same for 10 µL of cell suspension dispensed using a handheld pipette are given in Table 4. A graphical comparison of the number of cells dispensed in the same volume using the two methods is made in Figure 41. Comparison of cell viability is shown in Figure 42.

The number of live cells, dead cells, total number of cells and percent viability were found comparable in both groups (p-value not significant for all categories). This indicates that the volume of cell suspension dispensed using the cell printer (and thus the number of cells dispensed) is the same as programmed. Thus, the observed difference in the average number of live and total cells dispensed in the cells dispensed in the previous experiment was probably due to uneven cell distribution in suspension rather than an error in the dispensing mechanism of the cell printer.

Additionally, the percent viability data obtained experiment using human fibroblasts indicates that the dispensing process using the cell printer does not affect the viability of the cells, which correlates well with the cell viability data obtained in the previous experiment using hMSCs.

Table 3: Number of cells per 10 µL of cell suspension dispensed using the cell printer*

Sample no.	Live cells	Dead cells	Total	Viability %
1	5889	222	6111	96.36
2	5444	222	5667	96.08
3	5022	200	5222	96.17
4	5267	267	5533	95.18
5	5578	244	5822	95.80
6	6267	311	6578	95.27
7	6000	467	6467	92.78
8	5311	467	5778	91.92
9	5378	156	5533	97.19
10	6422	67	6489	98.97
Average	5658	262	5920	**95.57**
Standard Deviation	463	126	468	**2.02**

Table 4: Number of cells per 10 µL of cell suspension dispensed using a handheld pipette*

Sample no.	Live cells	Dead cells	Total	Viability %
1	5133	244	5378	95.45
2	5333	156	5489	97.17
3	5333	289	5622	94.86
4	6289	333	6622	94.97
5	4822	422	5244	91.95
6	6067	222	6289	96.47
7	5800	178	5978	97.03
8	6244	222	6467	96.56
9	6044	378	6422	94.12
10	6222	200	6422	96.89
Average	5729	264	5993	**95.55**
Standard Deviation	530	89	517	**1.64**

*p-value was found to be non-significant for all categories (live cells, dead cells, total cells and viability %) between the two groups with the null-hypothesis that there is no difference between the two groups (cell printer and handheld pipette) tested using an unpaired two-tailed Student's T-test assuming independent populations with unequal variances.
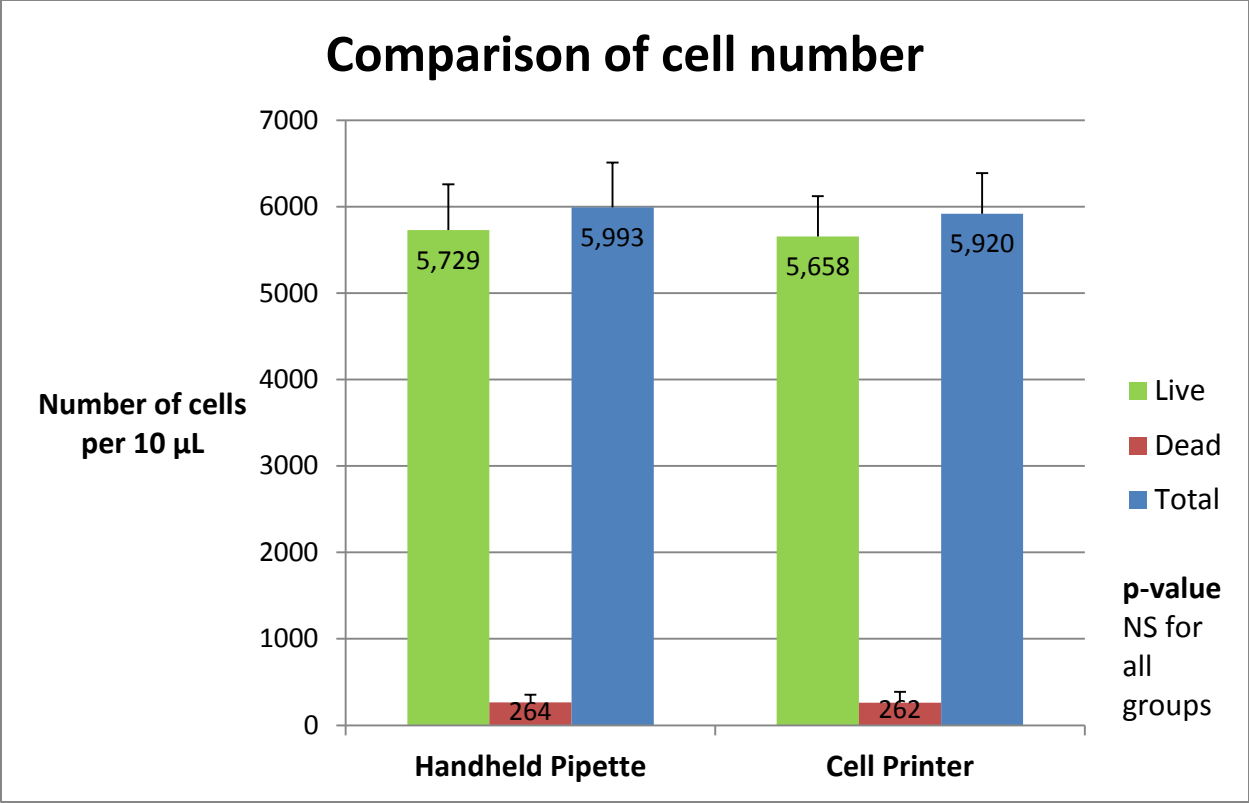
Figure 41: Comparison of number of cells (human fibroblasts) dispensed per 10 μL of cell suspension using a handheld pipette and the cell printer
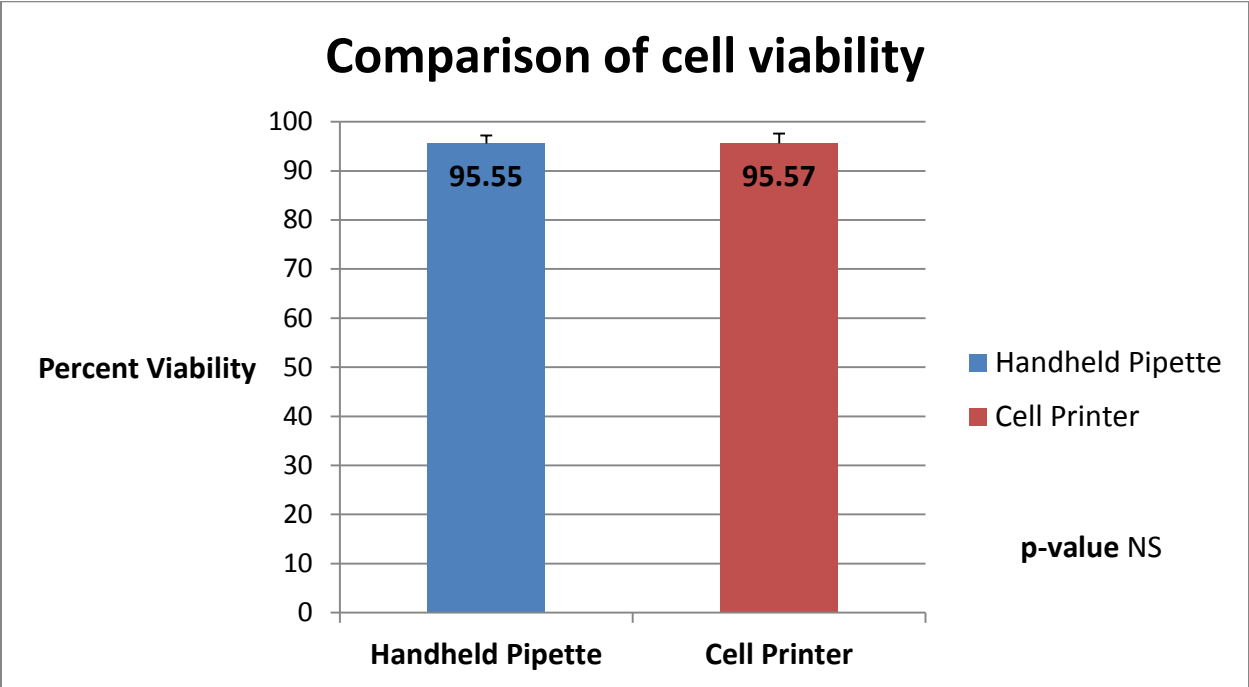

Figure 42: Comparison of cell viability of human fibroblasts dispensed using a handheld pipette and the cell printer

The presented data from the viability experiment using hMSCs and human fibroblasts indicates that the dispensing (or 'printing') process from the cell printer does not affect the viability of the cells. This is consistent with findings of previous in-house studies by Digilab, Inc. in which viability of other cell types was assessed at different time points after dispensing using the cell printer and was found to be satisfactory: mean viability of human myosatellite (satellite) cells assessed 3 hours post-printing was 98.4 %, and that of rat arterial smooth muscle cells 12 hours post-printing was 97.5 % (unpublished data from Digilab, Inc.; via personal communication).

Considering that the mechanical forces acting on the cell suspension when it is aspirated and dispensed using the cell printer with sufficiently low flow velocity are not very different from those that the suspension would experience in a hand-held pipette, the consistent high cell viability observed post-printing with different cells types is not unexpected (described in the discussion chapter). This observation has far reaching implications if various current and possible applications of the cell printer are considered – the cell printer is equivalent to a handheld pipette as far as viability of cells is concerned, with the added advantages of robotic dispensing, automation and user-specified pattern generation in two and three dimensions of space.

Other cell printing technologies such as inkjet printers modified for bioprinting and laser-induced forward transfer (LIFT) bioprinters have their limitations with regard to cell viability, undesirable mechanical or other physical stresses on the cells, low throughput, and commercial non-availability of printing equipment (3), (63), (5) (detailed in Discussion chapter). These technologies have a sub-micron level printing accuracy and may be the method of choice for applications where such accuracy of cell printing is desired. However, for applications where printing accuracy of tens of microns is acceptable, Digilab's automated liquid handling technology on which the cell printer is based has distinct advantages over Inkjet and Laser-based bioprinters.

Having determined that the printing process on the cell printer following a certain set of parameters does not affect the viability of human mesenchymal stem cells, whether the printer could deliver cells to a linear target such as a fibrin thread bundle was explored. As described in the methods and materials, a bioreactor assembly was developed for mounting the thread bundles onto the printer's deck (Figure 30, Figure 31) so that a fibrin thread bundle could be held horizontal suspended in mid-air, parallel to the deck to be presented to the printer's dispense tip.

## 5.2: Dispensing hMSCs on fibrin thread bundles:

With a combination of the bioreactor assembly designed to present a fibrin thread bundle to the cell printer's dispense tip and a print program written with special precautions to keep dispense parameters conducive to allowing the dispensed cell suspension cling onto the thread bundle, a highly precise delivery of the cell suspension onto the thread bundle was achieved. These precautions included dispensing cell suspension at low flow velocities (5 µL/sec), maintaining minimal distance between the dispense tip and target (thread bundle) (< 100 µm), slow movement of the dispense head (5 mm/sec), and dispensing the total solutions in aliquots of individual droplets of small volume (50 nL) distributed over a 2 cm length of the bundle with sufficient inter-droplet distance, to prevent accumulation and subsequent spillage at any single point on the thread bundle.

The total 10 µL of cell suspension was distributed over 2 cm length of the thread bundle using repeated side to side movement of the print head, distributing the suspension uniformly over the length, over a period of 10 minutes. The evaporation of media over the 10 minutes allowed just enough media to remain on the thread bundle to be accommodated in the 2 cm length of the bundle, with some excess for subsequent 20-min incubation period.

Briefly reiterating the staining and imaging protocol, after the 24-hour incubation period, seeded thread bundles were fixed and stained with Phalloidin and Ethidium Homodimer-1. Stained bundles were visualized using confocal microscopy from end to end in partially overlapping segments. Each segment of the bundle was visualized in a series of parallel planes, starting from the most superficial going progressively deeper by 2 µm with each plane, until half the circumference of the bundle was reached. Images of all planes of that segment were then overlaid to form a 'maximum projection' yielding a single image showing half the circumference of the bundle in that segment. Each segment required between 120 to 130 images to cover half the circumference depending upon thickness of the thread bundle.

Maximum projections of individual segments were 'stitched' together using software (Adobe Photoshop) to yield a single image of half the circumference of the entire thread bundle. Number of cells visible in this image was counted to obtain the count of total number of threads seeded on the bundle, and from that, the seeding efficiency. This was done for all thread bundles seeded with hMSCs using either of the two seeding methods – tube rotator or cell printer, to compare the seeding efficiency.

Sample images of thread bundles stained, visualized and stitched as described above are given in Figure 43.
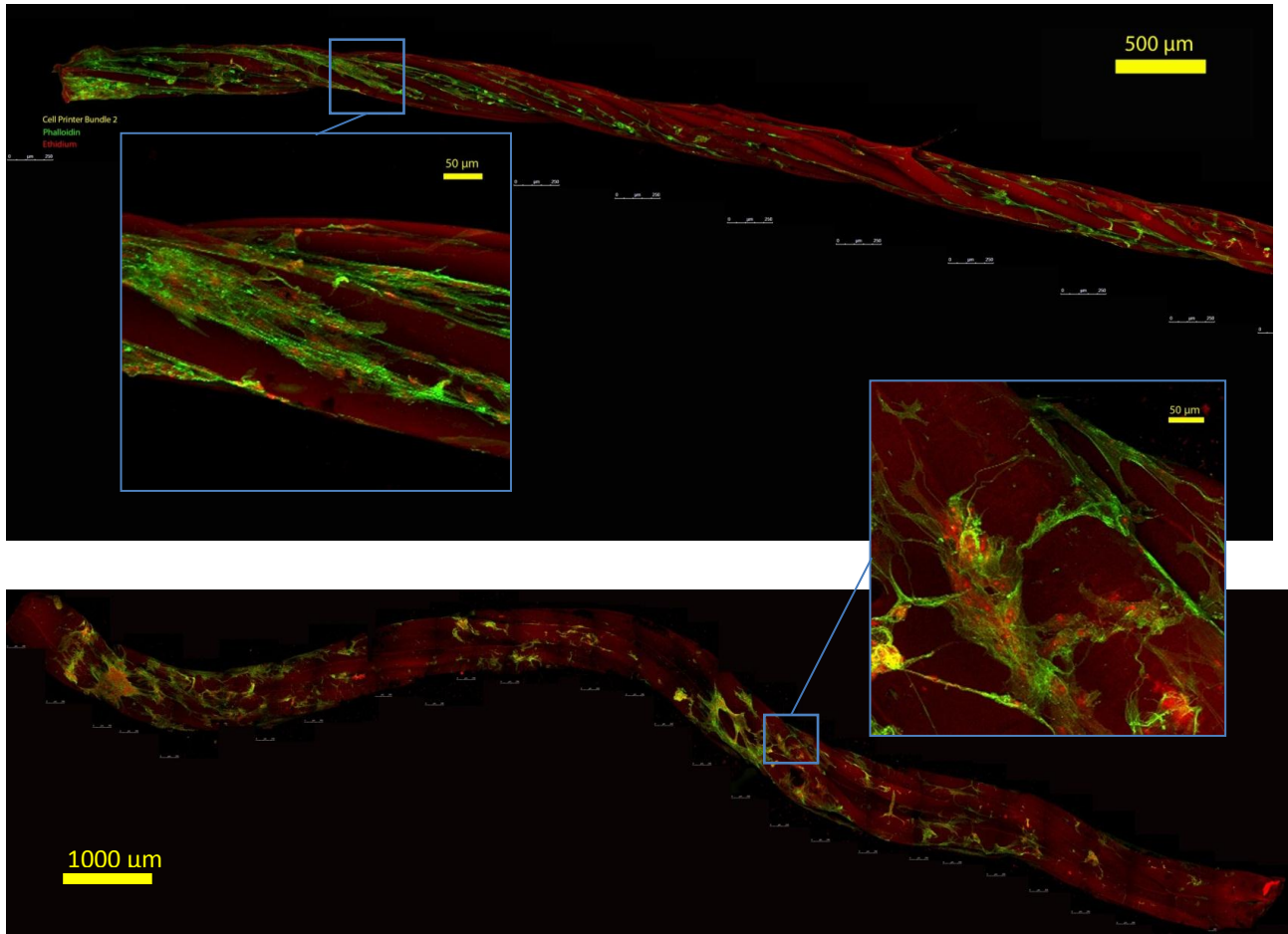
Figure 43: Stitched image of fibrin thread bundles seeded with hMSCs using the cell printer (top) and tube rotator method (bottom), stained with Phalloidin and Ethidium Homodimer-1 and visualized by confocal microscopy. Approximately half the length of a fibrin thread bundle seeded with hMSCs using the cell printer is shown in the top image and the entire bundle length of another bundle seeded using the tube rotator method is show in the bottom image. Cytoskeletal protein F-Actin shows a bright green Phalloidin signal while nucleic acids, predominantly nuclear DNA, show a bright red Ethidium Homodimer-1 signal. Due to reasons not entirely known, the fibrin thread bundles were observed emitting a signal in the Ethidium range, appearing dark red. The twisting of the individual fibrin microthreads on each other is visible in both bundles. Seeding of the cells appeared to be patchy and non-uniform, with preferential seeding in the grooves in between the individual microthreads. Each image was constructed by stitching several individual maximum projection images of segments of the respective bundle from one end to the other. One such segment from each bundle is shown in an inset alongside images of both bundles.

From the image of the entire thread bundle, the number of cells seeded for each bundle was counted manually by at least two individuals and the average of all counts was considered for calculation of seeding efficiency.

In order to account for variations in the length from bundle to bundle, seeding efficiency was calculated per millimeter length for all bundles as explained in the methods and materials chapter. The number of cells per millimeter length of the bundle for each bundle is given in Table 5.

Table 5: Count of number of cells seeded per millimeter length of thread bundle

Thread bundle	Number of cells seeded per mm	Length of thread bundle in mm
Cell-Printer-1	37.89	20.96
Tube-Rotator-1	196.65	17.73
Cell-Printer-2	181.13	16.41
Tube-Rotator-2	250.99	14.02
Cell-Printer-3	70.87	20.08
Tube-Rotator-3	51.95	8.78

The seeding efficiencies calculated on the basis of these numbers per millimeter length of the bundle for each seeded bundle are given in Table 6.

Table 6: Seeding efficiency per millimeter length of thread bundle

Thread bundle pair number	Cell Printer method	Tube Rotator method
1	1.59 %	6.97 %
2	5.94 %	7.04 %
3	2.85 %	0.91 %
Average	**3.46 %**	**4.97 %**
Standard Deviation	2.24 %	3.52 %
p-value	**0.57 (ns)**	

The bundle 'Tube-Rotator-3' was inadvertently damaged during the staining process leaving only about half the original length for staining and examination. The physical damage to the bundle is likely to have caused some attached cells to come off the bundle in addition to damaging the ones that remained attached to the half that was available for analysis. The effect of this damage was evident in the morphology of the thread bundle when the image of the entire bundle was generated. Additionally, the count of cells seeded per mm was markedly lower than those on the other two bundles seeded with the same method (Table 5). Also, when seeding efficiency calculations were performed, the calculated per millimeter cell seeding efficiency was noticeably low as is evident in Table 6.

Due to time constraints, a repeat of the cell seeding experiment on one more pair of bundles was not possible. In light of these events and observations, and bound by the limited available data, the average of per mm seeding efficiency of the other two bundles ('Tube-Rotator-1' and 'Tube-Rotator-2') was used as the representative seeding efficiency of the damaged bundle ('Tube-Rotator-3'), and a revised comparison of seeding efficiency was made. (Table 7, Figure 44)

Table 7: Revised comparison of seeding efficiency per mm length of thread bundle, after correcting for damaged bundle ('Tube-Rotator-3')

Thread bundle pair number	Cell Printer method	Tube Rotator method
1	1.59 %	6.97 %
2	5.94 %	7.04 %
3	2.85 %	7.01 %
Average	**3.46 %**	**7.01 %**
Standard Deviation	2.24 %	0.03 %
p-value	**0.11 (ns)**	

A detailed discussion of the rationale and impact of using the average of per mm seeding efficiency of the former two bundles to represent the latter is done in the Discussion chapter.
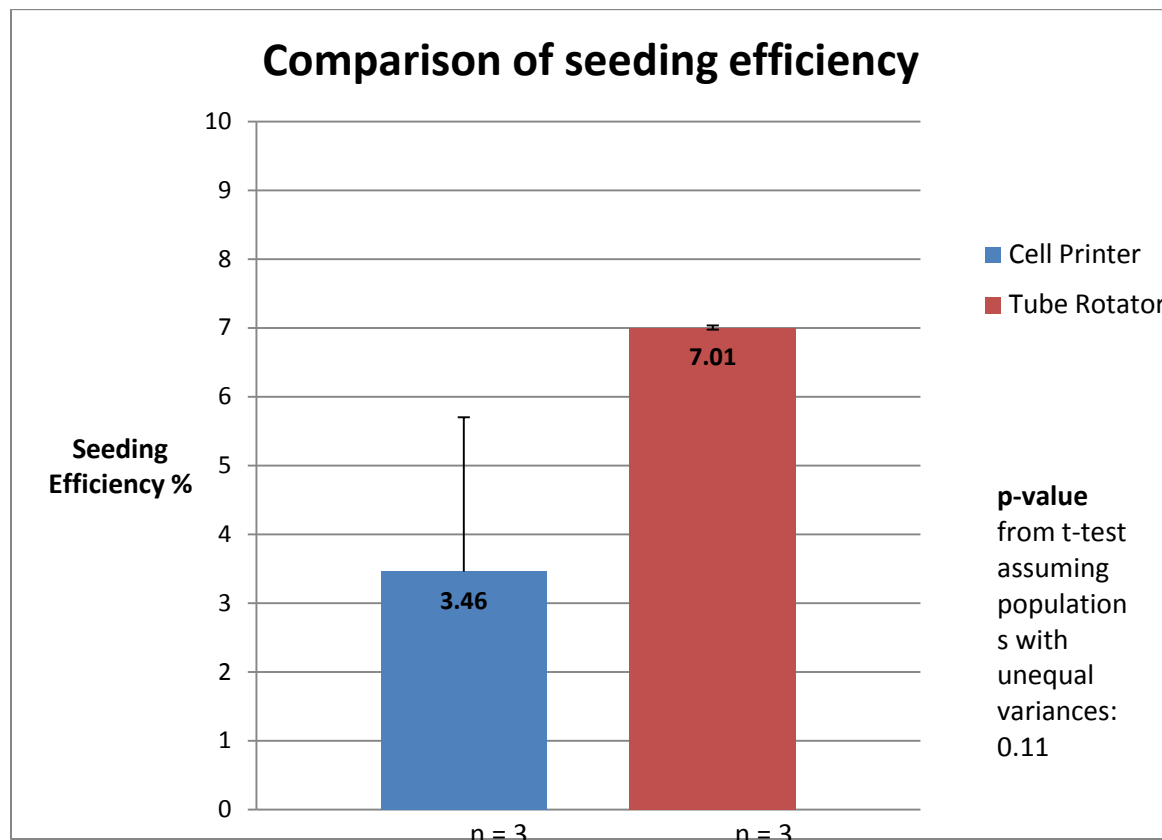

Figure 44: Comparison of efficiency of two methods to seed hMSCs onto Fibrin thread bundles

87

Even though hMSCs did show attachment to the fibrin thread bundle after being dispensed by the cell printer onto the bundle, lower number of cells seeded per mm length of bundle and lower seeding efficiency was observed using the cell printer. Probable factors contributing to this observation were sought.

The factor contributing most to low hMSC attachment and survival is thought to be dehydration of cells due to drying of thread bundles during the dispensing process in the laminar flow environment of the biosafety cabinet housing the cell printer, and during the 20-minute incubation period that immediately followed.

The deck of the prototype cell printer was open to laminar flow of air of the biosafety cabinet in which the printer was housed. As a result local temperature, humidity and gas level control on the deck of the printer was not possible and the evaporation of media from the bundle could not be prevented. The rationale behind incubating the freshly bundle freshly loaded with cell suspension for 20 minutes inside the cell culture incubator, before adding any additional media was to allow initial attachment of hMSCs onto the bundle. (Transferring the freshly loaded bundle into a bioreactor containing media would cause the unattached cells to disperse in the culture media, yielding the same, if not lesser, seeding efficiency as the tube rotator method). However, this additional 20-minute incubation period also meant that further drying of the seeded bundle and more dehydration of the cells.

If a theoretical scenario is considered where local temperature, humidity and gas level control was available, and conditions similar to a cell culture incubator could be established on the deck of the cell printer (37°C with atmospheric oxygen, 5% carbon dioxide and 85% or higher relative humidity), the seeding efficiency is highly likely to improve, as described in detail in the Discussions chapter.

The purpose of this study was to explore the feasibility of using Digilab's prototype cell printer to deliver cell suspension onto thin linear targets such as a fibrin thread bundle as a seeding method. 10 µL of cell suspension was delivered to the bundle each time, uniformly distributed over the 2 cm length of the bundle, with repeatable precision without any visible spillage on each occasion. Thus, the capability of the printer to perform such delivery of cell suspension was convincing established.

Additionally, attachment of human mesenchymal stem cells on fibrin thread bundles was observed, albeit with lower efficiency than the current method. Substantial addition to existing knowledge was made by means of this project in that the probable factors to improve the seeding efficiency were identified, thus laying groundwork for further development of this method towards similar applications.

Chapter 6: Discussion

Results of experiments performed in this project indicate that the printing process does not affect the viability of hMSCs, as determined 24 hours after printing. Additionally, it was demonstrated that the cell printer could deliver microliter volumes of cell suspension onto fibrin thread bundles suspended in mid-air, in a manner that allows the cells to seed over 24 hours. The significance of these results will be discussed in this chapter. The rationale behind certain protocols followed in this work will also be detailed.

6.1: High Post-printing cell viability

Probable reasons for high post-printing cell viability observed using Digilab's cell printer are:

1. **Aspirate-dispense mechanism:** If the design of the cell printer's print, head and the mechanism of aspiration and dispense are considered, the mechanical forces experienced by cells in suspension while the suspension is handled by the cell printer are not very different from those that the cells might experience when dispensed using a hand-held pipette. Theoretically ignoring the microsolenoid valve for the time being (or considering that it is permanently open), the aspirate-dispense mechanism at the dispense tip of the printer is identical to that of a pipette. When negative pressure is applied at the dispense tip as liquid due to withdrawal of the plunger by the synQUAD pump, it causes the cell suspension to be aspirated into the dispense tip, while positive pressure applied at the dispense tip when the plunger is pushed into the syringe causes the cell suspension to be dispensed.

2. **Gentle handling of cells:** The cell printer allows the user to adjust the flow velocities during aspirate and dispense steps, which in turn lets the user to set aspirate and dispense speeds to low settings such that cell suspension is handled gently and minimal shear stress is caused on the cells while they flow through the narrowest segments of the fluid path (typically orifice of the dispense tip).

3. **Positioning the dispense tip close to the print surface:** Because the cell printer has a Z-axis control, it allows the user to position the dispense tip close to the dispense surface while droplets of cell suspension are released. In combination with the low dispense velocity, bringing the dispense tip close to the print surface prevents the cells from crashing onto the surface. A gentle landing is facilitated which contributes to preservation of cell viability.

4. **Reservoir for aspirated cells & lack of need to pass through a valve:** The 300 µL reservoir for aspirated cells (coiled tubing directly above the dispense tip on the head of the cell printer, see Figure 45) was designed specifically for high cell viability.
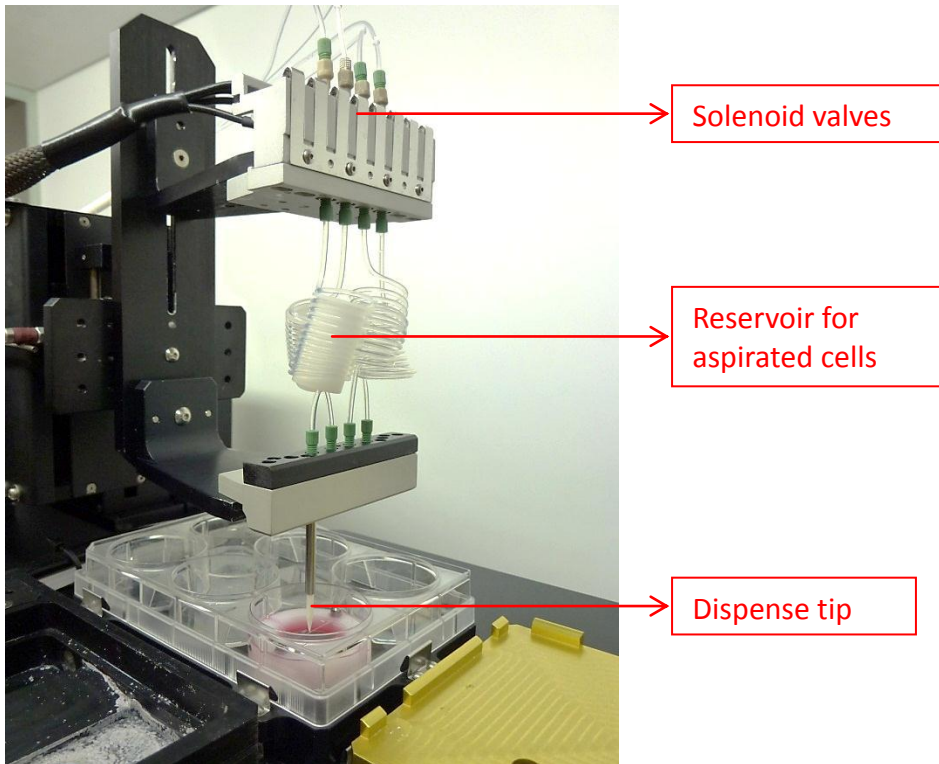
Figure 45: Reservoir for aspirated cells in between solenoid valves and dispense tip.
The coil of transparent tubing connecting the solenoid valve(s) to the dispense tip(s) acts as a reservoir for aspirated cells in suspension, preventing them from passing through the solenoid valve opening and closing at high frequency.

Because this reservoir is situated between the solenoid valves above and the dispense tip below, cells present in a suspension that is aspirated by the tip remain contained inside this reservoir (coil of transparent tubing) and do not reach the microsolenoid valve above. This prevents the cells from being constricted at the valve lumen as the valve fires open and close at high frequency.

Comparing to other technologies used for cell printing such as laser or inkjet based bioprinters, Digilab's cell printer's aspirate-dispense mechanism is simpler, more intuitively understood due to its likeness to the handheld pipette, and is a major advantage.

Inkjet printers used to print cells rely on modification of existing commercial printers designed to print ink on paper which are thermal or piezo-electric inkjet printers (3). These modified versions of commercial inkjet printers require the cell suspensions to either come in contact with a heating

element with temperatures ranging from 250 - 600°C momentarily in order to dispense the cell suspension (thermal inkjet), or constrict the cell suspension in order dispense it in a droplet form (3). Additionally, cell suspension is dispensed through narrow microfluidic channels (25 – 75 µm or smaller depending upon type of ink cartridge used) at high velocity, causing shear stress on the cells. Such thermal and mechanical stresses may affect the cell viability or may lead to undesirable physiological phenomena. In fact, certain types of thermal inkjet printers are known to cause transient cell membrane defects, a phenomenon that has been exploited to transport macromolecules across the membrane into the cell (63). Additionally, to dispense the cells with this technique, cells must be suspended in a concentrated salt solution (3x PBS or equivalent) in order to shrink their size by osmosis, to reduce damage when they pass through narrow channels of the print cartridge (63). Such stresses may not be desirable while handling highly sensitive cells such as embryonic or adult stem cells or other primary cell types.

Laser induced forward transfer (LIFT) or its modifications such as absorbing film assisted LIFT (AFA-LIFT) employ a high-energy laser pulse to 'transfer' cells suspended in a viscous medium loaded on a cartridge to the print substrate (5). The cartridge consists of a special film of silver or other material on top of which the cells to be transferred are laid in a thin layer of culture medium. The laser pulse is fired at the cartridge from the other side, such that it first contacts the silver film. The silver film (or equivalent) absorbs most of the laser energy preventing it from scorching the cells, while imparting kinetic energy to the film of cells in culture medium on the other side, causing them to detach ('desorb') from the cartridge and get deposited onto the print substrate placed opposite the cartridge (Figure 46). The biggest advantage of laser based bioprinters is their printing accuracy in terms of position, which is usually in the submicron range. This is advantageous when printing individual proteins or substances with subcellular dimensions, but has limited application when it comes to dispensing live cells, which have dimensions in tens of microns. Laser bioprinting requires modification of high-capital equipment and considerable technical expertise in printing technology, electronics and optics, before it can be adapted for cell printing. Additionally, it is limited by throughput because of the need to reload the print cartridge repeatedly, and is thus not suitable for bulk dispensing as of yet. Limited Z-axis movement is also an issue, if 3-dimensional constructs are desired.

Overall, despite advantages of micron or sub-micron level accuracy of inkjet and laser bioprinting techniques, both these techniques have limitations with regard to cell viability, undesirable mechanical or other physical stresses on the cells, low throughput, and commercial non-availability of printing equipment. Digilab's prototype (and commercial) cell-printer shows consistently high cell viability, does not induce any undue physical stresses on the cells, has an option of bulk dispensing for throughput and has a commercially available version of the equipment for use and repeatability by independent researchers. When acceptable positional accuracy for bioprinting is in tens of microns, Digilab's cell printer has distinct advantages over these two cell printing technologies. Other syringe based bioprinters such as Envision TEC's 3D bioplotter or Sciperio's BioAssembly Tool may have similar dispense mechanics as well.
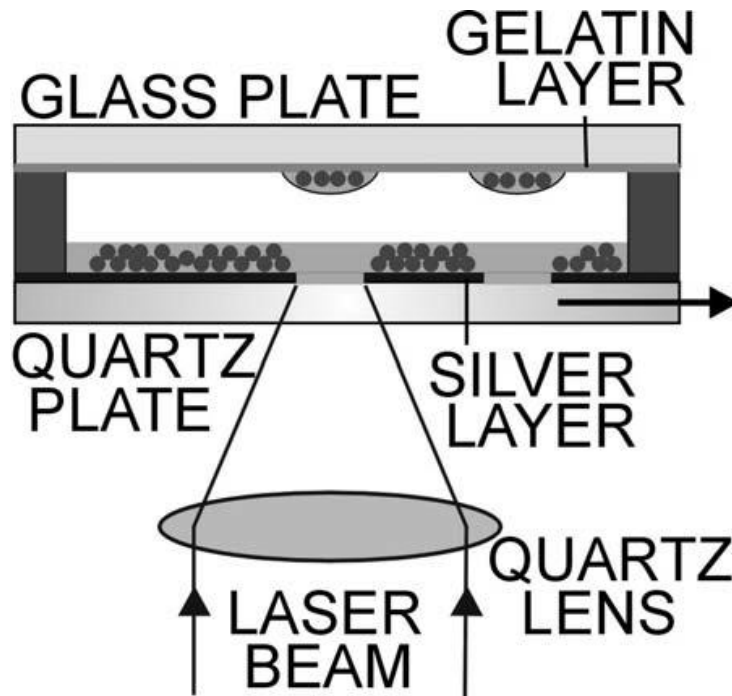
Figure 46: Mechanism of absorbing film-assisted laser-induced forward transfer (AFA-LIFT) of printing cells. Experimental arrangement for the absorbing film-assisted laser-induced forward transfer (AFA-LIFT) of living cells used by a group of researchers in University of Szaged, Szaged, Hungary, is depicted **(5)**. The silver layer served as the absorbing and carrying layer. During the transfer process this layer absorbed the laser energy, and transformed the electronic excitation into kinetic energy that caused the film contain the cells to detach and transfer to the print substrate (acceptor plate). To avoid the extreme hard impact of transferred cells the acceptor plate was covered with a gelatin layer.

6.2: Seeding hMSCs onto fibrin thread bundles using the cell printer

Using the cell printer for delivering cell suspension to fibrin microthreads in order to allow the cells to efficiently attached turned out to be more difficult than estimated at the start of this project. Several problems arose, and many were addressed in this project, while few others remain for future work.

Designing a bioreactor for mounting fibrin thread bundles

In order to deliver cell suspension onto a fibrin thread bundle using the cell printer, a device to mount the bundle onto the printers deck, so that it could be presented to the printer's dispense tip for laying the cell suspension on. It also had to be sterilizable, biocompatible and facilitate sterile mounting and handling of the bundle before and after the cell suspension was dispensed.

Additionally, it had to be large enough to accommodate at least 2 cm length of the thread bundle when held straight, preferably a little more than that, so that the printer could dispense cell

suspension onto 2 cm length of the bundle to make the method comparable to the length of bundles currently used in the tube rotator method. Considering all these factors, a ring assembly could be accommodated into a standard 6-well plate well was determined to fulfill the criteria.

The initial design of the bioreactor assembly is shown in Figure 47.
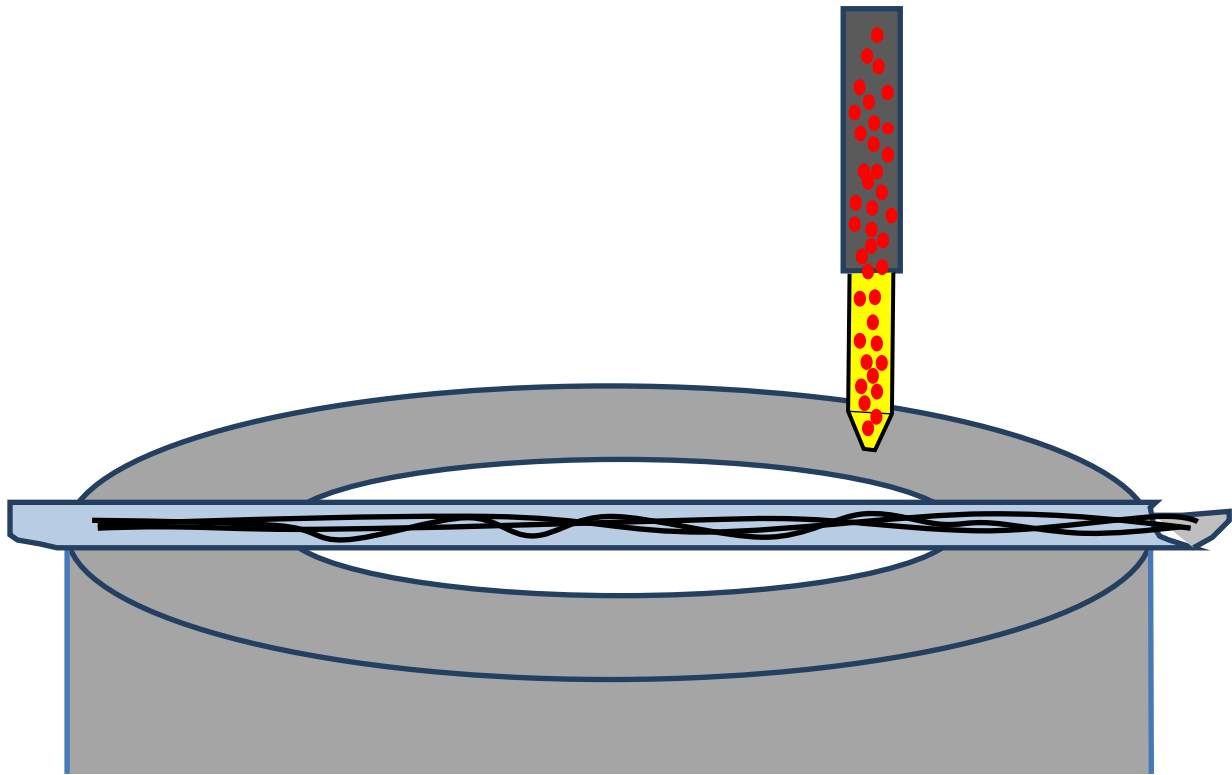
Figure 47: Initial design of bioreactor assembly to mount fibrin thread bundles onto cell printer. A delrin plastic ring that could support the positioning of a silastic tubing that was cut into a semi-cylinder along its diameter to act as a trough to hold the fibrin thread bundle (indicated by horizontal wavy black lines bundled together) was conceptualized in the early stages of the seeding assembly design. This would allow the printer's dispense tip (indicated by yellow vertical structure tapering at its bottom positioned above the horizontally placed thread bundle) would be able to dispense a small amount of concentrated cell suspension (indicated by red dots inside the tip) onto the bundle, with the cell suspension pooling around the bundle inside the trough. This would allow the cell suspension to remain in close contact with the bundle while coating its entire circumference by capillary action. Additionally, the trough formed by the silastic tube would also allow pooling of small amounts of culture media that could be added periodically to the seeded bundle to prevent dehydration and cell death.

After the delrin rings were machined, initial experiments to test the working of the assembly were performed, which revealed the flaws in the concept. Because the thread bundle was not anchored at the diametrically opposite ends in this assembly, upon hydration the bundle would curl up, or become wavy at the very least and not retain a linear shape. Programming the cell printer to dispense the cell suspension along the curves of the hydrated bundle sitting in the trough formed by the semi-cylindrical silastic tubing was not feasible. Alternatively, the cell suspension could be dispensed into the trough holding the wavy bundle assuming that the bundle would be sitting at the bottom of the trough and the cell suspension would gravitate onto it. However, parts of the bundle would very often not sit at the bottom of the trough, but rather stick to its sides or sometimes even protrude out of it a little bit. This prevented the cell suspension from reaching all parts of the bundle.

Secondly, the cell suspension dispensed onto the trough was observed to seep out through the ends of the semi-cylindrical trough of silastic tubing, sometimes in a matter of minutes. This would leave very little, if any, cells available for attachment onto the bundle. Attempts were made to block both ends of the trough by sterile sodium alginate, but were not successful.

Even if the seeping problem was corrected, the bundles would still not remain straight after hydration if they were not fixed at diametrically opposite ends of the delrin ring. Considering this fact, dowel pins made of stainless steel were introduced in the design of the assembly to act as anchors or posts for the fibrin thread bundle at diametrically opposite ends of the delrin ring, which is the assembly as was finally used for seeding. (Figure 30) Additionally, the trough of silastic tubing was removed altogether to prevent cell suspension from seeping out.

The problem of holding the thread bundle straight for printing cell suspension onto it in a straight line was addressed with this modification. However, the lack of a collection trough below the thread bundle meant that a very small amount of cell suspension (or media) could be dispensed onto the bundle at a time, if overflowing and spillage was to be avoided. This led to problems of thread dehydration and drying, which could only be addressed with local temperature and humidity control on the printer's deck, as discussed later in this section.

However, it was decided to use this bioreactor assembly for seeding cells with the cell printer in this project as it conceptually allowed for very high seeding efficiency, pending modifications on the printer's deck.

Counting cell seeded on fibrin thread bundles
To compare efficiency of seeding methods, a reliable way to count cells seeded on fibrin thread bundle had to be developed. This also was challenging task.

Murphy *et al.* had developed a method to count cells seeded on a bundle of four fibrin microthreads after fixing and staining the cells attached to the bundle, on the bundle itself, and

visualizing them using fluorescence microscopy (17). However, with twelve fibrin microthreads in each bundle, this was extremely tedious using epifluorescent microscopy because of the considerable depth of field with the average diameter of thread bundle being in the range of 300 – 400 μm, and the cells seeding on the entire circumference which could be visualized only in parts at each focal plane.

Fakharzadeh *et al.* had developed a method to count the cells using the hemocytometer after detaching them from the bundle using trypsin (18). However, the duration of trypsinization required to detach the majority of cells from the thread bundle was quite long (30 minutes), which caused several cells to die in the process of detachment. This was evident from the subsequent Trypan blue staining performed for counting the cells after trypsinization using a hemocytometer. Additionally, the cell suspension contained a lot of debris from the fibrin degradation. This, along with several dead and fragmented cells, made counting cells using this method quite difficult and unreliable. Also, any count obtained using this method would inevitably under-count the number of cells seeded by a variable and unknown proportion, because of considerable cell death in the trypsinization process.

Methods based on measuring amount of DNA present in a particular sample as a representation of the number of cells present such as CyQuant Cell Proliferation Assay (Molecular probes, Life technologies, Carlsbad, CA), also had limitations. These assays typically perform well only in a specific range of cell counts (50 to 50,000 cells for CyQuant, from manufacturer's product data sheet), and require that the cell suspension be prepared in a certain manner in a medium containing minimal impurities. Such methods are not tested for accuracy in presence of impurities such as fibrin degradation products (which would be present in suspension if seeded threads were trypsinized to detach seeded cells before counting) and thus could not be relied upon for counting for the purpose of this project.

Finally, a method to visualize one surface of a thread bundle in its entirety was developed in this study, using confocal microscopy, as described in the methods and materials section. In addition to being able to visualize cells seeded on half the circumference of each seeded bundle for counting the cells, this method also offered valuable qualitative data such as the morphology of the cells – whether they were spread out or bunched, what was their distribution along the length of the bundle, what part of the bundle did they preferentially attach to. This data can be used for extracting a lot of valuable information regarding the process of seeding and factors that affect cell attachment may be evaluated. Because individual microthreads were also visible in the confocal images due to their mild auto-fluorescence in the emission range of Ethidium Homodimer-1, the morphology of the bundle and cells could be evaluated with respect to each other, and compared from bundle to bundle. Thus, this method had several advantages in addition to offering a way to count the seeded hMSCs.

However, owing to the twisting geometry of the thread bundle with the individual fibrin microthreads twisting on one another, several cells would seed in the grooves in between

individual microthreads. The confocal images showed only the surface of the bundle. As a result, only the cells that could be seen on the surface were counted. It is likely that the cells sitting deep inside grooves between individual microthreads or inside the bundle between microthreads (if any) were missed and thus were not included into the counts considered for calculating seeding efficiency. Thus, the seeding efficiency calculated from the number of cells seeded as counted from images from confocal microscopy, was probably falsely low. It is hard to determine by what factor were the calculations off, however the number of cells seeded using the tube rotator method correlated well with previously obtained counts in the lab (18). From this, it was assumed that the magnitude of error was small and not significant, an assumption that can be tested when a more accurate counting method is developed. However, considering that this method of counting was consistently applied to all seeded bundles in both groups, the comparison of seeding efficiency between the two groups can be considered scientifically valid.

Compensating for damaged thread bundle 'Tube-Rotator-3'

As described in the results section, the third bundle in the tube rotator group was inadvertently damaged during the staining process, leaving only about half of the bundle available for analysis. Upon imaging and counting, the bundle was found to have unusually low amount of seeded cells compared to previously observed numbers for the same method. For this reason, the original count of cells on this bundle was not considered for seeding efficiency calculations of this group.

Instead, the average of the seeding efficiency of the remaining two bundles in the group was considered as representative seeding efficiency for the third bundle. This can be justified considering the fact that the tube rotator method is fairly consistent from bundle to bundle, when the number of cells used for seeding is the same, the passage of cells used is comparable and the bundles used have similar diameters.

This is evident from the measurements of seeding efficiency obtained from bundles seeded using this method during experiments performed while refining the seeding protocol for the cell printer (Table 8, Table 9). The average per mm seeding efficiency of the bundles is 9.44% which is close to the 7.05% seeding efficiency obtained by taking the average of seeding efficiency of bundles 'Tube-Rotator-1' and 'Tube-Rotator-2'.

Table 8: Number of cells per mm of thread bundle for bundles seeded with tube rotator method in developmental phases of seeding protocol for cell printer

Thread bundle	Number of cells seeded per mm	Length of thread bundle in mm
Expt_3_Tube_Rotator	280	18.60
Expt_4_Tube_Rotator	302	14.02

Table 9: Seeding efficiency per mm length of thread bundle for bundles seeded with tube rotator method in developmental phases of seeding protocol for cell printer

Thread bundle	Seeding Efficiency
Expt_3_Tube_Rotator	10.42 %
Expt_4_Tube_Rotator	8.47 %
Average	**9.44 %**

Although cell seeding data from only 3 bundle pairs (which were seeded after refinement of seeding protocol) has been admitted for the purpose of comparison of seeding efficiency in the results section of this study, more bundles had been seeded successfully with cells using the tube rotator method as comparison for the cell printer method, during the developmental stages of the seeding protocol. The above data is obtained from two such bundles. For seeding each bundle, 50,000 cells (P9 hMSCs) were used.

Local temperature, humidity & gas control on the cell printer's deck

The factor contributing most to low hMSC attachment and survival observed in the cell printer group to seed cells onto a fibrin thread bundle using the cell printer is thought to be dehydration of cells due to visible drying of thread bundles during the dispensing process in the laminar flow environment of the biosafety cabinet housing the cell printer, and during the 20-minute incubation period that immediately followed.

The deck of the prototype cell printer was open to laminar flow of air of the biosafety cabinet in which the printer was housed. As a result local temperature, humidity and gas level control on the deck of the printer was not possible and the evaporation of media from the bundle could not be prevented.

If a theoretical scenario is considered where local temperature, humidity and gas level control was available, conditions similar to a cell culture incubator could be established on the deck of the cell printer (37°C with atmospheric oxygen, 5% carbon dioxide and 85% or higher relative humidity). This would eliminate the need to transfer the seeded thread bundle to an incubator to allow cells to survive and attach to the bundle.

Additionally, the cell printer could be used to rehydrate the thread bundle as often as required in small, frequent aliquots of warmed media, to prevent dehydration of the cells, in addition to providing the necessary nutrition to the cells. The media could be added in aliquots small enough to prevent any of it from spilling or overflowing from the thread bundle, thus not causing any inadvertent loss of cells into the well below the thread bundle.

This would allow the entire bulk of cell suspension containing 50,000 cells to remain in contact with the thread bundle for an extended period of time, in conditions favorable to cell growth and attachment, and would also eliminate the need to place the bundle on a tube rotator. Such static seeding process, which is closer to culture conditions the hMSCs are used to seeing compared to the dynamic method of seeding in the tube rotator, is likely to result in a higher rate of cell attachment and thus increase seeding efficiency.

If localized temperature, humidity and gas control are introduced on the deck of the cell printer, several other bioprinting applications involving use of temperature sensitive hydrogels such as Collagen or Agarose, in addition to live cells, will become possible, opening doors for exciting possibilities of novel tissue constructs.

Future work:

The feasibility to use this automated liquid handling technology to deliver cells to biological scaffolds in specified patterns to develop vehicles for cell therapy was shown in this study, with plenty of room for improvement.

Options for local temperature, humidity and gas control on the cell printer's deck should be explored, inasmuch as this is a highly desirable feature for creating constructs with live cells.

Seeding other cell types on scaffold materials other than fibrin or a combination of materials, in more complex patterns in 2 and 3 dimensions may also be attempted. Loading selective portions of the scaffolds with growth factors or multiple cell types, or loading them in different concentrations at different parts of the scaffold may allow creation of 'gradients' of these biological agents.

Once methods to generate biologically relevant constructs for therapy, testing or research are established using the cell printer, the potential for automation of parts or whole of the construction method and scaling up the technology for manufacturing on a larger scale may also be evaluated.

De novo tissue construction of multilayered 3 dimensional constructs, starting from relatively simple tissues such as skin, to more complex tissues, is an exciting, challenging and promising prospect that the cell printer offers. As knowledge boundaries of biology, material science, and engineering disciplines expand, this approach which is in its infancy right now may become a reality with tools such as this cell printer.

Conclusion

A novel cell printing technology – Digilab's prototype cell printer, was explored in this work, and was found to handle human mesenchymal stem cells and human fibroblasts as gently as manual pipetting, preserving the viability of cells – a highly desirable quality for a bioprinter. Printing accuracy of the cell printer was found to be sufficient to consistently dispense small volumes of cell suspension directly onto fibrin thread bundles, a thin linear target suspended in mid-air, without any observable spillage. Cell attachment to the surface of fibrin thread bundles (seeding) was demonstrated following such delivery of cell suspension to the bundles and factors likely to contribute to better seeding efficiency were identified. In sum, the cell printer shows considerable potential to develop novel vehicles for cell therapy. It empowers researchers with a supervision-free, patterned cell dispensing robotic tool while preserving cell viability. In the future, de novo biofabrication of tissue replicates on a small scale using this technology by dispensing cells, extracellular matrices, and growth factors in different combinations is a very realistic possibility.

References

1. *Biofabrication: a 21st century paradigm.* **Mironov, V., Trusk, T., Kasyanov, V., Little, S., Swaja, R., Markwald, R.** s.l. : IOP Publishing, June 2009, Biofabrication, Vol. 1, pp. 1-16.

2. *Drop-on-demand printing of cells and materials for designer tissue constructs.* **Boland, T., Tao, X., Damon, B.J., Manley, B., Kesari, P., Jalota, S., Bhaduri, S.** s.l. : Elsevier Publications, 2007, Material Science and Engineering C, Vol. 27, pp. 372-376.

3. *Drop-on-demand inkjet printing: a primer.* **Binder, K.W., Allen, A.J., Yoo, J.J., Atala, A.** 1, s.l. : World Scientific Publishing Company, 2011, Vol. 6, pp. 33-49.

4. *Computer-assisted designing and biofabrication of 3-D hydrogel structures towards thick 3-D tissue engineering.* **Nakamura, M., Arai, K., Toda, H., Iwanaga, S., Ito, K., Genci, C., Nikaido, T.** s.l. : Materials Research Society, 2011, MRS Proceedings, Vol. 2011 Fall Proceedings.

5. *Survival and Proliferative Ability of Various Living Cell Types after Laser-Induced Forward Transfer.* **Hopp, B., Smausz, T., Kresz., N., Barna, N., Bor, Z., Kolozsvari, L., Chrisey, D.B., Szabo, A., Nogradi, A.** 11/12, s.l. : Many Ann Liebert, Inc., 2005, TISSUE ENGINEERING, Vol. 11, pp. 1817-1823.

6. *Biological laser printing: A novel technique for creating heterogeneous 3-dimensional cell patterns.* **Barron, J.A., Wu, P., Ladouceur, H.D., Ringeisen, B.R.** 2, 2004, Biomedical Microdevices, Vol. 6, pp. 139-147.

7. *Construction of Vasculature Structure within Fluidic Channel using Three-Dimensional Bio-Printer.* **Lee, V.K., Lee, W., Yoo, S.S., Dai, G.** s.l. : IEEE, 2011.

8. *Three-dimensional BioAssembly tool for generating viable tissue-engineered constructs.* **Smith, C.M., Stone, A.L., Parkhill, R.L., Stewart, R.L., Simpkins, M.W., Kachurin, A.M., Warren, W.L., Williams, S.K.** 9/10, s.l. : Mary Ann Liebert, Inc., 2004, Tissue Engineering, Vol. 10, pp. 1566-1576.

9. *Rapid prototyping of scaffolds derived from thermoreversible hydrogels and tailored for applications in tissue engineering.* **Landers, R., Hubner, U., Schmelzeisen, R., Mulhaupt, R.** s.l. : Elsevier Publications, 2002, Biomaterials, Vol. 23, pp. 4437-4447.

10. **American Heart Association.** Heart Disease and Stroke Statistics--2011 Update : A Report From the American Heart Association. 2011.

11. *Regenerating the heart.* **Laflamme, M., Murry, C.** 7, 2005, Nature Biotechnology, Vol. 23, pp. 845-856.

12. *Human mesenchymal stem cells improve myocardial performance in a splenectomized rat model of chronic myocardial infarction.* **Liu, J., et al.** 2, 2008, J Formos Med Assoc, Vol. 107, pp. 165-174.

13. *Mesenchymal stem cells from ischemic heart disease patients improve left ventricular function after acute myocardial infarction.* **Grauss, R., et al.** 4, 2007, Am J Physiol Heart Circ Physiol, Vol. 293, pp. H2438-H2447.

14. *A tissue engineering approach to progenitor cell delivery results in significant cell engraftment and improved myocardial remodeling.* **Simpson, D., et al.** 9, 2007, Stem Cells, Vol. 25, pp. 2350-2357.

15. *Bioengineered cardiac grafts: A new approach to repair the infarcted myocardium?* **Leor, J., et al.** 19 Suppl 3, 2000, Circulation, Vol. 102, pp. III56-III61.

16. *Master's thesis: Collagen and Fibrin Biopolymer Microthreads for bioengineered ligament generation.* **Cornwell, K.** Worcester : s.n., 2007, Dept. of Biomedical Engineering, Worcester Polytechnic Institute.

17. *Master's Thesis: Fibrin Microthreads Promote Stem Cell Growth for Localized Delivery in Regenerative Therapy.* **Murphy, M.K.** Worcester : s.n., 2008, Dept. of Biomedical Engineering, Worcester Polytechnic Institute.

18. *Master's Thesis: Delivering stem cells to the heart.* **Fakharzadeh, M.** Worcester : s.n., 2010, Dept. of Biomedical Engineering, Worcester Polytechnic Institute.

19. *Organ printing: computer-aided jet-based 3D tissue engineering.* **Mironov, V., Boland, T., Trusk, T., Forgacs, G., Markwald, R.R.** 4, s.l. : Cell Press, April 2003, Trends in Biotechnology, Vol. 21, pp. 157-161.

20. *Effects of Dispensing Pressure and Nozzle Diameter on Cell Survival from Solid Freeform Fabrication–Based Direct Cell Writing.* **Chang, R., Nam, J., Sun, W.** 1, s.l. : Mary Ann Liebert, Inc., 2008, Tissue Engineering: Part A, Vol. 14, pp. 41-48.

21. *Laser-guided direct writing of living cells.* **Odde, D.J., Renn, M.J.** 3, s.l. : John Wiley and Sons, Inc., February 2000, Biotechnology and Bioengineering, Vol. 67, pp. 312-318.

22. *Cell transfer printing from patterned poly(ethylene glycol)-oleyl surfaces to biological hydrogels for rapid and efficient cell micropatterning.* **Takano, T., Yamguchi, S., Matsunuma, E., Komiya, S., Shinkai, M., Takezawa, T., Nagamune, T.** 1, s.l. : Wiley Periodicals, Inc., January 2012, Biotechnology and Bioengineering, Vol. 109, pp. 244-251.

23. *High-throughput laser printing of cells and biomaterials for tissue engineering.* **Guillemot, F., et al.** 7, s.l. : Elsevier, July 2010, Acta Biomaterialia, Vol. 6, pp. 2494-2500.

24. *On-Demand Three-Dimensional Freeform Fabrication of Multi-Layered Hydrogel Scaffold with Fluidic Channels.* **Lee, W., et al.** 6, 2010, Biotechnology and Bioengineering, Vol. 105, pp. 1178-1186.

25. *Modular tissue engineering: engineering biological tissues from the bottom up.* **Khademhosseini, A., Nichol, J.W.** 2009, Soft Matter, Vol. 5, pp. 1312-1319.

26. *Functional arteries grown in vitro.* **Niklason, L.E., et al.** 5413, 1999, Science, Vol. 284, pp. 489-493.

27. *Bone morphogenetic proteins-2, -12, and -13 modulate in vitro development of engineered cartilage.* **Gooch, K.J, et al.** 4, 2002, Tissue Engineering, Vol. 8, pp. 591-601.

28. *Mechanical properties and remodeling of hybrid cardiac constructs made from heart cells, fibrin, and biodegradable, elastomeric, knitted fabric.* **Boublik, J., et al.** 7-8, 2005, Tissue Engineering, Vol. 11, pp. 1122-1132.

29. *The tissue-engineered small-diameter artery.* **Tranquillo, R.T.** 2002, Ann. N. Y. Acad. Sci., Vol. 961, pp. 251-254.

30. *Rods, tori, and honeycombs: the directed self-assembly of microtissues with prescribed microscale geometries.* **Dean, D.M.** 2007, FASEB J., Vol. 21, pp. 4005-4012.

31. *Micromolding of shape-controlled, harvestable cell-laden hydrogels.* **Yeh, J.** 2006, Biomaterials, Vol. 27, pp. 5391-5398.

32. *A completely biological tissue-engineered blood vessel.* **L'Heureux, N., et al.** 1, 1998, FASEB J., Vol. 12, pp. 47-56.

33. **American Heart Association.** Heart Disease and Stroke Statistics - 2011 Update. *A report from American Heart Association.* 2011.

34. **Thom, T., et al.** Heart disease and stroke statistics -- 2006 update: a report from the American Heart Association Statistics Committee and Stroke Statistics Subcommittee. *Circulation.* 2006, Vol. 113, 6, pp. e85-151.

35. **Braunwald, E. and Pfeffer, M.** Ventricular enlargement and remodeling following acute myocardial infarction: mechanisms and management. *American Journal of Cardiology.* 1991, Vol. 68, 14, pp. 1D-6D.

36. *Influence of the internal-mammary-artery graft on 10-year survival and other cardiac events.* **Loop, F.D., et al.** 1, Jan 2, 1986, New England Journal of Medicine, Vol. 314, pp. 1-6.

37. *Surgical ventricular restoration in the treatment of congestive heart failure due to post-infarction ventricular dilation.* **Athanasuleas, C., et al.** 7, 1991, Journal of American College of Cardiology, Vol. 44, pp. 1439-1445.

38. *Ventricular structure and surgical history.* **Buckberg, G.** 4, 2004, Heart Failure Review, Vol. 9, pp. 255-268.

39. *Mobilized bone marrow cells repair the infarted heart, improving function and survival.* **Orlic, D., et al.** 18, 2001, Proceedings of National Academy of Science U S A, Vol. 98, pp. 10344-10349.

40. *Regenerating functional myocardium: improved performance after skeletal myoblast transplantation.* **Taylor, D.A., et al.** 8, 1998, Nature Medicine, Vol. 4, pp. 929-933.

41. *Engraftment of engineered ES cell-derived cardiomyocytes but not BM cells restores contractile function to the infarcted myocardium.* **Kolossov, E., et al.** 10, 2006, Journal of Experimental Medicine, Vol. 203, pp. 2315-2327.

42. *Adult cardiac stem cells are multipotent and support myocardial regeneration.* **Beltrami, A.P., et al.** 6, 2003, Cell, Vol. 114, pp. 763-776.

43. *Mesenchymal stem cells and their potential as cardiac therapeutics.* **Pittinger, M. and Martin, B.** 1, 2004, Circulation Research, Vol. 95, pp. 9-20.

44. *Cellular cardiomyoplasty -- cardiomyocytes, skeletal myoblasts, or stem cells for regenerating myocardium and treatment of heart failure?* **Reffelmann, T., and Kloner, R.** 2, 2003, Cardiovascular Research, Vol. 58, pp. 358-368.

45. *Human mesenchymal stem cells differentiate to a cardiomyocyte phenotype in the adult murine heart.* **Toma, C., et al.** 1, 2002, Circulation, Vol. 105, pp. 93-98.

46. *Transplantation of mesenchymal stem cells from human bone marrow improves damaged heart function in rats.* **Hou, M., et al.** 2, 2007, International Journal of Cardiology, Vol. 115, pp. 220-228.

47. *Effects of bone marrow derived mesenchymal stem cells transplantation in acutely infarcting myocardium.* **Piao, H.,.** 5, 2005, European Journal of Heart Failure, Vol. 7, pp. 730-738.

48. *Mesenchymal stem cells modified with Akt prevent remodeling and restore performance of infarcted hearts.* **Mangi, A., et al.** 9, 2003, Nature Medicine, Vol. 9, pp. 1196-1201.

49. *Systemic delivery of bone marrow-derived mesenchymal stem cells to the infarcted myocardium: feasibility, cell migration, and body distribution.* **Barbash, et al.** 7, 2003, Circulation, Vol. 108, pp. 863-868.

50. *Mesenchymal stem cells participate in angiogenesis and improve heart function in rat model of myocardial ischemia with reperfusion.* **Tang, et al.** 2, 2006, European Journal of Cardiothoracic Surgery, Vol. 30, pp. 353-361.

51. *High resolution mechanical function in the intact porcine heart: mechanical effects of pacemaker location.* **Azeloglu, E.U., et al.** 4, 2006, Journal of Biomechanics, Vol. 39, pp. 717-725.

52. *Dose-dependant effects of intravenous allogenic mesenchymal stem cells in the infarcted porcine heart.* **Wolf, D., et al.** 2, 2009, Stem cells development, Vol. 18, pp. 321-329.

53. *Repairing damaged myocardium: evaluating cells used for cardiac regeneration.* **Schuldt, A., et al.** 1, 2008, Current Treatment Options in Cardiovascular Medicine, Vol. 10, pp. 59-72.

54. *Injectable fibrin scaffold improves cell transplant survival, reduces infarct expansion, and induces neovasculature formation in ischemic myocardium.* **Christman, K., et al.** 3, 2004, Journal of American College of Cardiology, Vol. 44, pp. 654-660.

55. *Fibrin glue alone and skeletal myoblasts in a fibrin scaffold preserve cardiac function after myocardial infarction.* **Christman, K., et al.** 3-4, 2004, Tissue Engineering, Vol. 10, pp. 403-409.

56. *A novel bioartificial myocardial tissue and its prospective use in cardiac surgery.* **Kofidis, T., et al.** 2, 2002, European Journal of Cardiothoracic Surgery, Vol. 22, pp. 238-243.

57. *Percutaneous transvenous cellular cardiomyoplasty. A novel nonsurgical approach for myocardial cell transplantation.* **Thompson, C., et al.** 11, 2003, Journal of American College of Cardiology, Vol. 41, pp. 1964-1971.

58. *Artificial matrix helps neonatal cardiomyocytes restore injured myocardium in rats.* **Zhang, P., et al.** 2, 2006, Artificial Organs, Vol. 30, pp. 86-93.

59. *Enhancing efficacy of stem cell transplantation to the heart with a PEGylated fibrin biomatrix.* **Zhang, G., et al.** 6, 2008, Tissue Engineering Part A, Vol. 14, pp. 1025-1036.

60. *A novel composite scaffold for cardiac tissue engineering.* **Park, H., et al.** 7, 2005, In vitro cellular & developmental biology, Vol. 41, pp. 188-196.

61. *Discrete crosslinked fibrin microthrea scaffolds for tissue regeneration.* **Cornwell, K. and Pins, G.** 2007, Journal of Biomedical Materials Research, pp. 104-112.

62. *Fibrin microthreads support mesenchymal stem cell growth while maintaining differentiation potential.* **Proulx, M.K., et al.** 2, February 2011, Journal of Biomedical Materials Research, Vol. 96, pp. 301-312.

63. *Creating Transient Cell Membrane Pores Using a Standard Inkjet Printer.* **Owczarczak, A.B., Shuford,S.O., Wood,S.T., Deitch, S., Dean, D.** 2012, Journal of Visualized Experiments, Vol. 61.

64. *Characterizing the effects of cell settling on bioprinter output.* **Pepper, M.E., Seshadri, V., Burg, T.C., Burg, K.J.L., Groff, R.E.** 1, 2012 : IOPScience, Biofabrication, Vol. 4, pp. 1-6.

65. *Custom design of the cardiac microenvironment with biomaterials.* **Davis, , M., et al.** 1, 2005, Circulation Research, Vol. 97, pp. 8-15.

Appendix A: Post-Printing Cell Viability Measurements

Cells dispensed using the cell printer – Calculation of number of nuclei belonging to live cells in each well			
Well address	Objects showing Hoechst signal (total # of nuclei) (A)	Objects showing Hoechst and Ethidium signal (nuclei of dead cells) (B)	Objects showing only Hoechst signal (nuclei of live cells) (A – B)
A5	2504	140	2364
A6	2045	57	1988
A7	1957	165	1792
A8	1955	119	1836
B1	1837	37	1800
B2	2246	88	2158
B3	2551	74	2477
B4	2854	126	2728
B5	3104	104	3000
B6	1984	105	1879
B7	2817	115	2702
B8	2225	130	2095

Cells dispensed manually using a hand-held pipette – Calculation of number of nuclei belonging to live cells in each well			
Well address	Objects showing Hoechst signal (total # of nuclei) (A)	Objects showing Hoechst and Ethidium signal (nuclei of dead cells) (B)	Objects showing only Hoechst signal (nuclei of live cells) (A – B)
C5	4422	134	4288
C6	4772	156	4616
C7	3402	103	3299
C8	3311	137	3174
D1	1823	228	1595
D2	3633	278	3355
D3	3446	142	3304
D4	3721	109	3612
D5	3657	64	3593
D6	4229	138	4091
D7	3718	83	3635
D8	4273	150	4123

Cells dispensed using the cell printer – Nuclei belonging to dead cells	
Well address	Objects showing Ethidium Homodimer-1 signal (nuclei of dead cells)
A5	247
A6	119
A7	351
A8	167
B1	70
B2	161
B3	120
B4	318
B5	197
B6	302
B7	270
B8	342

Cells dispensed manually using a hand-held pipette – Nuclei belonging to dead cells	
Well address	Objects showing Ethidium Homodimer-1 signal (nuclei of dead cells)
C5	190
C6	235
C7	196
C8	323
D1	746
D2	804
D3	230
D4	191
D5	177
D6	342
D7	152
D8	439